



UNIVERSITÀ POLITECNICA DELLE MARCHE
FACULTY OF ENGINEERING

Master's Degree Course: Environmental Engineering

**Harmonizing Satellite Thermal Data with Ground-based Observations for
Climate Long-term Monitoring.**

Supervisor:

Prof. Eva Savina Malinvernì

Candidate:

Qudratullah Ramzi

Co-Supervisor

Eng. Sanità Marsia

Abstract

Estimating land surface temperature (LST) usually is challenging because urban areas are made up of many different material, each with distinct thermal properties and emissivity. This study evaluates LST data from two satellite sensors, Landsat 8 TIRS, ECOSTRESS, against temperature readings from 50 ground-based sensors installed across a range of urban surfaces in Ancona city, Italy. For this purpose, the first part of the study focused on land-use classification, dividing the area into four categories for the years 1996 to 2025. This step aimed to assess how much the urban area has expanded over time and how this growth has contributed to the rise of the Urban Heat Island (UHI) effect and its influence on Land Surface Temperature (LST). In addition, the study analysed the temporal trends of LST in Ancona from 1996 to 2025 to determine how much surface temperatures have increased over the past three decades and to better understand the relationship between urban development and thermal changes in the city.

To reduce differences between the satellite products, a harmonization process was implemented. This included matching spatial resolution, aligning acquisition times within ± 15 minutes, and normalizing surface emissivity. The agreement between satellite and ground data was then analysed using standard accuracy metrics such as RMSE, MAE, bias, and Pearson's correlation coefficient(R). Among all datasets, ECOSTRESS shows lower MAE and RMSE, with smaller errors overall. Landsat 8 has slightly smaller bias and higher correlation, indicating it tracks the pattern of temperature changes a bit more consistently. The differences are not huge, but ECOSTRESS tends to estimate better temperature magnitudes, while Landsat 8 provides stronger temporal/spatial consistency with ground trends.

Looking across all the analysed dates, the surface-specific metrics show: 1- Vegetation shows the best agreement between satellite and ground temperatures. 2- Soil performs moderately, with stable correlations but slightly higher error magnitudes. 3- Asphalt/concrete remains the most challenging, with the highest errors due to thermal complexity and extreme heating behaviour.

Keywords

- Land Surface Temperature (LST)
- Urban Heat Island (UHI)
- Harmonization
- Landsat 8 TIRS
- ECOSTRESS
- Google Earth Engine (GEE)
- QGIS
- Urbanization
- Validation Metrics (RMSE, MAE, Bias, Pearson R)
- Ancona, Italy
- Spatial and Temporal Analysis
- Thermal Infrared Remote Sensing

Table of Contents

Abstract.....	1
Keywords	2
List of Figures	5
List of Tables.....	6
1 Introduction.....	7
1.1 Motivation & Background	8
1.2 Study Objectives	8
2 - State of the Art.....	9
3 Methods and Materials.....	14
3.1 Study Area.....	14
3.2 Input data	15
3.2.1 Landsat Data (Landsat 8).....	15
3.2.2 ECOSTRESS Level 2 Product.....	18
3.3 Software /Platform Used.....	19
3.3.1 Google Earth Engine (GEE)	19
3.3.2 Quantum GIS (QGIS)	20
3.4 Calculation of LST in QGIS	21
3.4.1 Image Analysis.....	21
3.5 Calculation of TOA (Top of Atmosphere) Reflectance.....	22
3.6 Conversion of TOA to Brightness Temperature.....	22
3.7 CALCULATE THE NDVI	22
3.8 Calculation of the Proportion of Vegetation	23
3.9 Calculate the land surface emissivity.....	23
3.10 Calculate the Land Surface Temperature	24
3.11 Workflow for Classification and Land Surface Temperature Trends Over Ancona.....	25
3.11.1 Land Cover Classification Overview	25
3.11.2 Random Forest (RF) Classifier	25
3.12 Workflow of Random Forest (RF) Classifier in GEE	26
3.13 Harmonizing Satellite Thermal Data with Ground-based Observations workflow	38
3.13.1 Ground-based Observations workflow	38
3.13.2 LST Workflow in Google Earth Engine.....	45
3.14 Harmonization workflow of.....	47
3.14.1 Spatial Harmonization of Satellite Data	47
3.14.2 Sampling Harmonization of Satellite and Ground Data	47

3.14.3 Temporal Interpolation for Ground–Satellite Harmonization.....	48
3.14.4 Average Weighted Temperature (AWT) for Mixed Surface Conditions	48
3.14.5 Residual Result After Harmonizations.....	52
3.15 Data Preparation and Validation Metric Computation in Python	53
3.15.1 Residual Analysis as a Validation Metric.....	54
3.15.2 Root Mean Square Error (RMSE) as a Validation Metric	54
3.15.3 Mean Absolute Error (MAE) as a Validation Metric	55
3.15.4 Bias (ΔT) as a Validation Metric.....	55
3.15.5 Correlation Analysis (Pearson’s R) - Evaluating the Relationship Between Satellite and Ground Temperatures.....	56
4 Result and Discussion.....	57
4.1 Land Cover Change Analysis in Ancona, Agugliano, and Camerata Picena	57
4.2 Urban Expansion Intensity (UEII)-Ancona	62
4.3 Land Surface Temperature (LST) Change in Ancona (1996–2025)	67
4.4 Urban Growth and Land Surface Temperature in Ancona.....	70
4.5 Urban Heat Island Dynamics and Land Surface Temperature Variations in Ancona (1996–2025).....	71
4.6 Urban Heat Island Intensity (UHII)/ Its Implications in Ancona (1996–2025)	73
4.7 Land Use Land Cover (LULC) and Urban Heat Island (UHI)-Ancona	74
4.8 Land Surface Temperature (LST) Derived from Landsat and ECOSTRESS Data (Ancona, 19 June 2025)	75
4.8.1 Metrics Results.....	76
4.9 Conclusion	79
4.10 References.....	80

List of Figures

Figure 1. study area.....	15
Figure 2. Landsat and ECOSTRESS. Source: google images	18
Figure 3. illustrates the sequential outputs generated during the Land Surface Temperature (LST) retrieval process using Landsat 8 imagery. The top row presents the intermediate products, including the Top of Atmosphere (TOA) radiance, Brightness Temperature (BT), and Normalized Difference Vegetation Index (NDVI). The bottom row displays the derived Proportion of Vegetation (PV), Land Surface Emissivity (ε), and the final LST map. .	24
Figure 4 this figure shows the training data collected form the area covered by water.....	28
Figure 5. this figure shows the data collected for vegetation across Ancona	29
Figure 6. this figure shows the data collected for covered area by soil across Ancona.....	29
Figure 7. this figure shows the data collected for build up area across Ancona	30
Figure 8. this figure shows the data collected for road network.....	30
Figure 9. this figure shows all the data collected for the random forest classification	31
Figure 10. this figure shows the RF classification along with training data for different classes	34
Figure 11. result of RF classification.....	34
Figure 12. this figure shows the total number of samples, training size and testing size	35
Figure 13. Final result of Training accuracy, Training Kappa, test accuracy, test kappa.....	36
Figure 14. iButton DS1921GH-F50 deployment	39
Figure 15. 50 iButton DS1921GH-F50 sensors across Ancona city.....	39
Figure 16. Google Earth Engine environment displaying the NASA LST script and the selected study area for LST analysis. Source: (Google Earth Engine screenshot)	45
Figure 17. Land Surface Temperature visualization.....	46
Figure 18. spatial harmonization of satellite image	47
Figure 19. sampling harmonization of satellite and ground data.....	47
Figure 20. Loading ECOSTRESS/Landsat and Sentinel raster data, converting both to vector format, and clipping the Sentinel vector data using the ECOSTRESS and Landsat boundaries.	49
Figure 21. Average Land Surface Temperature, or LST, for different vegetated areas.....	50
Figure 22. Average Land Surface Temperature (LST) for Soil Areas	50
Figure 23. Average Land Surface Temperature (LST) for Asphalt/Concrete Areas	51
Figure 24. steps of LST calculation of one Landsat/ECOSTRESS pixel.....	51
Figure 25. Data Preparation and Validation Metric Computation in Python	53
Figure 26. land cover classification	57
Figure 27. land cover classification	58
Figure 28. land cover classification	59
Figure 29. land cover classification	60
Figure 30. land cover classification	61
Figure 31. Urban area growth and expansion intensity (Ancona, 1996 to 2025).....	62
Figure 32. Relationship Between Land Cover Types and Land Surface Temperature	63
Figure 33. Ancona Road network and Land Surface Temperature	64
Figure 34. Relationship Between build-up area and LST.....	65
Figure 35. Relationship Between LST and DEM	66
Figure 36. Land Surface Temperature (LST) Change in Ancona (1996–2025)	67
Figure 37. LST trends in Ancona	69
Figure 38. Urban Growth and Land Surface temperature.....	70
Figure 39. UHI dynamics and LST	71
Figure 40. urban and rural LST trends.....	72
Figure 41. UHII and its Implications in Ancona	73
Figure 42. Land cover distribution by year 1996 to 2025	74
Figure 43 Land Surface Temperature Ancona 19 June 2025.....	75
Figure 44 Land Surface Temperature Ancona 26 June and 5 July 2025	75

List of Tables

<i>Table 1. Landsat 8 OLI and TIRS band specifications.....</i>	16
<i>Table 2. overview of Landsat 5-9.....</i>	17
<i>Table 3. Recorded sensor LST values in degrees Celsius along with location descriptions on June 19, 2025.....</i>	41
<i>Table 4. Recorded sensor LST values in degrees Celsius along with location descriptions on June 23, 2025.....</i>	42
<i>Table 5. Recorded sensor LST values in degrees Celsius along with location descriptions on June 26, 2025.....</i>	43
<i>Table 6. Recorded sensor LST values in degrees Celsius along with location descriptions on June 19, 2025, and descriptions about the sensors which their location were changed.....</i>	44
<i>Table 7. temporal trends in LST 1996-2025 over Ancona.....</i>	68
<i>Table 8. urban and rural LST statistics, Ancona 199-2025</i>	71
<i>Table 9. metrics results consistent</i>	76
<i>Table 10. metric result for LANDSAT data on July 5th, 2025</i>	77
<i>Table 11. metric result for LANDSAT data on June 19th, 2025.....</i>	77
<i>Table 12. metric result for ECOSTRESS data on June 19th, 2025</i>	77
<i>Table 13. metric result for ECOSTRESS data on June 23th, 2025</i>	77
<i>Table 14. metric result for LADSAT data on June 26th, 2025</i>	77

1 Introduction

Our planet's surface is constantly changing. Cities are expanding, forests are shrinking, and climates are warming. To understand these changes, scientists rely on a combination of satellite observations and ground-based measurements. Satellites like Landsat and ECOSTRESS in space, capturing detailed snapshots of the Earth's surface temperature, while ground sensors provide the precision and local context that satellites sometimes miss ([Ewa Głowienka, 2025](#)).

The Landsat satellite series provides high-resolution data ideal for local LST analysis, but many retrieval algorithms require detailed input parameters and calibration constants that are not always easy to access. Although some datasets exist online, processing them often involves handling large data volumes. The Google Earth Engine (GEE) platform simplifies this process by offering direct access to Landsat Level 1 and Level 2 data for large-scale analysis without local computing resources. However, high-resolution LST products from Landsat have only recently become available on GEE (Sofia L. Trigo, 2020) QGIS (Quantum Geographic Information System) offers a wide range of plugins designed to assist users with different geospatial tasks. These plugins act as additional tools that simplify complex workflows. However, there is currently no dedicated plugin that automatically computes land surface temperature (LST). At present, LST must be calculated manually in QGIS using the Raster Calculator, which involves several detailed steps. Developing a specialized plugin would greatly simplify and streamline the LST calculation process, making it more efficient and user-friendly (Mohammad Ramahillah 2020).

Rapid and ongoing urbanization has led to various environmental challenges, one of the most significant being the Urban Heat Island (UHI) effect. Built-up areas in cities tend to absorb and retain more solar energy, causing them to emit higher surface temperatures compared to nearby rural regions(Mehmet Cetin, 2024).

Satellites offer broad, repeated views of Earth's surface heat (for example, Land Surface Temperature), while ground stations give precise, local temperature readings, but the two don't always match because of differences in resolution, sensor calibration, surface heterogeneity, and timing. To bridge that gap, scientists align data in space and time (for example, only comparing satellite passes within ± 30 minutes of a ground reading), correct for emissivity and atmospheric effects, and normalize between sensors so their scales match. A harmonized dataset lets us monitor long-term climate trends more reliably, reduce bias in urban vs. rural areas, and confidently track subtle warming signals over decades. One recent study used sensors like Landsat 8, ECOSTRESS, MODIS, and Sentinel-3 alongside 50 in-situ thermal sensors across urban surfaces and performed spatial reprojection, temporal alignment, and emissivity normalization to reduce discrepancies; they validated differences using metrics like RMSE, bias, and correlation. (Eva Savina Malinverni, 2025).

The main part this report explores how these two satellite data sources (Landsat and ECOSTRESS) can be harmonized to better monitor land surface temperature (LST) and urban heat patterns over time. Focusing on the Municipalities (commune) Ancona, Agugliano and Camerata Picena in central Italy. This study focuses on understanding how surface temperatures change over time in the given commune, using satellite data, and comparing the satellite sensor with ground-based measurements to understand how much the satellite data is accurate. Using the framework of "Harmonizing Satellite Thermal Data with

Ground-based Observations for Climate Long-term Monitoring,” the research analyses Landsat data from 1996 to 2025 to explore how the given urban growth, vegetation, and land cover influence temperature distribution and the Urban Heat Island (UHI) effect. To improve accuracy, Landsat 8 TIRS and ECOSTRESS thermal data were harmonized with ground sensor observations through spatial and temporal alignment. Statistical validation metrics such as bias, MAE, RMSE, and correlation were applied to assess consistency between datasets. The results enhance the reliability of satellite-derived temperatures and provide valuable insights for long-term climate monitoring, urban heat assessment, and sustainable city planning.

1.1 Motivation & Background

Land Surface Temperature (LST) is one of the most important variables for understanding how our environment is changing, especially when it comes to urban heat islands (UHI), heat-related health risks, and long-term city planning. Satellites equipped with thermal infrared (TIR) sensors allow us to monitor surface temperatures over large areas, providing the big picture of how heat is distributed across urban and rural landscapes. However, these satellite observations are not perfect, they differ in spatial resolution, overpass times, and calibration accuracy, which can lead to inconsistencies. That is why validation with ground-based measurements is critical. Ground sensors, such as weather stations or surface radiometers, offer highly precise, direct measurements of temperature at specific points. The drawback is that they cover only limited areas and often cannot represent the spatial variability of complex urban environments. By harmonizing and validating satellite observations with ground-based data, researchers can combine the strengths of both approaches: the broad coverage of satellites and the accuracy of local sensors. This synergy ensures more reliable LST data, which is vital for applications ranging from climate monitoring to urban heat risk management and sustainable urban design. (Qihao Weng, 2009), (Zhao-Liang Li 2015).

1.2 Study Objectives

The main goal of this study is to evaluate how well satellite-derived Land Surface Temperature (LST) agrees with ground-based observations and to reduce the gaps that often appear between the two. Specifically, focus on comparing LST from Landsat 8 TIRS and ECOSTRESS sensors with in-situ measurements from ground stations. Since each sensor collects data under different spatial resolutions and overpass times, a harmonization workflow is applied to align them both spatially and temporally. This step is essential to minimize mismatches and ensure that when we compare values, we are truly looking at the same surface and conditions.

To assess accuracy, we calculate a set of statistical residuals including Root Mean Square Error (RMSE), Mean Absolute Error (MAE), bias, and correlation coefficients which provide a quantitative measure of agreement between satellite and ground data.

2 - State of the Art

Understanding land surface temperature (LST) and its role in climate and urban area studies has been an active part of research for several years or decades. With the increasing availability of satellite data and the growing need to monitor environmental change, a large body of scientific work has explored how thermal infrared remote sensing, ground-based observations, and harmonization techniques can be combined to produce reliable temperature datasets. In the following sections I will summarize the main scientific relevant to LST retrieval, thermal sensors, urban heat island studies, harmonization approaches, and validation practices.

Remote Sensing of Land Surface Temperature and Urban Heat Islands:

Land Surface Temperature (LST) has become one of the most informative variables for examining how urban areas respond to climate change, land use dynamics, and the expansion of built-up surfaces. Over the past decade, satellite-based thermal data have been widely used to map surface temperature patterns and to quantify the Urban Heat Island (UHI) effect. Much of this work relies on linking LST with vegetation indicators such as NDVI and built-up indices like NDBI, which together help explain the spatial distribution of heat within a city.

A substantial body of research consistently shows that vegetation plays a clear cooling role in urban environments. Areas with higher NDVI values generally exhibit lower surface temperatures, confirming the influence of evapotranspiration and shading in reducing heat accumulation. In contrast, built-up areas—captured through indices such as NDBI—tend to record higher LST values. This is attributed to the thermal properties of impervious materials, reduced moisture, and the density of artificial surfaces, all of which contribute to the intensification of local UHI effects.

Studies comparing different years often report that, regardless of changes in absolute temperature values due to atmospheric conditions, the spatial pattern of heat remains strongly tied to land cover. Vegetated zones consistently appear cooler, while densely constructed areas form temperature hotspots. When NDVI and NDBI are analysed together with LST, the negative correlation between vegetation and heat, and the positive correlation between built-up surfaces and heat, become evident and stable across time.

Research carried out in regions with strong seasonality further emphasizes how land cover modulates LST. Seasonal analyses commonly show very large differences between summer and winter temperatures, especially in areas exposed to extreme climates. Summer LST values can reach exceptionally high levels, whereas winter temperatures drop sharply. However, even in such conditions, the cooling influence of vegetation and water bodies remains visible, while bare soil and urban structures continue to amplify heat. These results demonstrate that remote sensing is highly effective at capturing both seasonal and spatial variability in thermal behaviour.

Taken together, the literature highlights a consistent set of patterns across different climatic and geographical contexts: vegetation reliably reduces surface temperature, built-up areas increase it, and seasonal cycles further reinforce the contrast between land cover types. These findings form the foundation for contemporary approaches to UHI assessment and long-term LST monitoring, showing the value of combining thermal satellite data with indices that describe the state of vegetation and the extent of urbanisation.

Importance of Sensor Calibration for Reliable Thermal Observations:

Accurate LST retrieval does not depend only on algorithm choice or land cover information, it also requires well-calibrated satellite sensors. Any bias in radiance / reflectance at the sensor level will propagate into temperature estimates and can distort the interpretation of UHI intensity, climate trends or comparisons with ground measurements. For this reason, a substantial part of recent research has focused on radiometric calibration and validation of thermal sensors such as those on Landsat.

The vicarious calibration work carried out for Landsat 9 Operational Land Imager (OLI) is a good example of this effort. Here I give an research example that Using a combination of ground-based measurements and dedicated test sites in Nevada, California and South Dakota. researchers evaluated how well the sensor's top-of-atmosphere spectral radiance and reflectance agreed with independent reference data. So, two complementary approaches were employed:

- the traditional reflectance-based method.
- automated measurements at the Radiometric Calibration Test Site (RadCaTS) in Railroad Valley.

The calibration framework is technically complex, but the idea is straightforward. Ground-viewing radiometers and portable spectroradiometers are used to measure surface bidirectional reflectance factor (BRF) at well-characterised sites, while Cimel sun photometers and other instruments record atmospheric conditions such as aerosol optical depth, water vapour and ozone. These measurements are then combined in a radiative transfer model (e.g. MODTRAN) to simulate the expected top-of-atmosphere radiance and reflectance. The simulated values are finally compared with what Landsat 9 actually records for the same place and time.

The results related to the example here, show that Landsat 9 OLI meets its design specifications, with radiance differences within $\pm 5\%$ and reflectance differences within $\pm 3\%$ across the bands. Multiple campaigns at RadCaTS, Ivanpah Playa and vegetated sites near Brookings (South Dakota) confirm this level of agreement and reveal no significant temporal drift in the calibration over the first years of the mission. In practice, this means that the reflectance and radiance values used as input for LST retrieval are stable and reliable, which is a prerequisite for any long-term climate analysis or for combining thermal data from different periods and sensors.

- Instruments and software used in this measurement:

- a) Camel Sun Photometer: The Camel sun photometer provides atmospheric data like aerosol optical depth (AOD), water vapor, and Angstrom exponent from AERONET.
- b) VRs (Ground-based Visible Radiometers): These devices measure reflected radiance from the surface at the RadCaTS.
- c) Portable Spectroradiometer: Used for collecting ground-based measurements of reflected radiance over a reference panel and the test site surface.
- d) LED (light emitting diode): LED is used as a light detector in a custom-built ground-viewing radiometer for RadCaTS.
- e) Automated Solar Radiometer (ASR): The ASR is used to measure solar irradiance extinction due to atmospheric absorption and scattering.
- f) CaTSSITTR (Calibration Test Site SI-Traceable Transfer Radiometer: The CaTSSITTR is a multispectral instrument developed to measure surface BRF with high accuracy in the field.
- g) RadCaTS (Radiometric Calibration Test Site): It is not a single instrument, is an automated test site that was used in this research for calibration purposes, as a more advanced approach than the traditional reflectance-based method.
- h) Radiative Transfer Code: This is a software-based tool, not an instrument, used to process the surface BRF data and atmospheric measurements to calculate TOA spectral radiance and reflectance.

For studies it is essential in the background. Knowing that sensors such as Landsat 8 and 9 are radiometrically well-behaved gives confidence that observed trends in LST and UHI are linked to real environmental changes rather than to sensor artefacts. It also underpins any attempt to harmonize satellite thermal data with ground observations: if the satellite measurements are poorly calibrated, no amount of statistical adjustment can fully compensate for that.

From Satellite Analyses to Harmonization with Ground Observations:

The three examples strands of literature described above-UHI analysis in Kayseri, seasonal LST variation in Babylon, and radiometric calibration of Landsat 9-have a common feature: they rely heavily on satellite data to derive spatially explicit thermal information. In the first two cases, ground data may be used for context, but the main focus is on mapping patterns and correlations from space. In the calibration study, ground measurements are used systematically, but mainly as a reference to tune the sensor rather than to describe local microclimates.

However, many urban and regional applications require both perspectives at the same time. Satellites provide the broad, spatially continuous view needed to understand how heat is distributed across a city and its surroundings, while ground sensors capture fine-scale conditions at specific locations, including variations that may occur between different materials, street canyons or local climate zones. For long-term climate monitoring and for detailed urban heat assessments, these two sources of information need to be brought together.

The literature so far shows that satellite-derived LST is sensitive to land cover, vegetation and season, and that well-calibrated sensors can achieve good radiometric accuracy. What is still less common, and where this thesis is positioned, is the explicit harmonization of

satellite thermal data with dense ground observations in a specific urban context. In the case of Ancona and the surrounding municipalities, this means taking advantage of reliable thermal products from sensors such as Landsat 8 and ECOSTRESS, while at the same time using ground-based loggers and stations to correct, validate and better interpret the satellite-based temperatures.

Relationship Between Air Temperature (Ta) and Land Surface Temperature (LST):

Land Surface Temperature (LST) and air temperature (Ta) are two fundamental indicators used to study the urban thermal environment, yet they represent different physical layers of the atmosphere surface system. LST measures the temperature of the Earth's surface as captured by satellite sensors, while Ta reflects the temperature of the air near the surface, which more directly affects human comfort and health.

Satellite derived LST data are widely used due to their consistent spatial coverage, they do not always accurately represent near-surface air temperature, especially in heterogeneous urban areas. The difference between LST and Ta depends strongly on urban form, land cover, and seasonal conditions. In general, LST tends to show greater spatial and seasonal variability than Ta. The gap between LST and Ta is typically wider in built-up areas than in natural or vegetated zones, particularly during warm seasons. This occurs because impervious materials like concrete and asphalt absorb and store more heat, increasing surface temperature, while vegetated areas promote cooling through shading and evapotranspiration.

Seasonal patterns play an important role as well. During summer and spring, LST values rise significantly due to higher solar radiation and longer daylight hours, often exceeding Ta by more than **10-30 °C** in some regions. In contrast, during winter, both LST and Ta become more stable, and their difference narrows. Additionally, distance from the sea can influence these dynamics: coastal areas usually experience smaller LST-Ta differences because of the moderating effect of sea breezes. (Marzia Naserika. 2023)

When analysed across different Local Climate Zones (LCZs), the relationship between LST and Ta is stronger in less dense and vegetated zones, while in compact built-up areas with high building density, the correlation weakens or can even become negative. This suggests that urban morphology—including factors like building height, sky view factor, and surface materials, significantly shapes local thermal behaviour.

Overall, while LST provides valuable information about surface heating patterns, it cannot be used as a direct proxy for air temperature, particularly in dense urban settings or during warm periods. A combined analysis of both LST and Ta offers a more realistic understanding of urban heat dynamics and supports better design and planning for thermal comfort and climate resilience. (Marzia Naserika. 2023).

Applications of Land Surface Temperature (LST):

Land Surface Temperature (LST) is widely used across multiple fields today. Below are some of its most common and valuable applications.

Agriculture:

1- Crop Stress Monitoring:

LST is an important input for energy balance-based evaporation models. These models help detect early signs of crop stress, allowing farmers to take timely action before major yield losses occur.

2- Phenological Development:

LST data can be used to calculate Growing Degree Days (GDD), a measure that helps track crop maturity. Unlike traditional air temperature measurements, LST-based GDD offers a more precise understanding of actual crop and pest growth conditions by directly assessing surface heat accumulation. This helps farmers better predict crop development stages and plan management strategies.

3- Seeding Depth Recommendations:

High-resolution LST maps help identify variations within a field. This information can be used to adjust seeding depth according to local soil and environmental conditions, improving crop emergence and ensuring a more uniform plant stand.

4- Yield Forecasting:

When combined with factors like soil water content and vegetation optical depth, LST becomes a key component in predicting crop yields. Changes or anomalies in land surface temperature can significantly impact productivity throughout different growth stages, making it an essential variable in regional yield models.

Weather and Climate Monitoring:

LST represents the "skin temperature" of the Earth's surface as measured by emitted radiation. It plays a crucial role in understanding heat exchange processes on land and helps monitor climate change, crop conditions, and land cover changes (Voogt & Oke, 2003; Xiao et al., 2008; Franzpc, 2019).

• Long-Term Climate Tracking:

By observing LST data over years or decades, scientists can identify both normal and abnormal temperature patterns for specific regions. This provides a solid foundation for understanding local and global climate trends.

- Heatwave and Drought Monitoring:

LST helps track extreme heat and dry conditions. Since temperature and soil moisture are closely linked, these measurements provide insight into drought severity and its effects on agriculture, ecosystems, and human populations.

- Urban Heat Island Analysis:

Cities tend to be warmer than surrounding rural areas a phenomenon known as the urban heat island effect. LST data can help pinpoint the hottest zones in urban environments, supporting governments and city planners in designing effective cooling and mitigation strategies.

Environmental Impact Assessment:

- Evaluating Restoration Efforts:

LST can be used to measure how land restoration or management projects affect local climates. By comparing pre- and post-restoration temperature data, researchers can assess the environmental outcomes of these interventions.

3 Methods and Materials

3.1 Study Area

This study focuses on three municipalities in central Italy Ancona, Agugliano, and Camerata Picena, as it is showed bellow, located along the Adriatic coast in the Marche Region. Together, these municipalities are home to an estimated population of about 107,000 people in 2025. The area is characterized by a transitional Mediterranean climate, which brings mild, wet winters and warm, dry summers, making it an important setting for studying heat dynamics and their impacts on urban life. The urban fabric is highly heterogeneous. Ancona, as the regional capital, combines a historic city centre with densely built residential districts, green parks, and extensive port and industrial areas. Agugliano and Camerata Picena, on the other hand, are smaller towns that contribute more suburban and rural land uses, providing a contrast in surface types and settlement patterns.

Observations for this study were carried out between 19 June, 23 June, 26 June, and again on 05 July 2025, under both clear-sky and cloudy-sky conditions. These dates were chosen to capture the thermal behaviour of the area during the early summer season, when surface heating is particularly relevant for urban heat island studies and climate monitoring.

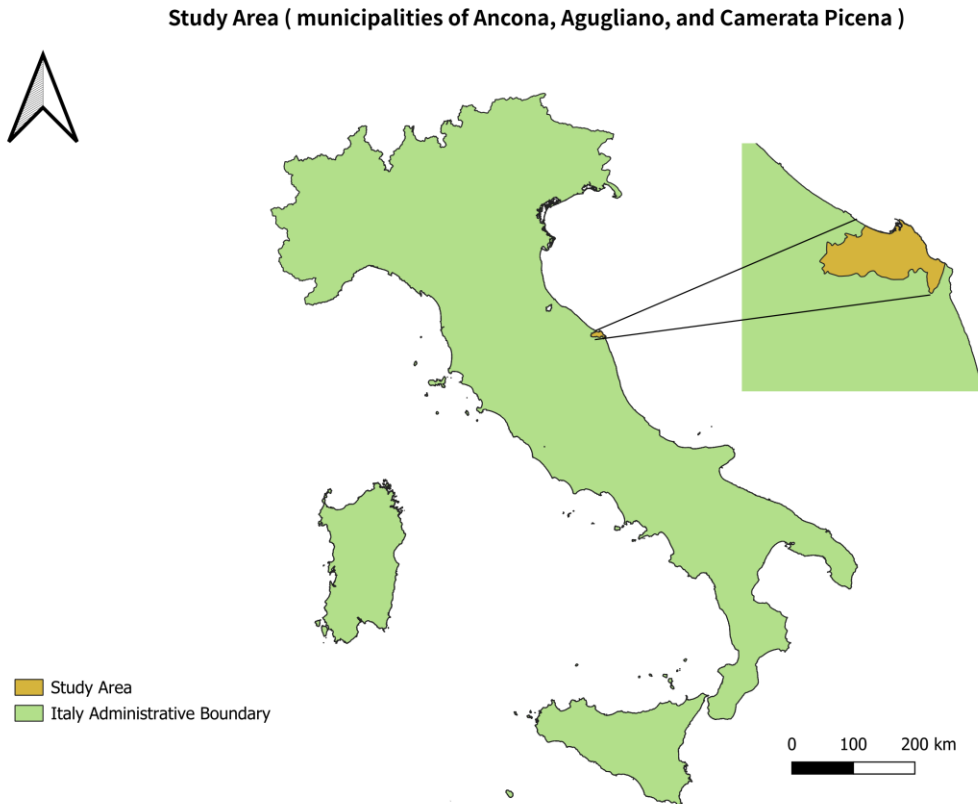


Figure 1. study area

3.2 Input data

3.2.1 Landsat Data (Landsat 8)

Landsat 8 launched on February 11, 2013, from Vandenberg Air Force Base, California, with the extended payload fairing (EPF) from United Launch Alliance, LLC ([2013](#)). The Landsat 8 satellite carries two main instruments, the Operational Land Imager (OLI) and the Thermal Infrared Sensor (TIRS), which work together to capture detailed images of Earth's surface. These sensors provide regular, seasonal coverage of land areas worldwide, with spatial resolutions of 30 meters for visible, near infrared, and shortwave infrared bands, 100 meters for thermal data, and 15 meters for the panchromatic band.

Landsat 8 was jointly developed by NASA and the U.S. Geological Survey (USGS). NASA was responsible for designing, building, launching, and calibrating the satellite, which was initially known as the Landsat Data Continuity Mission (LDCM). After its successful launch and initial testing, USGS assumed operational control on May 30, 2013, officially designating it as Landsat 8. Since then, USGS has managed satellite operations, data calibration, and the distribution and archiving of imagery through the Earth Resources Observation and Science (EROS) Centre ([Landsat-8](#))

The United States Geological Survey (USGS) provides Top-of-Atmosphere (TOA) brightness temperature data for the thermal infrared (TIR) bands of the Landsat satellites. These

datasets, available in Google Earth Engine (GEE) for Landsat 4-9 Collection 1, which are pre-processed and ready for analysis. The TOA values are generated by the USGS from raw, orthorectified digital number data using the appropriate radiometric calibration coefficients (Sofia L. Ermida 2021).

The first dataset for this studying comes from **Landsat 8's Thermal Infrared Sensor (TIRS)**, which provides thermal imagery at a spatial resolution of 100 meters. For this research, I used Level-2 surface temperature products that include NDVI-based emissivity correction, ensuring more accurate estimates of how different land cover types emit thermal radiation.

Landsat 8 Operational Land Imager (OLI) and Thermal Infrared Sensor (TIRS) Band Specifications:

Band	Description	Wavelength (μm)	Spatial Resolution
Band 1	Coastal / Aerosol	0.435 – 0.451	30 m
Band 2	Blue	0.452 – 0.512	30 m
Band 3	Green	0.533 – 0.590	30 m
Band 4	Red	0.636 – 0.673	30 m
Band 5	Near Infrared (NIR)	0.851 – 0.879	30 m
Band 6	Shortwave Infrared 1 (SWIR-1)	1.566 – 1.651	30 m
Band 7	Shortwave Infrared 2 (SWIR-2)	2.107 – 2.294	30 m
Band 8	Panchromatic (Pan)	0.503 – 0.676	15 m
Band 9	Cirrus	1.363 – 1.384	30 m
Band 10	Thermal Infrared 1 (TIR-1)	10.60 – 11.19	100 m
Band 11	Thermal Infrared 2 (TIR-2)	11.50 – 12.51	100 m

Table 1. Landsat 8 OLI and TIRS band specifications

To compare Landsat-8 derived temperatures with ground-based observations, spatial and temporal matching procedures were applied. Spatial matching was performed using the reprojection based on the geographic coordinates of the sites. For temporal alignment, two ground LST measurements closest to the Landsat overpass time were **linearly interpolated** to create a corresponding match.

Finally, images in three dates 19 and 26 of June and July 5 were retained according to the Landsat product. In total, 3 Landsat LST images were collected between June 19, 2025, and July 5, 2025. After applying all spatial– harmonization and temporal harmonization were applied for both.

Landsat 5-9 Satellite Missions: Key Characteristics and Applications:

Characteristics	Landsat 5	Landsat 7	Landsat 8	Landsat 9
General Information	Developed by NASA and launched from Vandenberg Air Force Base in California. And the longest operating earth observation satellite. Circled the Earth every 99 minutes, fourteen orbits a day	The same as Landsat 5 Developed by NASA and launched from Vandenberg Air Force Base in California.	The same as Landsat 5,7 Developed by NASA. The satellite carries the Operational Land Imager (OLI) and the Thermal Infrared Sensor (TIRS) instruments. The TIRS measures land surface temperature in two thermal bands with a new technology	This Landsat is a partnership between the U.S. Geological Survey (USGS) and the National Aeronautics and Space Administration (NASA).
Launch year	March 1,1984	April 15, 1999	2013	September theh2021
Status	Decommissioned in June (2013), but it delivered Earth imaging for 29 years.	Active (with scan line corrector failure)	Active	Active
Sensor(s)	Thematic Mapper (TM), and Multispectral Scanner (MSS)	Enhanced Thematic Mapper Plus (ETM+), it is improved from previous instrument design.	Tow sensors: Operational Land Imager (OLI), Thermal Infrared Sensor (TIRS)	OLI-2, TIRS-2
Number of Bands	7 Thematic mapper (TM), and 4 multispectral scanners (MSS)	8 bands, spectral bands, including one thermal and one panoramic.	11 bands, including two thermal bands with 100m resolution.	11 bands
Spatial Resolution	30m (Multispectral), 120m (Thermal), 79m (MSS)	30m for Multispectral, 15m for Panchromatic, and 60m Thermal	30m (Multispectral), 15m (Panchromatic), 100m (Thermal)	30m (Multispectral), 15m (Panchromatic), 100m (Thermal)
Temporal Resolution	After every 16 days	After every 16 days	16 days as well	16 days as well
Swath Width	185 km in a single pass	185 km in a ...	185 km....	185 km
Main Applications	Land cover change, vegetation monitoring, water resources	Agriculture, forestry, urban planning, environmental monitoring	Climate studies, water quality, natural disaster assessment	Continuation of Landsat 8 applications with improved reliability, provide a unique resource for those who work in agriculture, geology, forestry, regional planning, education, mapping, and global change research.
Orbital altitude	705 km form the earth surface in a sun synchronous Landsat-5	Previous with 705 km altitude, but now it on 697 km Landsat-7	705 km Landsat-8	705 km ... Landsat-9

Table 2. overview of Landsat 5-9

3.2.2 ECOSTRESS Level 2 Product

The ECOSTRESS Level 2 Land Surface Temperature and Emissivity (LST&E) product was downloaded from the [NASA Earth data Search Portal](#). This dataset is generated using a physics-based Temperature Emissivity Separation (TES) algorithm, which simultaneously retrieves both land surface temperature (LST) and surface emissivity (LSE) from ECOSTRESS Level 1 data. The LST&E product includes 15 scientific data layers (SDSs), such as LST, its associated error, emissivity and emissivity error for five spectral bands, broadband emissivity, precipitable water vapor, and quality control (QC) indicators for both temperature and emissivity.

To compare satellite-derived temperatures with ground-based observations, spatial and temporal matching procedures were applied. Spatial matching was performed using the nearest neighbor sampling method, based on the geographic coordinates of the validation sites. For temporal alignment, two ground LST measurements closest to the [ECOSTRESS overpass time were linearly interpolated](#) to create a corresponding match. I incorporated data from NASA's ECOSTRESS (ECOsystem Spaceborne Thermal Radiometer Experiment on Space Station), which captures thermal information at a finer resolution of about 70 meters. ECOSTRESS Level-2 products rely on emissivity values derived from the ASTER spectral library, allowing detailed retrieval of land surface temperature patterns. For this study, ECOSTRESS observations were available for 19 June, and June 23.

Finally, only two images in two dates 19 and 23 of June were retained according to the ECOSTRESS product. In total, 2 ECOSTRESS LST images were collected between June 19, 2025, and June 23, 2025. After applying all spatial–harmonization and temporal harmonization were applied for both.

Source	Date 1	Date 2	Date 3	Date 4
Landsat 8	19 June 2025		26 June 2025	5 July 2025
ECOSTRESS	19 June 2025	23 June 2025		
Ground Sensors	19 June 2025	23 June 2025	26 June 2025	5 July 2025

Table 3 Satellite Overpass Dates and ground sensor measurements dates



Figure 2. Landsat and ECOSTRESS. Source: google images

Emissivity in Landsat 8 (C2 L2) and ECOSTRESS Products:

Both Landsat 8 and ECOSTRESS provide Level 2 Land Surface Temperature (LST) products, where emissivity corrections have already been applied [U.S. Geological Survey \(USGS\)](#) and [ECOSTRESS \(Ecosystem Spaceborne Thermal Radiometer Experiment on Space Station\) \(NASA mission\)](#). This is important because emissivity essentially, how efficiently a surface emits thermal radiation varies by land cover type, and without correcting for it, satellite-derived temperature estimates can be misleading. Landsat 8 uses an **NDVI-based approach** to estimate emissivity, linking vegetation cover to surface thermal properties, while ECOSTRESS relies on emissivity values from the ASTER spectral library, which provides a well-established reference for different materials. Since both products already incorporate emissivity corrections, researchers can directly compare their LST outputs without having to reprocess emissivity themselves, saving both time and effort.

In contrast, Landsat 8 Level 1 products only provide the Top of Atmosphere (TOA) radiance/reflectance and raw thermal bands (Band 10 and Band 11). At this stage, neither atmospheric correction nor emissivity correction is applied. If researchers want to retrieve LST from Level 1 data, they need to go through a multi-step process to remove the influence of atmospheric gases and aerosols (Huanya Xhang, 2025).

3.3 Software /Platform Used

3.3.1 Google Earth Engine (GEE)

Google Earth Engine (GEE) is a powerful cloud-based platform developed by Google for planetary-scale geospatial analysis. It provides access to a vast public archive of satellite imagery and geospatial datasets, including data from Landsat, Sentinel, MODIS, and many other sensors. One of GEE's main advantages is that it allows users to process and analyse large volumes of remote sensing data directly online, without the need for local data storage or high-performance computing resources. Users can write scripts in JavaScript or Python through the GEE Code Editor or API to visualize, process, and export geospatial products efficiently. This capability has made GEE one of the most widely used platforms in environmental monitoring, land cover mapping, urban heat analysis, and climate research (Sofia L. Ermida 2023).

Land Surface Temperature (LST) represents the temperature of the Earth's surface as measured by thermal infrared (TIR) sensors onboard satellites. It plays a crucial role in understanding surface energy balance, evapotranspiration, vegetation stress, and urban heat island effects. LST is derived by converting the thermal radiance recorded by satellite sensors into temperature values, accounting for factors such as surface emissivity and atmospheric effects. Among the available sensors, the Landsat series (particularly Landsat 8 and Landsat 9) are often used to estimate LST because they provide thermal data at relatively high spatial resolution (around 100 meters) suitable for local and regional studies (Sofia L. Ermida, 2023).

I combined, GEE and LST retrieval methods offer an efficient and scalable approach for temperature mapping. GEE provides direct access to Landsat thermal bands, surface reflectance products, and atmospheric correction data, enabling automated and consistent LST

estimation over large spatial and temporal scales. This integration allows researchers to monitor land surface thermal behaviour, detect spatial temperature variations, and assess environmental changes in a reproducible way, all within a cloud-based computational environment.

3.3.2 Quantum GIS (QGIS)

QGIS (formerly Quantum GIS) is a leading open-source Geographic Information System (GIS) that allows users to visualize, analyse, and manage spatial data. Since its creation in 2002 by **Gary Sherman**, it has grown from a simple map viewer into a powerful, full-featured platform used by researchers, planners, and organizations worldwide.

What makes QGIS remarkable is its community-driven development model it is built and maintained by a global network of developers, researchers, and volunteers who contribute new features, plug-ins, and documentation. Unlike proprietary software, QGIS promotes digital sovereignty by giving users complete freedom to use, modify, and share the software without licensing restrictions (Anita Graser 2025).

- Key Features and Capabilities:

QGIS integrates vector, raster, mesh, and point cloud data, supporting formats like Post GIS, Geo TIFF, and cloud-optimized data types. It includes tools for:

- 1- Cartography and map composition - creating high-quality, publication-ready maps with customizable symbology and labelling.
- 2- Data analysis – using the Processing Toolbox and plug-ins for spatial statistics, geoprocessing, and modelling workflows.
- 3- Automation and customization – through its well-documented Python API, users can build custom plug-ins and automate workflows.
- 4- Web mapping - QGIS Server and QGIS Web Client allow for publishing maps and spatial data online using OGC standards such as WMS and WFS.

The platform's open nature has led to an ecosystem of third party extensions, including Q Field, Margin Maps, and Liz Map, which extend its capabilities to mobile data collection and web publishing (Anita Grasis 2025).

- QGIS Applications of QGIS in Real-World Studies:

QGIS's flexibility allows it to be applied across diverse domains from urban planning and environmental monitoring to public health and transportation (Prof. S.V. Sabale 2021).

Some key applications include:

- 1- Mapping Road Accidents: QGIS was used to identify accident “hotspots” using heat maps and Kernel Density Estimation (KDE). These visualizations help local authorities plan safety measures, allocate emergency resources, and reduce accident frequency.
- 2- Tracking COVID-19 Cases: During the pandemic, QGIS helped map infection hotspots, allowing policymakers to visualize and manage outbreak zones through spatial analysis.
- 3- Optimizing ATM Locations - By overlaying population density, road networks, and existing ATM locations, QGIS helped determine ideal sites for new ATMs, improving accessibility and customer convenience.

Through these examples, it's clear that QGIS serves not just as a data analysis tool but as a decision-support system that transforms complex spatial data into actionable insights.

- Governance and Sustainability:

The QGIS project is managed by the QGIS.ORG Association, a non-profit organization based in Switzerland. It oversees governance, finances, and community coordination. The project is funded through sustaining memberships, donations, and crowdfunding campaigns. Annual financial reports are publicly available, reflecting the transparency that defines the open-source ethos QGIS Releases are scheduled every four months, with Long-Term Releases (LTR) providing stable versions for institutional use. This ensures a balance between innovation and reliability (Prof.S.V. Sabale. 2021).

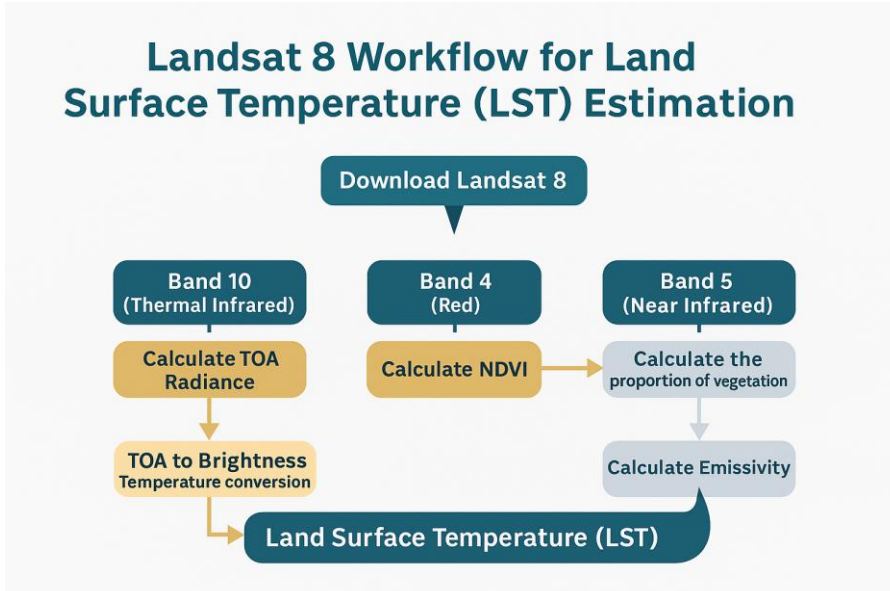
- Why QGIS Matters

QGIS stands out not just for its functionality but for what it represents, the democratization of spatial technology. It empowers researchers, governments, and individuals worldwide to analyse their environment without the financial or technical barriers of commercial GIS platforms. QGIS embodies (spatial without compromise) a tool that combines scientific rigor, openness, and inclusivity to make geographic knowledge truly accessible.

3.4 Calculation of LST in QGIS

3.4.1 Image Analysis

The image processing workflow was carried out using QGIS. In this study, the Thermal Infrared Band (Band 10) from Landsat 8 was utilized to derive brightness temperature, while Bands 4 (Red) and 5 (Near Infrared) were employed to calculate the Normalized Difference Vegetation Index (NDVI). The Land Surface Temperature (LST) estimation followed the methodology provided by the U.S. Geological Survey (USGS, 2024b) for computing Top of Atmosphere (TOA) spectral radiance. The overall procedure for LST retrieval is illustrated in Figure 3.



3.5 Calculation of TOA (Top of Atmosphere) Reflectance

The Top of Atmosphere (TOA) Reflectance represents the proportion of solar radiation that is reflected by the Earth's surface and atmosphere relative to the incoming solar radiation. It is a dimensionless parameter that can be derived from satellite-based measurements of spectral radiance, taking into account the mean solar spectral irradiance and the solar zenith angle.

For Landsat Level-1 data, TOA spectral radiance should calculate using the radiance rescaling factors provided in the image's metadata (MTL file). These parameters are described in the technical documentation that accompanies the Landsat 8 data available from the U.S. Geological Survey (USGS) Earth Explorer platform.

The TOA spectral radiance ($L\lambda$) can be computed using the following equation:

$$L\lambda = ML * Qcal + AL$$

- $L\lambda$ = TOA spectral radiance (Watts / (m²·sr·μm))
- ML = Band-specific multiplicative rescaling factor (from metadata)
- AL = Band-specific additive rescaling factor (from metadata)
- $Qcal$ = Quantized and calibrated standard product pixel values (Digital Numbers, DN)

In QGIS, this formula can be applied using the Raster Calculator tool. The equation used in this study for Band 10 is:

$$TOA = 0.0003342 \times "Band10" + 0.1$$

3.6 Conversion of TOA to Brightness Temperature

Thermal band data from Landsat 8 can be converted from Top of Atmosphere (TOA) spectral radiance to brightness temperature by applying the thermal conversion constants provided in the metadata (MTL) file. This process translates the measured radiance into the equivalent blackbody temperature of the surface. The conversion is performed using the following equation:

$$B_T = \frac{K_2}{\ln(\frac{K_1}{K_2}) + 1} - 273.15$$

BT = Top of Atmosphere brightness temperature (Kelvin)

$L\lambda$ = TOA spectral radiance

K_1 = Band-specific thermal conversion constant (from metadata)

K_2 = Band-specific thermal conversion constant (from metadata)

In QGIS, this equation can be implemented using the Raster Calculator tool.

3.7 CALCULATE THE NDVI

The normalized difference vegetation index (NDVI), which is derived from remote-sensing (satellite) data, is closely linked to drought conditions. To determine the density of green on a patch of land, the distinct colours (wavelengths) of visible and near-infrared sunlight reflected

by the plants are observed; red and near-infrared bands i.e. Band 4 and Band 5 respectively must be used for calculating the Normal NDVI. The importance of estimating the NDVI is essential since the amount of vegetation present is an important factor and NDVI can be used to infer general vegetation condition. The calculation of the NDVI is important because, afterward, the proportion of the vegetation (Pv) should be calculated, and they are highly related with the NDVI, and emissivity (ϵ) should be calculated, which is related to the Pv.

$$NDVI = \frac{NIR(Band\ 5) - Red(Band\ 4)}{NIR(Band\ 5) + Red(Band\ 4)}$$

3.8 Calculation of the Proportion of Vegetation

The proportion of vegetation (also known as the Vegetation Fraction) represents the percentage of ground area covered by vegetation when viewed vertically. Variations in vegetation cover significantly influence surface energy balance and hydrological processes by affecting transpiration, surface albedo, emissivity, and surface roughness.

In this study, the vegetation proportion (Pv) was derived based on the Normalized Difference Vegetation Index (NDVI) values for vegetation and soil. The proportion of vegetation calculate using the following equation:

$$P_v = \left(\frac{NDVI - NDVI_{min}}{NDVI_{max} - NDVI_{min}} \right)^2$$

NDVI max = Maximum NDVI value, representing dense vegetation.

NDVI min = Minimum NDVI value, representing bare soil.

3.9 Calculate the land surface emissivity

Land Surface Emissivity (ϵ) represents the efficiency with which the Earth's surface emits thermal radiation and is a key parameter for accurate Land Surface Temperature (LST) estimation. The emissivity depends on the surface type, vegetation cover, and wavelength (Qihao Weng. 2004).

The emissivity can be calculated using the proportion of vegetation (Pv) as follows:

$$\epsilon_\lambda = \epsilon_v P_v + (1 - p_v) + C_\lambda$$

ϵ_λ – Effective emissivity of the pixel at wavelength λ

ϵ_v – Emissivity of vegetation (typically around 0.985–0.990)

ϵ_s – Emissivity of bare soil (typically around 0.960–0.970)

Pv – Proportion of vegetation within the pixel (derived from NDVI)

C_λ – Surface roughness correction term, generally a small constant (≈ 0.005)

3.10 Calculate the Land Surface Temperature

The emissivity corrected land surface temperatures (S_t) were calculated as follows (Jose Sobrino 2023) (Sholihah, 2019):

$$S_t = \frac{B_t}{1 + \left[\left(\frac{\lambda * B_T}{\rho} \right) * \ln_{\varepsilon\lambda} \right]}$$

Ts: Land Surface Temperature

TB: Brightness Temperature

λ : Wavelength of emitted radiance (meters), $\sim 10-12 \mu\text{m}$ for thermal infrared bands.

ε : Surface emissivity (dimensionless), Ratio of emitted energy to blackbody emission at the same temperature (ranges 0.95–0.99).

ρ : A constant derived from Planck's law, $\rho = \sigma h / c = 1.438 \times 10^{-2} \text{ m}$.

h : Planck's constant = $6.626 \times 10^{-34} \text{ J}\cdot\text{s}$

c : Speed of light = $2.998 \times 10^8 \text{ m/s}$

σ : Boltzmann constant = $1.38 \times 10^{-23} \text{ J/K}$

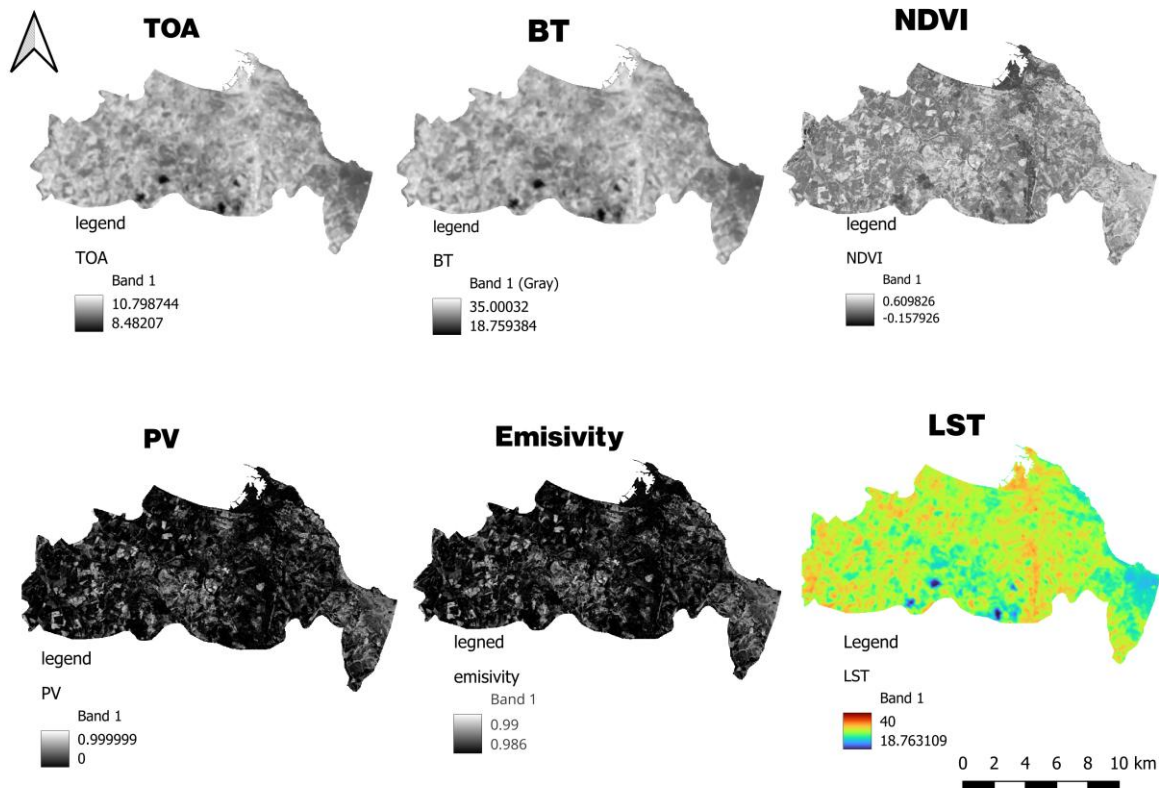


Figure 3. illustrates the sequential outputs generated during the Land Surface Temperature (LST) retrieval process using Landsat 8 imagery. The top row presents the intermediate products, including the Top of Atmosphere (TOA) radiance, Brightness Temperature (BT), and Normalized Difference Vegetation Index (NDVI). The bottom row displays the derived Proportion of Vegetation (PV), Land Surface Emissivity (ε), and the final LST map.

3.11 Workflow for Classification and Land Surface Temperature Trends Over Ancona

3.11.1 Land Cover Classification Overview

Land cover classification is a technique used in remote sensing to identify and map different types of surface cover on the Earth such as forests, grasslands, water bodies, agricultural lands, and built-up areas. It's essential for understanding environmental changes, resource management, and land-use planning.

In remote sensing, classification usually involves analysing satellite imagery and assigning each pixel to a specific land cover type based on its spectral characteristics (reflectance in various bands such as red, green, NIR, SWIR, etc.). Recent advances in cloud-based platforms like Google Earth Engine (GEE) have made large-scale land cover mapping more efficient. GEE allows researchers to access vast satellite archives (like Landsat and Sentinel data), process them in the cloud, and apply machine learning algorithms for classification without needing high-end local computing power. A critical step before classification is image composition, which involves combining multiple images to minimize cloud and snow interference and create clearer composites (Thanh Noy Phan 2020).

3.11.2 Random Forest (RF) Classifier

The Random Forest (RF) algorithm is one of the most widely used machine learning techniques for land cover classification. It belongs to the family of ensemble learning methods, meaning it builds multiple decision trees and combines their results to improve prediction accuracy and reduce overfitting (Thanh Noy Phan 2020).

- RF operates by:
 - 1- Randomly selecting subsets of the training data and input features to build each decision tree.
 - 2- Aggregating (through majority voting) the results from all trees to decide the final class of each pixel.
- The advantages of RF include:
 - 1- High accuracy and robustness: It performs well even with noisy or incomplete data and handles large, complex datasets effectively.
 - 2- Variable importance ranking: RF can estimate which features (spectral bands or indices) contribute most to classification accuracy.
 - 3- Good generalization: It minimizes overfitting by averaging results from multiple trees.

3.12 Workflow of Random Forest (RF) Classifier in GEE

1- Definition of temporal window and study area.

- The RF classification is done in Google Earth Engine (GEE) using Landsat (surface reflectance and surface temperature) data.
- Definition a temporal window from 1 July 2010 to 31 July 2010.

```
// choose a valid Landsat 7 period
var startDate = '2010-07-01';
var endDate   = '2010-07-31';
```

- Loading Landsat 7 collection to GEE.
- Filtration of the Image collection to the Area of Interest (AOI) using `filterBounds(AOI)`, so only overlapping area is considered.
- Filtered the considered date (start Date, end Date).

```
// Load Landsat 7 collection
var landsat7 = ee.ImageCollection('LANDSAT/LE07/C02/T1_L2')
  .filterDate(startDate, endDate)
```

2- Preprocessing of Landsat 7 data:

- Radio metric scaling: The Level 2 Landsat 7 images are delivered as scaled integers. Here it is converted these to physically meaningful units using the official scale factors.
- Optical surface reflectance bands: Bands SR_B1– SR_B5 and SR_B7 were converted to surface reflectance by:

$$\rho = DN * 0.0000275 - 0.2$$

In GEE applied by this formula:

```
// Apply scaling factors
var optical = img.select('SR_B.*').multiply(0.0000275).add(-0.2);
```

- Surface temperature band: The thermal band ST_B6 was converted to surface temperature (in Kelvin) by:

$$T = DN * 0.003418020 + 149.0$$

In GEE applied by this formula:

```
var thermal = img.select('ST_B.*').multiply(0.00341802).add(149.0);
```

3- Cloud and Shadow masking

To improve data quality, I masked out clouds and cloud shadows using the QA_PIXEL band, means that QA_PIXEL band used to remove or mask out the cloudy pixels and cloud shadow pixels.

Below in the GEE it is extracted the QA_PIXEL band and used bitwise operations on the cloud and shadow bits:

```
// Cloud/shadow mask
var qa = img.select('QA_PIXEL');
var cloudShadow = 1 << 3;
var clouds      = 1 << 5;
var mask = qa.bitwiseAnd(cloudShadow).eq(0)
            .and(qa.bitwiseAnd(clouds).eq(0));
return img.updateMask(mask);
};
```

What these formula means: Every Landsat image comes with a special band called QA_PIXEL. This band tells you which pixels in the image are: clouds, cloud shadows, snow or water. These conditions are stored using bits. So here in the code Bit 3 = cloud shadow, and Bit 5 is the cloud.

So it is kept only the pixels where:

bit 3 = 0 → not cloud shadow

bit 5 = 0 → not cloud

4- Compositing and band selection:

After applying the scaling and cloud/shadow mask to each image via this code: .map(scale And Mask)), all images within July 2010 were combined using the median composite (.median()). This reduces noise from residual clouds and temporal variability. The composite was then clipped to the AOI (.clip(AOI)). So at it is retained only the optical bands required for classification: which are [SR_B1 (blue), SR_B2 (green), SR_B3 (red), SR_B4 (near-infrared), SR_B5 (short-wave infrared 1), SR_B7 (short-wave infrared 2)].

```
.filterBounds(AOI)
.map(scaleAndMask)
.median()
.clip(AOI)
.select(['SR_B1', 'SR_B2', 'SR_B3', 'SR_B4', 'SR_B5', 'SR_B7']); // optical bands
```

5- Calculation of spectral indices (NDVI and NDBI)

To enhance separability between land-cover classes, it is derived two spectral indices from the composite:

- Normalized Difference Vegetation Index (NDVI): Computed from NIR (SR_B4) and red (SR_B3) bands.

$$NDVI = \frac{NIR - Red}{NIR + Red}$$

- Normalized Difference Built-up Index (NDBI): Computed from SWIR (SR_B5) and NIR (SR_B4) bands.

$$NDBI = \frac{SWIR - NIR}{SWIR + NIR}$$

In GEE used this formula to calculate NDVI and NDBI:

```
// Add NDVI and NDBI
var NDVI = landsat7.normalizedDifference(['SR_B4','SR_B3']).rename('NDVI');
var NDBI = landsat7.normalizedDifference(['SR_B5','SR_B4']).rename('NDBI');
var newdata = landsat7.addBands([NDVI, NDBI]);
```

6- Preparation of training data:

- Land-cover classes and reference polygons: defined five land-cover classes, each represented by a Feature Collection in GEE: **Water, Vegetation, Soil, Urban (buildings), Roads**. Each sample feature contained a property LC storing the class ID (1–5). The individual Feature Collections (water, vegetation, soil, buildings, road) were merged into a single training Feature Collection (training FC) using .merge().
- Water training data collection: for the water covered area considered 16 points samples data which is showed bellow.

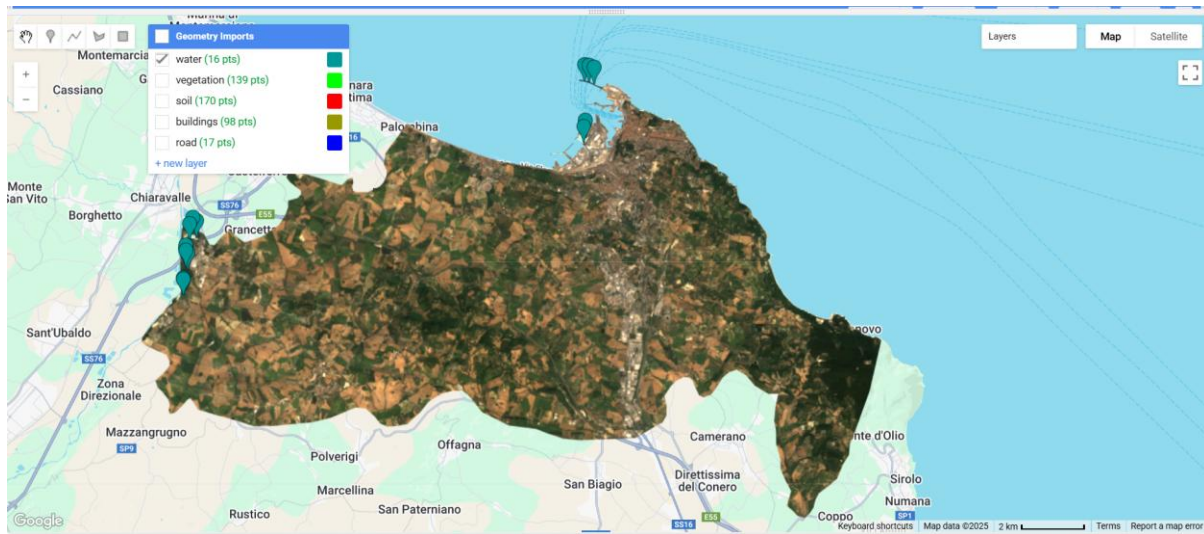


Figure 4 this figure shows the training data collected form the area covered by water

- Vegetation data collection: As shown in the figure below, a total of 139 sample points were collected for the vegetation class.

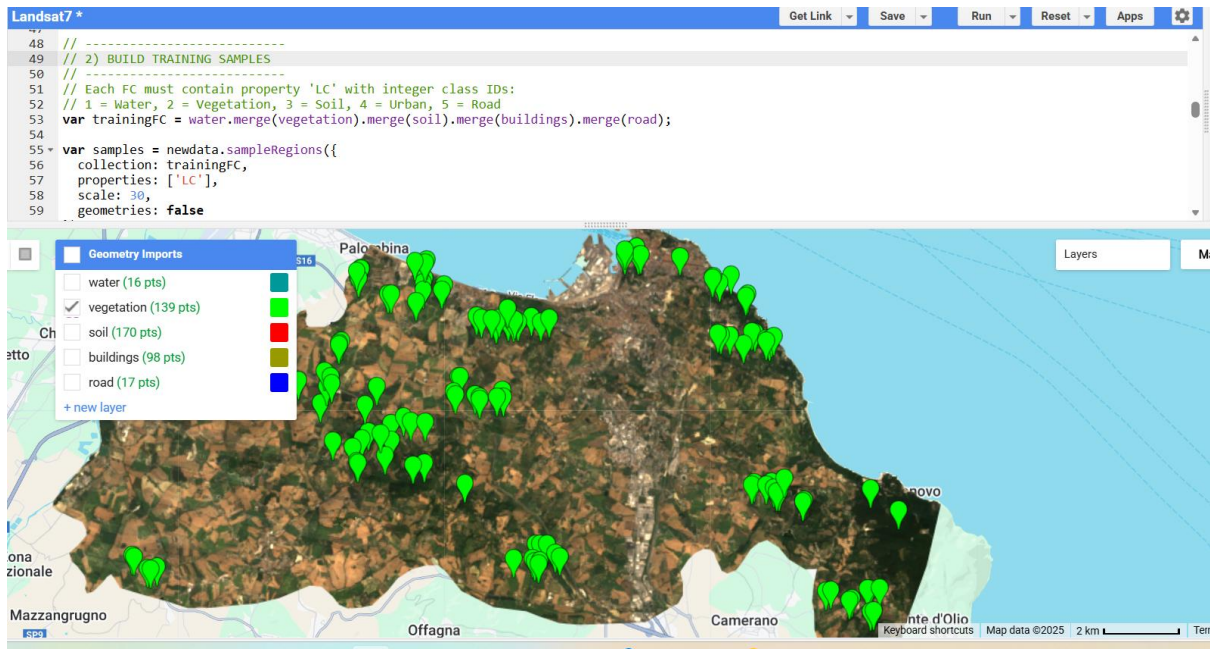


Figure 5. this figure shows the data collected for vegetation across Ancona

- Soil data collection: As shown in the figure below, the soil class covers a relatively wide area; therefore, 170 sample points were collected for this category.

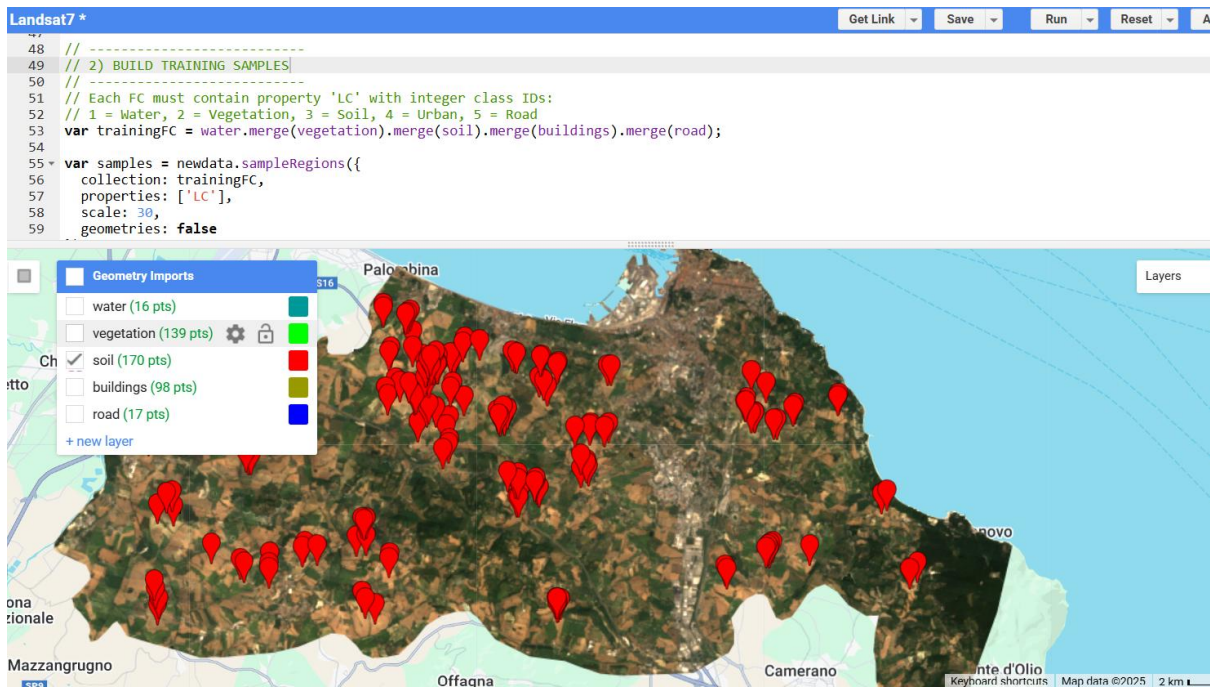


Figure 6. this figure shows the data collected for covered area by soil across Ancona

- Data Collection of Build-up Area: For the built-up area, a total of 98 sample points were collected that is showed in figure bellow.

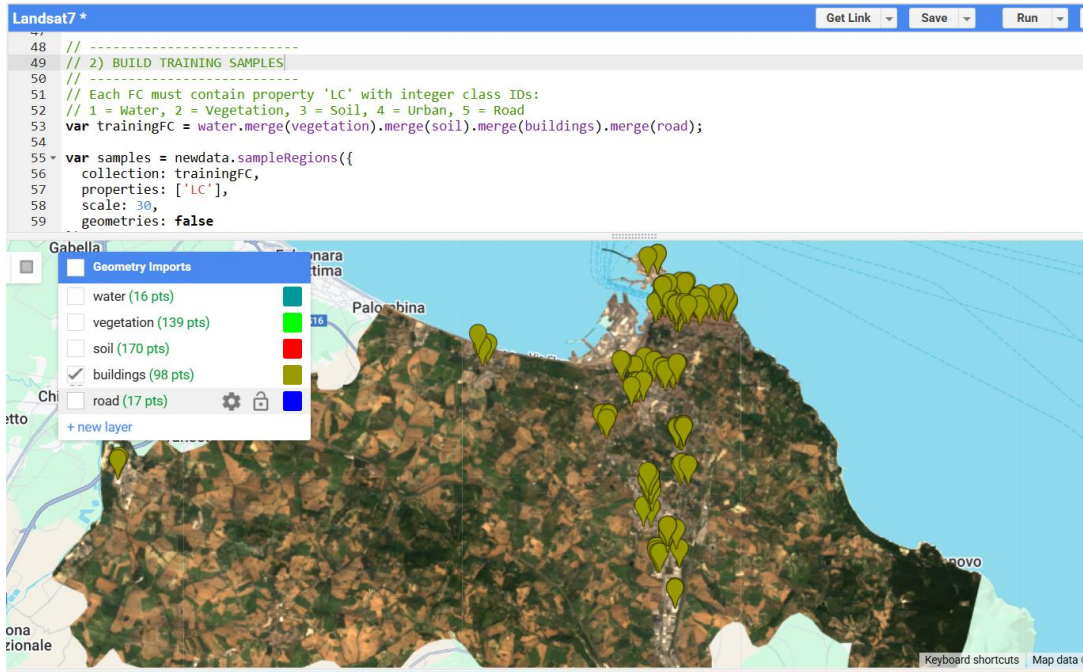


Figure 7. this figure shows the data collected for build up area across Ancona

- Data Collection of Road Network: Because of the relatively low spatial resolution of Landsat 7, only 17 sample points could be collected for this area that is showed in the figure bellow. However, these points were ultimately merged with the built-up class in QGIS for further calculations, and this had no meaningful impact on the final classification results.

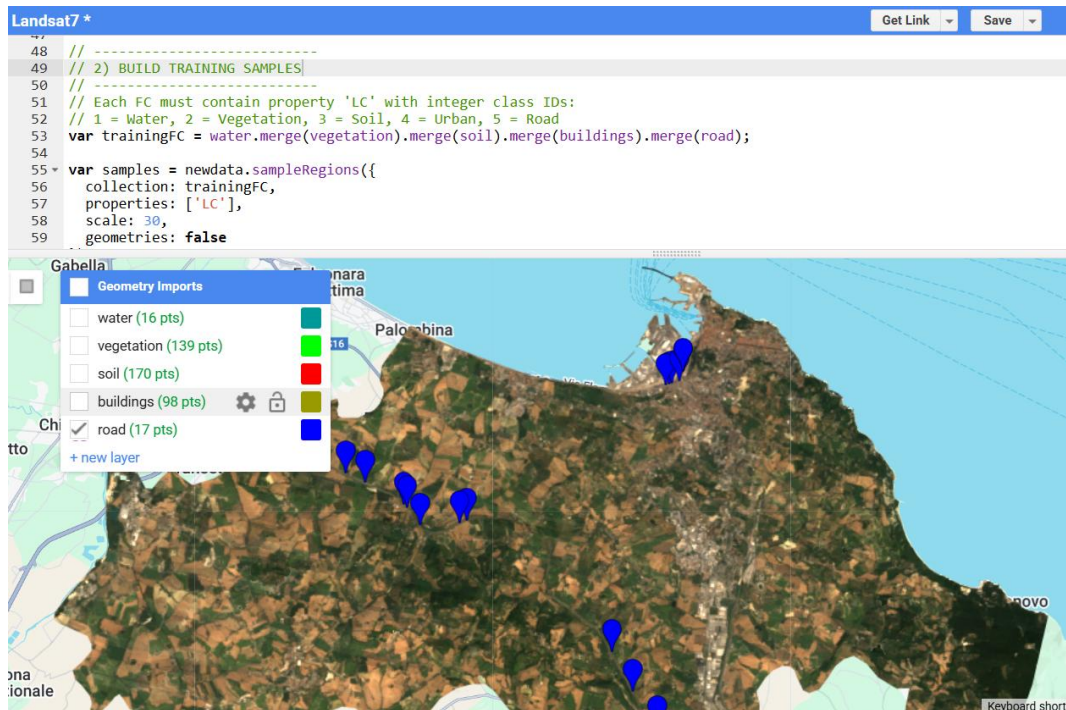


Figure 8. this figure shows the data collected for road network

At the end, all the data collected for training and testing are shown in the figure below, which displays the total number of sample points.

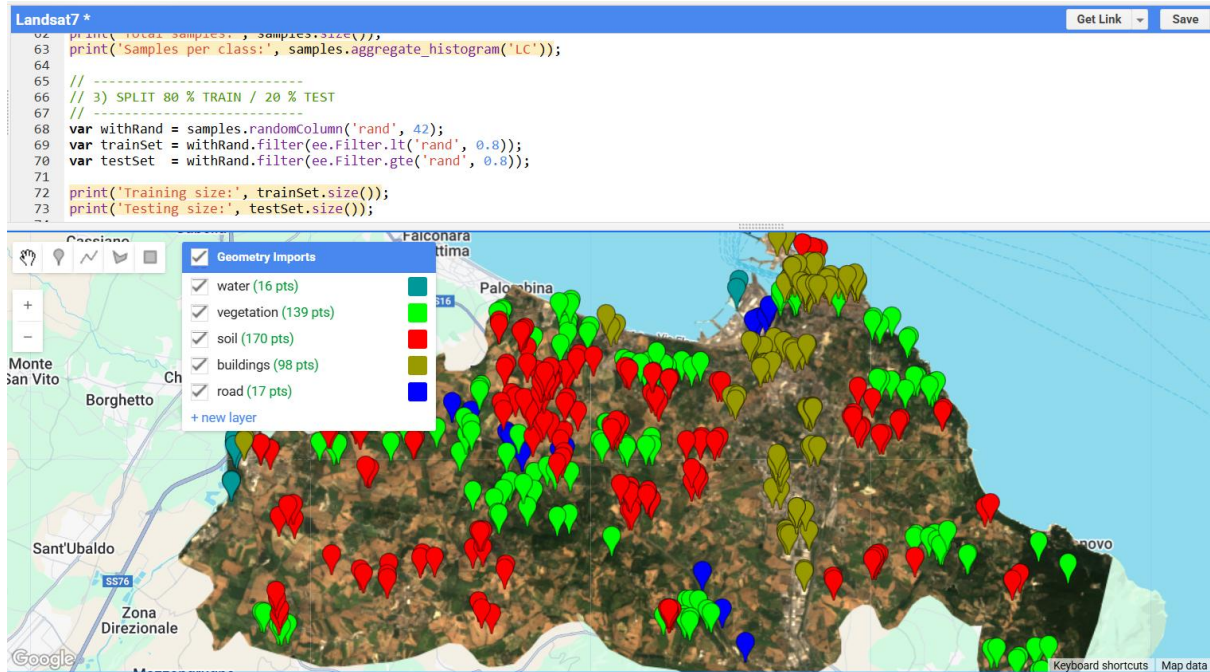


Figure 9. this figure shows all the data collected for the random forest classification

7- Extraction of pixel values (sample Regions):

Training samples were generated by extracting spectral and index values from new data at the locations of the reference polygons: I used sample Regions () with:

- collection: training FC.
- properties: ['LC'] to carry the class label.
- scale: 30 m, corresponding to the native Landsat resolution.

This produced a table (samples) where each row corresponds to one sampled pixel and contains:

- Predictor variables: all bands from new data.
- Response variable: LC (land-cover class).

And then checked:

- Total number of samples.
- Number of samples per class (using aggregate histogram ('LC')).

In GEE used this formula for these calculations that explained above.

```

var samples = newdata.sampleRegions({
  collection: trainingFC,
  properties: ['LC'],
  scale: 30,
  geometries: false
});

print('Total samples:', samples.size());
print('Samples per class:', samples.aggregate_histogram('LC'));

```

8- Training and Test Data split (80/20)

To evaluate the classifier on independent data, I split the sample dataset into training and test subsets: A random value between 0 and 1 was added to each sample using random Column ('rand', 42), with a fixed seed (42) to ensure reproducibility.

- Training set (80%): samples with rand < 0.8
- Test set (20%): samples with rand ≥ 0.8

```

// 3) SPLIT 80 % TRAIN / 20 % TEST
// -----
var withRand = samples.randomColumn('rand', 42);
var trainSet = withRand.filter(ee.Filter.lt('rand', 0.8));
var testSet = withRand.filter(ee.Filter.gte('rand', 0.8));

print('Training size:', trainSet.size());
print('Testing size:', testSet.size());

```

It is created two groups from sample data:

- Training data → used to teach the Random Forest model 80%
- Testing data → used to check how good the model is 20%

9- Random Forest classification model

I trained a Random Forest classifier using the GEE smile Random Forest implementation:

- Number of trees: 200
- Random seed: 42 (for reproducibility)

Training parameters:

- features: train Set - table of training samples
- class Property: 'LC' - target variable (land-cover class)
- input Properties: new data.band Names - all spectral bands + indices in new data used as predictors.

The result was a trained Random Forest classifier (rf), which learned the relationship between the multi-band predictors (spectral reflectance and indices) and the land-cover classes.

```
//  
var rf = ee.Classifier.smileRandomForest({  
    numberOfTrees: 200,  
    seed: 42  
}).train({  
    features: trainSet,  
    classProperty: 'LC',  
    inputProperties: newdata.bandNames()  
});
```

10- training accuracy:

First, I evaluated the classifier on the training set:

I computed the training confusion matrix directly from the classifier using rf.confusionMatrix(). From this matrix, I derived:

- Overall accuracy (proportion of correctly classified samples)
- Cohen's kappa coefficient (agreement corrected for chance)

These metrics describe how well the model fits the data it was trained on (training accuracy). In GEE it used these formulas.

```
// (a) training accuracy  
var trainCM = rf.confusionMatrix();  
print('Training Confusion Matrix', trainCM);  
print('Training Accuracy:', trainCM.accuracy());  
print('Training Kappa:', trainCM.kappa());
```

11- test accuracy:

To obtain an unbiased estimate of performance, I evaluated the classifier on the test set:

- It is classified the test samples using testSet.classify(rf), obtaining predicted labels in the classification field.
- It is built a confusion matrix with errorMatrix('LC', 'classification'), comparing the true class (LC) with the predicted class (classification).
- From this confusion matrix (testCM), I computed:
 - Overall accuracy
 - Kappa coefficient
 - Producer's accuracy (by class) - probability that a reference pixel is correctly classified.
 - User's accuracy (by class) - probability that a pixel classified into a given class is that class.

```
// (b) test accuracy  
var testPred = testSet.classify(rf);  
var testCM = testPred.errorMatrix('LC', 'classification');  
print('Test Confusion Matrix', testCM);  
print('Test Accuracy:', testCM.accuracy());  
print('Test Kappa:', testCM.kappa());  
print('Producer's Accuracy:', testCM.producersAccuracy());  
print('User's Accuracy:', testCM.consumersAccuracy());
```

12-Class distribution within the Area Of Interest (AOI)

To quantify the spatial distribution of land-cover classes, I computed the frequency of each class over the AOI. The result is a histogram of class IDs and their pixel counts, which can be converted to areas by multiplying by the pixel area (30 m × 30 m).

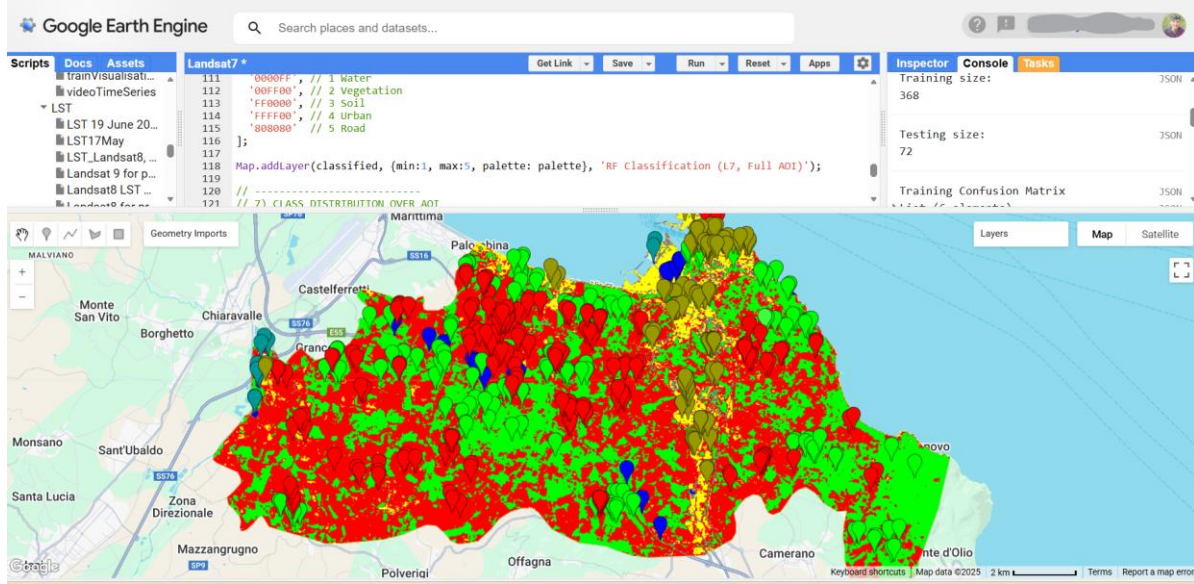


Figure 10. this figure shows the RF classification along with training data for different classes

13-Final Result of Classification

The final result of the classification is shown below and is ready for export and further analysis in QGIS. After completing the Random Forest classification in Google Earth Engine, the output was exported as a TIFF file and imported into QGIS. In QGIS, the area covered by each land-cover class was calculated, and the results were then arranged and visualized in map format, as presented in the following sections.

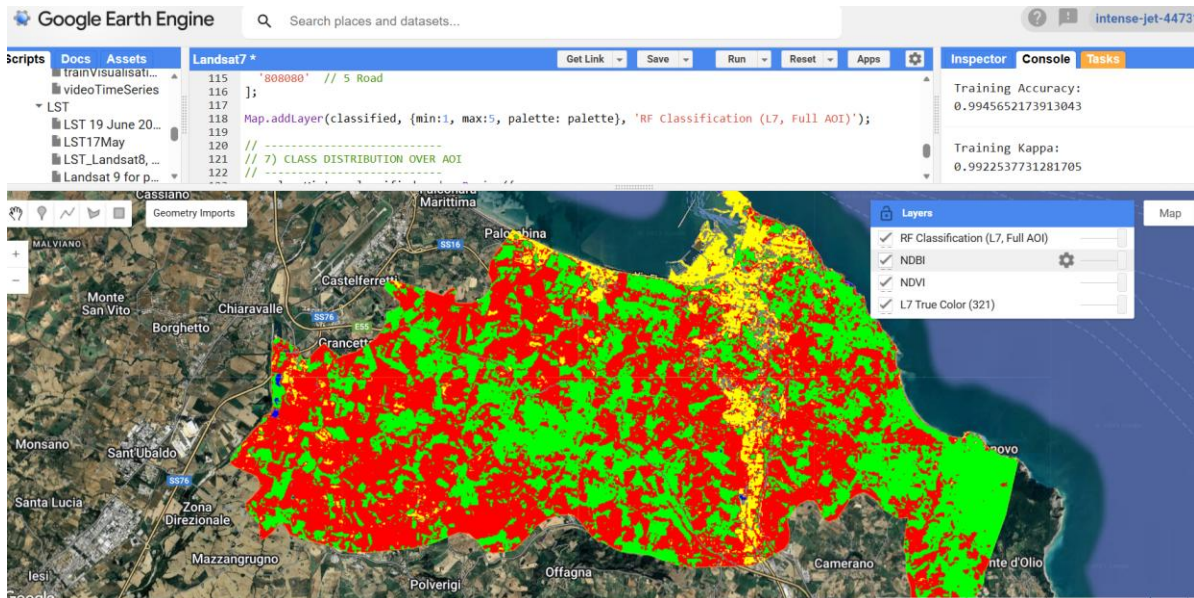
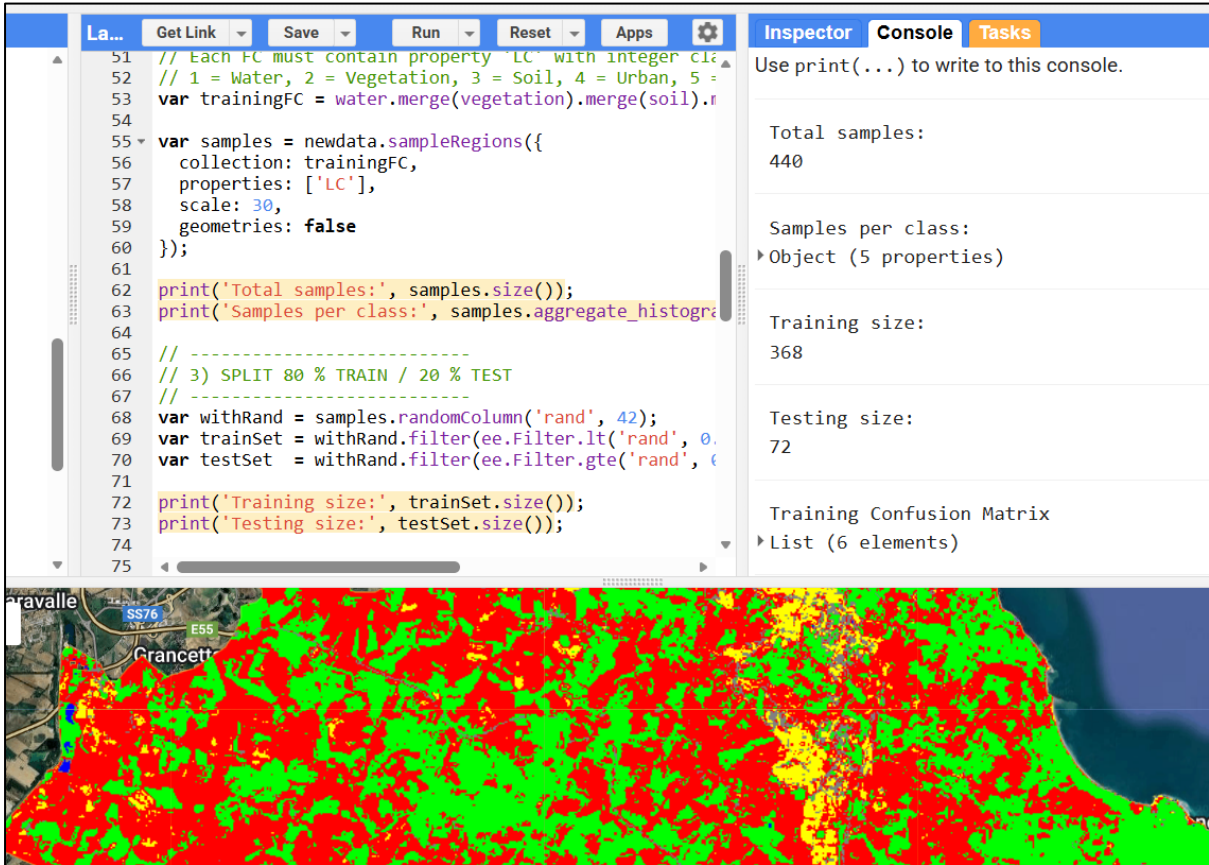


Figure 11. result of RF classification

14- Total Samples, Training Size Testing Size and Training Confusion Matrix:

In total, 440 samples were collected for the classification process that is showed in the figure bellow. These samples were distributed across the five land-cover classes used in the study. Following the standard 80/20 approach, the dataset was randomly divided into 368 samples for training and 72 samples for independent testing. The training set was used to build the Random Forest classifier, while the test set was reserved for evaluating the model's performance. A confusion matrix was then generated for the training data to assess how well the classifier learned the patterns of each class.



The figure shows a screenshot of the Earth Engine code editor interface. On the left, there is a code editor window containing JavaScript code for sample selection and data splitting. On the right, there is a panel with tabs for 'Inspector', 'Console', and 'Tasks'. The 'Console' tab is active, displaying output related to the sample selection process. Below the code editor is a map visualization showing land cover classification results. The map displays various land cover types in different colors (red, green, yellow, blue) over a geographic area. Labels like 'Grancetti' and 'SS76' are visible on the map.

```
La... Get Link Save Run Reset Apps
51 // Each FC must contain property 'LC' with integer class values
52 // 1 = Water, 2 = Vegetation, 3 = Soil, 4 = Urban, 5 = Residential
53 var trainingFC = water.merge(vegetation).merge(soil).filter(ee.Filter.notNull('LC'))
54
55 var samples = newdata.sampleRegions({
56   collection: trainingFC,
57   properties: ['LC'],
58   scale: 30,
59   geometries: false
60 });
61
62 print('Total samples:', samples.size());
63 print('Samples per class:', samples.aggregate_histogram('LC'));
64
65 // -----
66 // 3) SPLIT 80 % TRAIN / 20 % TEST
67 // -----
68 var withRand = samples.randomColumn('rand', 42);
69 var trainSet = withRand.filter(ee.Filter.lt('rand', 0.8));
70 var testSet = withRand.filter(ee.Filter.gte('rand', 0.8));
71
72 print('Training size:', trainSet.size());
73 print('Testing size:', testSet.size());
74
75
```

Inspector Console Tasks

Use `print(...)` to write to this console.

Total samples:
440

Samples per class:
Object (5 properties)

Training size:
368

Testing size:
72

Training Confusion Matrix
List (6 elements)

Figure 12. this figure shows the total number of samples, training size and testing size

15- Training Accuracy, Kappa, Test confusion Matrix, Test accuracy and Test Kappa Coefficient

The performance of the Random Forest RF classifier was evaluated using both the training dataset and the test dataset. The model achieved a high training accuracy of 0.9946, with a corresponding kappa coefficient of approximately 0.99234. These values indicate excellent agreement between the predicted and actual classes during training, so this suggesting that the model successfully learned the distinguishing characteristics of each land-cover type.

For the test dataset, the classifier also demonstrated a strong performance, achieving an accuracy of 0.97222 and a kappa value 0.9593 that is showed in the figure bellow. Since the test data were not used during model training, these results confirm that the classifier generalizes well and maintains high reliability when applied to unseen data. The high kappa values further show that the classification accuracy is not due to random chance, reflecting a robust and consistent model.

The screenshot shows the Earth Engine code editor interface. On the left, the code is written in JavaScript:

```
1 // Each FC must contain property 'LC' with integer class values
2 // 1 = Water, 2 = Vegetation, 3 = Soil, 4 = Urban, 5 = Residential
3 var trainingFC = water.merge(vegetation).merge(soil).filter(
4   ee.Filter.eq('LC', 1)
5 );
6 var samples = newdata.sampleRegions({
7   collection: trainingFC,
8   properties: ['LC'],
9   scale: 30,
10  geometries: false
11 });
12 print('Total samples:', samples.size());
13 print('Samples per class:', samples.aggregate_histogram('LC'));
14
15 // -----
16 // 3) SPLIT 80 % TRAIN / 20 % TEST
17 // -----
18 var withRand = samples.randomColumn('rand', 42);
19 var trainSet = withRand.filter(ee.Filter.lt('rand', 0.8));
20 var testSet = withRand.filter(ee.Filter.gte('rand', 0.8));
21
22 print('Training size:', trainSet.size());
23 print('Testing size:', testSet.size());
```

On the right, the 'Console' tab displays the following output:

```
Training Accuracy:  
0.9946562173913043  
  
Training Kappa:  
0.9922537731281705  
  
Test Confusion Matrix  
List (6 elements)  
  
Test Accuracy:  
0.9722222222222222  
  
Test Kappa:  
0.9593105397004805
```

Below the code editor is a map visualization showing land cover classification. The map area is predominantly red (Vegetation), with some green (Soil) and yellow (Urban) patches. Labels like 'Grancett', 'SS76', 'E55', and 'OVO' are visible. A 'Layers' button is in the top right corner of the map.

Figure 13. Final result of Training accuracy, Training Kappa, test accuracy, test kappa

- The accuracy of classification

Assessing the accuracy of a land cover classification is a crucial step in remote sensing analysis, as it determines how reliable the results are for subsequent interpretation or modeling.

The Overall Accuracy (OA) represents the proportion of correctly classified pixels compared to the total number of pixels evaluated. It provides a straightforward measure of performance essentially showing how often the classification agrees with reference data or ground truth. The formula for overall accuracy is expressed as:

$$Accuracy = \frac{\text{total correct prediction}}{\text{total prediction}} * 100$$

While overall accuracy gives a general sense of classification performance, it does not account for agreements that might occur purely by chance. To address this, we use the Kappa Coefficient (κ), a more robust statistical measure that evaluates how well the classification results align with reference data beyond random agreement. Kappa values range from 0 to 1, where:

- 1- $\kappa = 0$ indicates no agreement beyond chance,
- 2- $\kappa = 1$ represents perfect agreement, and
- 3- Values closer to 1 signify good or very good agreement between the classified and reference datasets.

By combining both Overall Accuracy and the Kappa Coefficient, we obtain a more complete understanding of how reliable the classification results are. Additionally, these metrics help identify strengths and weaknesses in the classification process, guiding improvements in data selection, algorithm performance, and feature optimization for future analyses.

3.13 Harmonizing Satellite Thermal Data with Ground-based Observations workflow

3.13.1 Ground-based Observations workflow

To complement the satellite data, I deployed 50 iButton DS1921GH-F50 temperature loggers across the city of Ancona. These sensors were installed in direct contact with different surface types and programmed to record temperatures at intervals of 10 to 30 minutes. With an accuracy of ± 1.0 °C and a resolution of 0.5 °C, the iButtons provide reliable, fine-scale measurements of surface temperature that serve as a critical reference for validating satellite-derived land surface temperature (LST).

The sensors were placed in locations representing three categories of the Local Climate Zone (LCZ) classification system, which is widely used in urban climate studies. The three LCZ types selected were:

- 1- Vegetated zones: areas dominated by trees, grass, or parks, where shading and evapotranspiration strongly influence thermal behaviour.
- 2- Impervious zones: areas dominated by built and sealed surfaces such as asphalt, concrete, rooftops, and pavements, which tend to store and radiate heat more intensely.
- 3- Mixed and soil zones: transitional areas that combine both vegetation and impervious materials, reflecting the complex surface composition typical of many urban environments.

This setup allows us to capture how different land cover types shape local temperature patterns and to compare them directly with satellite observations. To validate these satellite-derived temperatures, I deployed **50 ground-based iButton DS1921GH-F50** loggers across different urban and natural surfaces. These loggers are compact temperature sensors with an accuracy of ± 1 °C, a resolution of 0.5 °C, and sampling intervals between 10 and 30 minutes. They were strategically distributed across sites representing vegetated, impervious, and mixed Local Climate Zones (LCZs). This deployment design ensured that ground measurements captured the diversity of surface conditions in the study area, making them highly suitable for harmonization with the satellite data.



Figure 14. iButton DS1921GH-F50 deployment

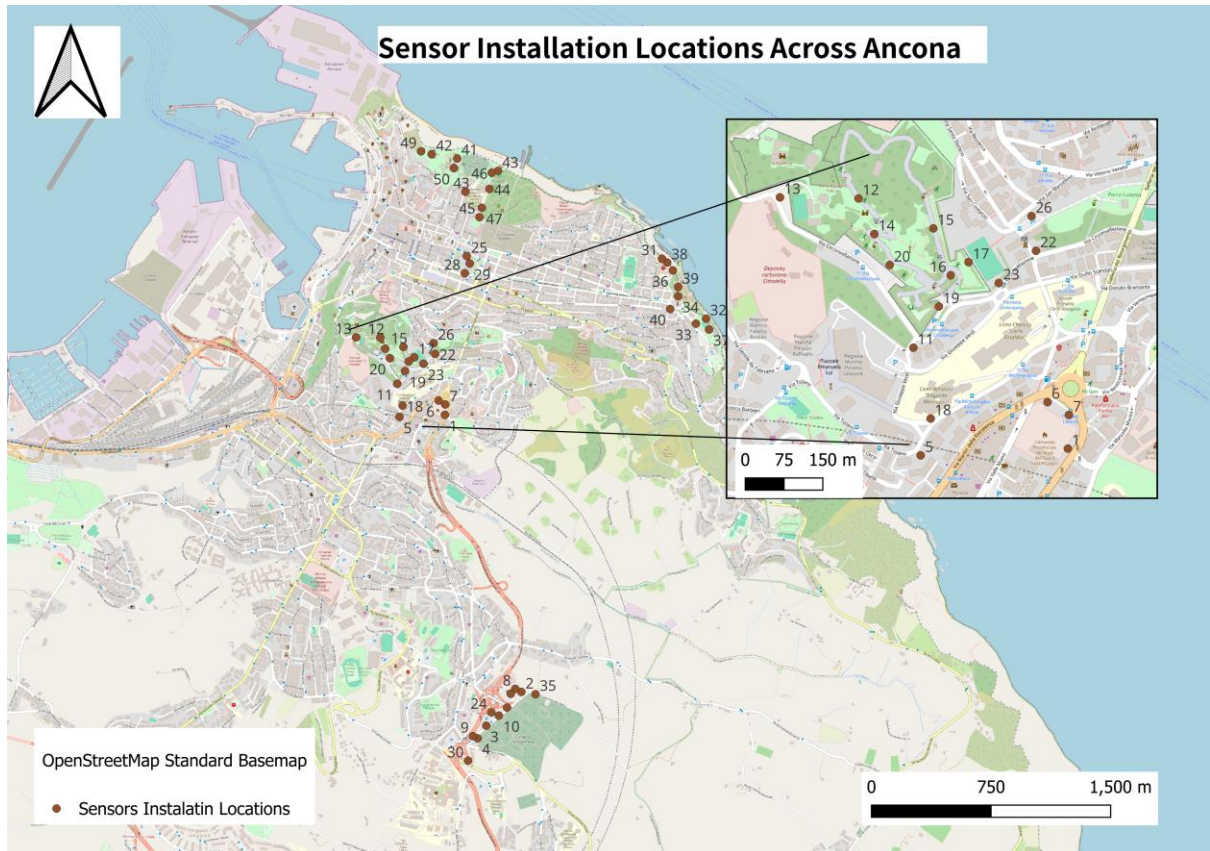


Figure 15. 50 iButton DS1921GH-F50 sensors across Ancona city

Sensors Data On 19 June 2025		
Sensor's Number	Sensor Location Details	Sensor's Value (°C)
1	On soil – exposed to direct sunlight	30
2	On soil, near a concrete surface	28.5
3	on concrete surface- exposed to direct sunlight.	28
4	on concrete, under tree- shaded by vegetation.	23
5	On concrete surface	40
6	On soil, under tree – shaded area	40.5
7	Over soil, under tree – shaded and surface.	26.5
8	Inside vegetation, near a concrete area	32.5
9	On concrete, under tree – shaded surface area.	37
10	On soil, near concrete	24
11	Over concrete- shaded surface by tree	24
12	Over soil- shaded by tree	28
13	Over soil- shaded by tree	26.5
14	Inside vegetation- partially shaded by tree.	23.5
15	Over soil- partially shaded by tree	24
16	Over soil- and shaded by tree	32
17	Inside vegetation- under tree	24
18	Over soil- shaded area	24
19	Inside vegetation- shaded by vegetation.	38
20	Over soil- under tree- completely shaded by tree.	26
21	Inside vegetation—and shaded area.	35
22	Over soil	29
23	Over soil	34.5
24	Over the concrete, completely shaded area.	23.5
25	Lost sensor	Lost sensor
26	Over soil- and near the concrete.	33
27	Over the concrete, completely shaded area by tree.	31
28	Over soil- but partially shaded area.	24
29	On the soil, but exposed to direct sunlight	36.5
30	On the soil- but completely shaded area	28
31	Over soil	40
32	Over soil	40
33	Inside vegetation- but exposed to direct sunlight	36
34	Inside vegetation- but exposed to direct sunlight	28.5
35	Shaded area- inside vegetation.	23.5
36	Over soil	26
37	Inside vegetation- under tree	27
38	Over soil- exposed to direct sunlight.	39
39	Over the soil	29
40	Inside vegetation	26
41	Over the concrete, shaded area	24
42	Inside vegetation	24.5
43	Over the concrete	27
44	Over the soil, shaded area	35

45	Inside vegetation, shaded area	25
46	Inside vegetation- but partially shaded area.	28
47	Vegetation area- partially shaded.	24
48	Completely shaded area.	23
49	Between vegetation	35
50	shaded area inside vegetation	33

Table 4. Recorded sensor LST values in degrees Celsius along with location descriptions on June 19, 2025

Sensors Data On 23 June 2025		
Sensors Number	Sensor location Details	Sensor Value (°C)
1	On soil – exposed to direct sunlight	34
2	On soil, near a concrete surface	30.5
3	On concrete surface- exposed to direct sunlight.	40
4	On concrete, under tree– shaded by vegetation.	25
5	On concrete surface	35
6	On soil, under tree – shaded area	40
7	Over soil, under tree – shaded and surface.	29
8	Inside vegetation, near a concrete area	30
9	On concrete, under tree – shaded surface area.	33
10	On soil, near concrete	26
11	Over concrete- shaded surface by tree	30
12	Over soil- shaded by tree	30
13	Over soil- shaded by tree	29
14	Inside vegetation- partially shaded by tree.	29.5
15	Over soil- partially shaded by tree	29.5
16	Over soil- and shaded by tree	30
17	Inside vegetation- under tree	29.5
18	Over soil- shaded area	30.5
19	Inside vegetation- shaded by vegetation.	31
20	Over soil- under tree- completely shaded by tree.	29.5
21	Inside vegetation—and shaded area.	30
22	Over soil	29.5
23	Over soil	30
24	Over the concrete, completely shaded area.	29.5
25	Lost sensor	Lost sensor
26	Over soil- and near the concrete.	29.5
27	Over the concrete, completely shaded area by tree.	29.5
28	Over soil- but partially shaded area.	30
29	On the soil, but exposed to direct sunlight	35
30	On the soil- but completely shaded area	30
31	Over soil	32
32	Over soil	32
33	Inside vegetation- but exposed to direct sunlight	30
34	Inside vegetation- but exposed to direct sunlight	29
35	Shaded area- inside vegetation.	28.5
36	Over soil	31

37	Inside vegetation- under tree	28
38	Over soil- exposed to direct sunlight.	40
39	Over the soil	30
40	Inside vegetation	30.5
41	Over the concrete, shaded area	25
42	Inside vegetation	26
43	Over the concrete	33
44	Over the soil, shaded area	27.5
45	Inside vegetation, shaded area	27.5
46	Inside vegetation- but partially shaded area.	29
47	Vegetation area- partially shaded.	24
48	Completely shaded area.	26
49	Between vegetation	32
50	Shaded area inside vegetation	28

Table 5. Recorded sensor LST values in degrees Celsius along with location descriptions on June 23, 2025

Sensors Data On 26 June 2025		
Sensor's N	Sensor Location Details	Sensor Value
1	On soil – exposed to direct sunlight	34
2	On soil, near a concrete surface	36.5
3	on concrete surface- exposed to direct sunlight.	35.5
4	on concrete, under tree- shaded by vegetation.	30.5
5	On concrete surface	43.5
6	On soil, under tree – shaded area	32
7	Over soil, under tree – shaded and surface.	33
8	Inside vegetation, near a concrete area	45
9	On concrete, under tree – shaded surface area.	44
10	On soil, near concrete	34
11	Over concrete- shaded surface by tree	28
12	Over soil- shaded by tree	33
13	Over soil- shaded by tree	29.5
14	Inside vegetation- partially shaded by tree.	30.5
15	Over soil- partially shaded by tree	30
16	Over soil- and shaded by tree	35
17	Inside vegetation- under tree	26
18	Over soil- shaded area	30
19	Inside vegetation- shaded by vegetation.	38
20	Over soil- under tree- completely shaded by tree.	30
21	Inside vegetation—and shaded area.	32
22	Over soil	34
23	Over soil	46
24	Over the concrete, completely shaded area.	27.5
25	Lost sensor	Lost sensor
26	Over soil- and near the concrete.	36.5
27	Over the concrete, completely shaded area by tree.	30
28	Over soil- but partially shaded area.	27.5

29	On the soil, but exposed to direct sunlight	42.5
30	On the soil- but completely shaded area	27.5
31	Over soil	46.5
32	Over soil	50.5
33	Inside vegetation- but exposed to direct sunlight	33
34	Inside vegetation- but exposed to direct sunlight	36.5
35	Shaded area- inside vegetation.	25
36	Over soil	32
37	Inside vegetation- under tree	33.5
38	Over soil- exposed to direct sunlight.	54.5
39	Over the soil	32.5
40	Inside vegetation	31
41	Over the concrete, shaded area	28.5
42	Inside vegetation	28.5
43	Over the concrete	30
44	Inside vegetation, shaded area	30
45	Inside vegetation- but partially shaded area.	28.5
46	Vegetation area- partially shaded.	Lost sensor
47	Completely shaded area.	30
48	NULL	27.5
49	Between vegetation	40
50	shaded area inside vegetation	31

Table 6. Recorded sensor LST values in degrees Celsius along with location descriptions on June 26, 2025

Sensors Data On 5 July 2025		
Sensors Number	Sensor Location Details	Sensors Value
1	On soil – exposed to direct sunlight	35
2	On soil, near a concrete surface	36
3	on concrete surface- exposed to direct sunlight.	34.5
4	on concrete, under tree- shaded by vegetation.	29
5	On concrete surface	39.5
6	On soil, under tree – shaded area	38.5
7	Over soil, under tree – shaded and surface.	31
8	On concrete (previously inside vegetation)	49.5
9	On concrete, under tree – shaded surface area.	45
10	On soil, near concrete	29
11	Over concrete- shaded surface by tree	28
12	Over soil- shaded by tree	32.5
13	Over soil- shaded by tree	29.5
14	Inside vegetation- partially shaded by tree.	29
15	Over soil- partially shaded by tree	33
16	Over soil- and shaded by tree	31
17	Inside vegetation- under tree	29
18	Over soil- exposed to direct sunlight (previously shaded area)	47
19	Inside vegetation- shaded by vegetation.	46

20	Over soil- under tree- completely shaded by tree.	31.5
21	Over concrete (previously Inside vegetation)	49
22	Over soil	31
23	Over soil	47
24	Over the asphalt (previously on concrete shaded area)	51
25	Lost sensor	Lost sensor
26	Over soil- and near the concrete.	44
27	Over asphalt (previously shaded area)	48.5
28	Over soil- but partially shaded area.	26.5
29	On the soil, but exposed to direct sunlight	41.5
30	On asphalt (previously on the soil)	53
31	Over soil	58
32	Over soil	47
33	Inside vegetation- but exposed to direct sunlight	34.5
34	Inside vegetation- but exposed to direct sunlight	32
35	On asphalt (previously inside vegetation)	46
36	Over soil	32
37	Inside vegetation- under tree	39.5
38	Over soil- exposed to direct sunlight.	48
39	Over the soil	32
40	Inside vegetation	29.5
41	Over the concrete, shaded area	29
42	Inside vegetation	28.5
43	Over the soil, exposed to direct sunlight (previously shaded area)	49
44	inside vegetation, shaded area	29.5
45	inside vegetation- but partially shaded area.	28.5
46	Vegetation area- partially shaded.	Lost sensor
47	Completely shaded area.	30
48	vegetation	29
49	On soil	40
50	Over soil (previously inside vegetation)	53

Table 7. Recorded sensor LST values in degrees Celsius along with location descriptions on June 19, 2025, and descriptions about the sensors which their location were changed. Sensors which changed their location for 5th of July is selected with different background colour in the tables above.

3.13.2 LST Workflow in Google Earth Engine

To process and analyse Land Surface Temperature (LST) over Ancona, I implemented a custom workflow in **Google Earth Engine (GEE)**. The workflow begins by loading a shapefile of the study area, which ensures that all computations are spatially constrained to the municipal boundaries. We then accessed the **Landsat 8 Collection 2, Level-2** data, specifically the thermal band (**ST_B10**), filtering images by date and cloud cover (<10%) to maintain reliable conditions.

The GEE's code converts raw pixel values from the thermal band into surface temperature in °C by applying the scaling factor and offset provided by USGS. Because these are Level-2 products, emissivity and atmospheric corrections were already applied, allowing us to focus on temperature scaling and spatial processing. The images were then clipped to the Ancona boundary and composited using the median function to minimize noise and cloud contamination.

To assess variability across dates, I calculated both mean and standard deviation (stdDev) of LST values over time. These statistics were extracted for the entire study region, providing summary indicators of Ancona's surface temperature distribution. The script also exported results as Geo TIFF files at 30 m resolution, making them available for further spatial analysis outside GEE in QGIS ([Google Earth Engine Platform](#))

For visualization, I used a colour palette ranging from 20 °C to 60 °C, with cooler areas displayed in blue and warmer hotspots shown in red and dark red. A legend and title panel were added to the map interface, improving clarity for interpretation and communication. The workflow was run for three key periods 19 June, 26 June, and 5 July 2025 coinciding with the field campaign. By combining automation, cloud computing, and satellite data archives, I was able to generate accurate, high-resolution LST products and visualize spatial patterns of heat across Ancona in near real-time ([GEE 2017](#))

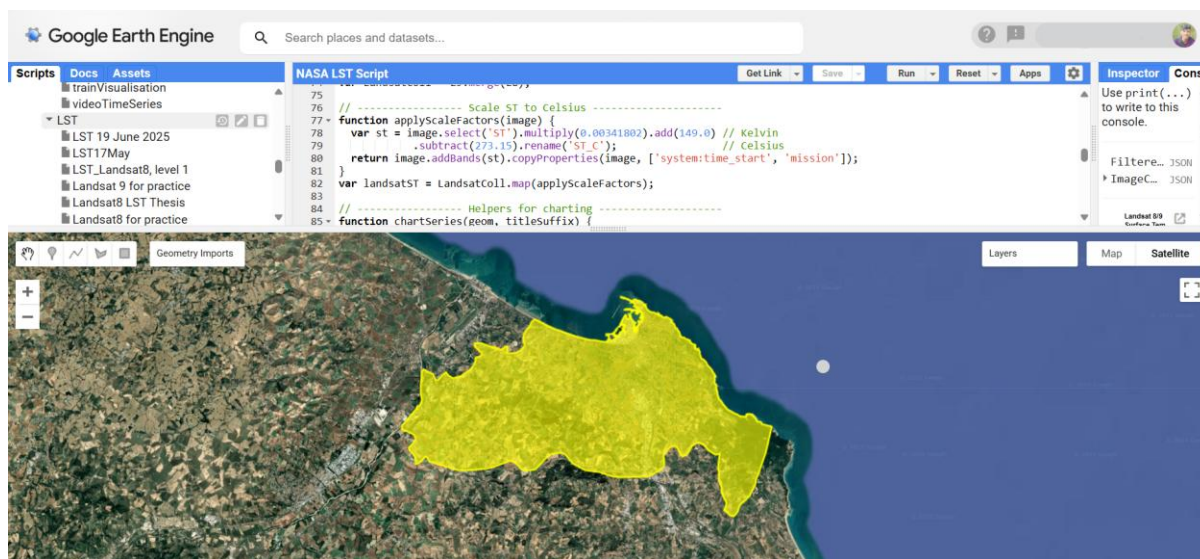


Figure 16. Google Earth Engine environment displaying the NASA LST script and the selected study area for LST analysis. Source: (Google Earth Engine screenshot)

- Outputs & Visualization

The final step of our analysis was to generate land surface temperature (LST) maps for Ancona and its surroundings. For each observation date 19, 23, and 26 June, and 5 July 2025, I produced detailed maps showing how surface temperatures varied across the study area. These maps use a colour ramp ranging from 20 °C to 60 °C, which helps to easily distinguish cooler vegetated zones from hotter impervious surfaces such as asphalt, concrete, and rooftops.

Alongside the maps, I calculated average LST values across Ancona, providing a summary of thermal conditions for each observation period. The outputs were exported as GeoTIFF files at high spatial resolution, making them suitable for both visualization and further spatial analysis.

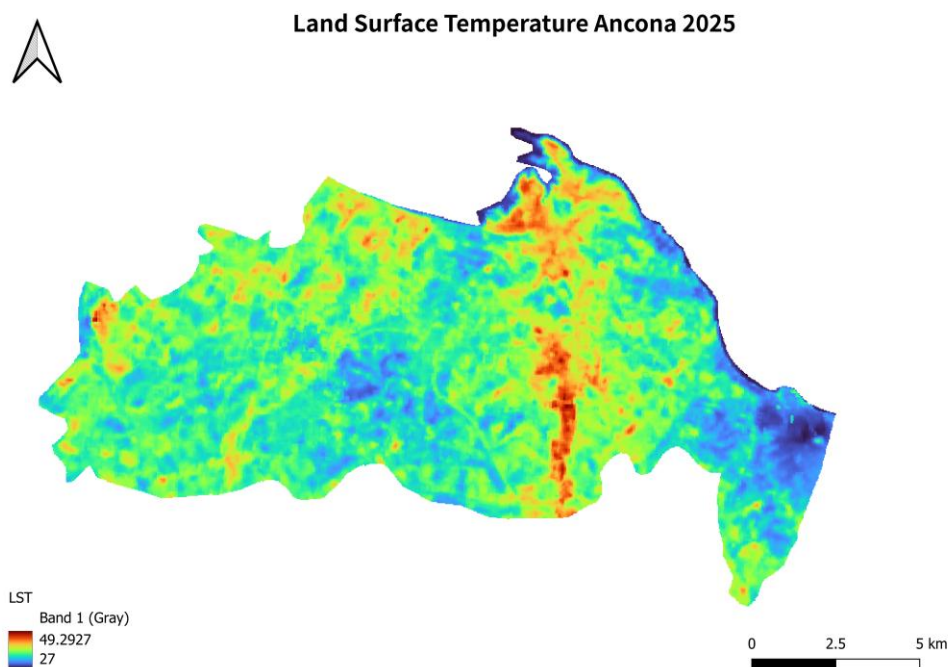


Figure 17. Land Surface Temperature visualization

3.14 Harmonization workflow of

3.14.1 Spatial Harmonization of Satellite Data

In this study, spatial harmonization was a crucial step to ensure that all datasets shared the same coordinate system and spatial alignment before comparison. The process involved reprojecting all raster datasets including Landsat 8 TIRS, ECOSTRESS data to a common coordinate system, **UTM Zone 33N (EPSG:32633)**. This projection was selected because it minimizes spatial distortion for the Ancona region, ensuring accurate pixel correspondence between multiple data sources.

The comparison in the figure highlights how reprojection improves spatial alignment. The “Not Reprojected” image shows noticeable pixel mismatches, while the “Reprojected” version achieves a consistent grid, allowing for precise pixel-to-pixel comparison between satellite and ground observations. Without this step, even small geographic discrepancies could introduce significant errors in temperature comparison, especially when harmonizing data from different satellite sensors with varying resolutions and acquisition geometries.

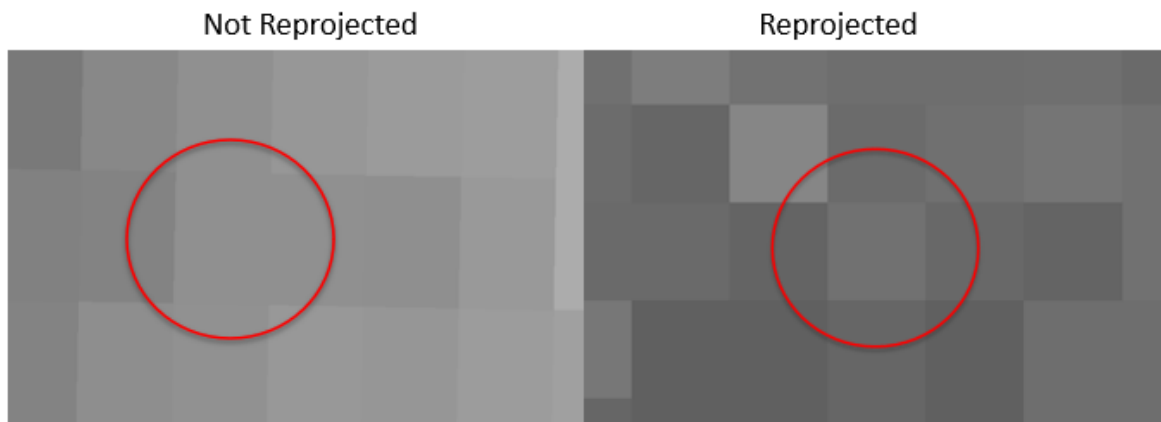


Figure 18. spatial harmonization of satellite image

3.14.2 Sampling Harmonization of Satellite and Ground Data

Sampling harmonization is an essential process that ensures consistency between satellite-derived data and ground-based temperature observations. In this step, pixel values were extracted from the satellite roasters at the locations of ground **sensor points**. This alignment allows for a direct comparison between the satellite-measured Land Surface Temperature (LST) and in situ measurements.

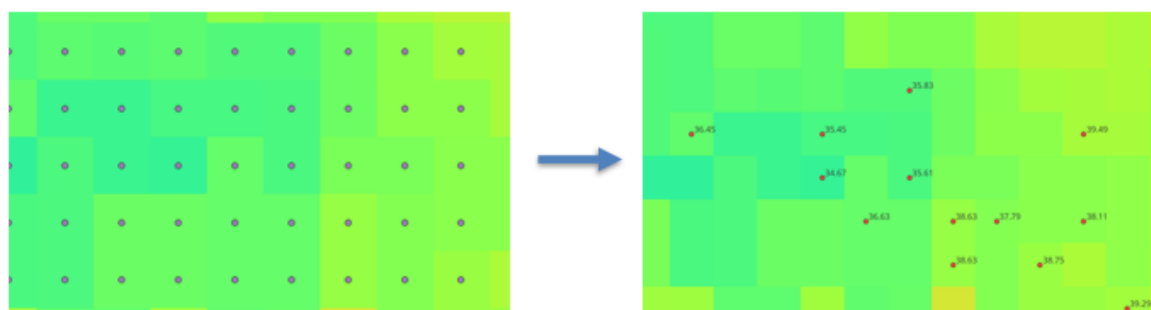


Figure 19. sampling harmonization of satellite and ground data

3.14.3 Temporal Interpolation for Ground–Satellite Harmonization

To ensure accurate comparison between satellite-derived Land Surface Temperature (LST) and ground-based sensor data, temporal harmonization was performed. Since satellite overpass times often do not perfectly align with ground sensor readings, the nearest in-situ measurement within ± 15 minutes was matched to the satellite acquisition time.

If no reading fell within this time window, linear interpolation was applied to estimate the ground temperature at the exact satellite overpass time. The interpolation formula uses two consecutive ground measurements one before and one after the satellite pass to calculate an intermediate value that reflects the temperature at the satellite observation time. This method minimizes temporal bias and improves the reliability of the satellite-ground LST correlation.

$$T_g(t)_s = T_g(t_1) + \frac{T_g(t_2) + T_g(t_1)}{t_2 - t_1} (t_s - t_1)$$

- t_1 : the earlier ground-sensor measurement time (for example 10:00)
- $T_g(t_1)$: the ground temperature recorded at that earlier time (for example 30 °C)
- t_2 : the later ground-sensor measurement time (for example 11:00)
- $T_g(t_2)$: the ground temperature recorded at that later time (for example 38 °C)
- t_s : the satellite overpass time (for example 10:30)
- $T_g^*(t_s)$: the estimated ground temperature at the satellite's overpass time (used for comparison)

3.14.4 Average Weighted Temperature (AWT) for Mixed Surface Conditions

To better represent surface temperatures in areas where multiple land cover types coexist such as partial vegetation and asphalt, an Average Weighted Temperature (AWT) approach was used. This method combines the contribution of different surface fractions (e.g., vegetation and impervious materials like asphalt) to estimate a more realistic local temperature. The formula applied is:

$$AWT = (f_{asphalt} * T_{asphalt}) + (f_{vegetation} * T_{vegetation})$$

Here, $f_{asphalt}$ and $f_{vegetation}$ represent the fractional coverage of asphalt and vegetation within a sensor's footprint, while $T_{asphalt}$ and $T_{vegetation}$ are their corresponding surface temperatures.

This approach accounts for the fact that few locations are entirely homogeneous or maybe there is no homogeneous location. Most urban environments include a mix of built-up and natural surfaces. By weighting the temperature contributions based on surface type, AWT provides a

more accurate representation of local microclimates especially in transitional areas such as tree-lined streets or partially shaded concrete zones.

- Workflow to Calculate the Average Weighted Temperature (AWT)

To determine the percentage of different land cover classes within a single pixel of Landsat or ECOSTRESS data, Sentinel-2 imagery was also used. The Sentinel-2 raster image was converted to a vector shapefile, and the same conversion was applied to the ECOSTRESS/Landsat image.

Since the spatial resolution of Landsat 8 and ECOSTRESS is 100 m and 70 m, while Sentinel-2 has a 10 m resolution, overlaying the Sentinel-2 vector data on the Landsat 8 or ECOSTRESS vectors allows identification of how many Sentinel-2 pixels fall within a single Landsat/ECOSTRESS pixel. By analysing how many Sentinel-2 pixels within that area are classified as vegetation, asphalt, or other land cover types, it becomes possible to estimate the percentage composition of land cover classes within each Landsat or ECOSTRESS pixel. This percentage information is then used to compute the Average Weighted Temperature (AWT) for that pixel.

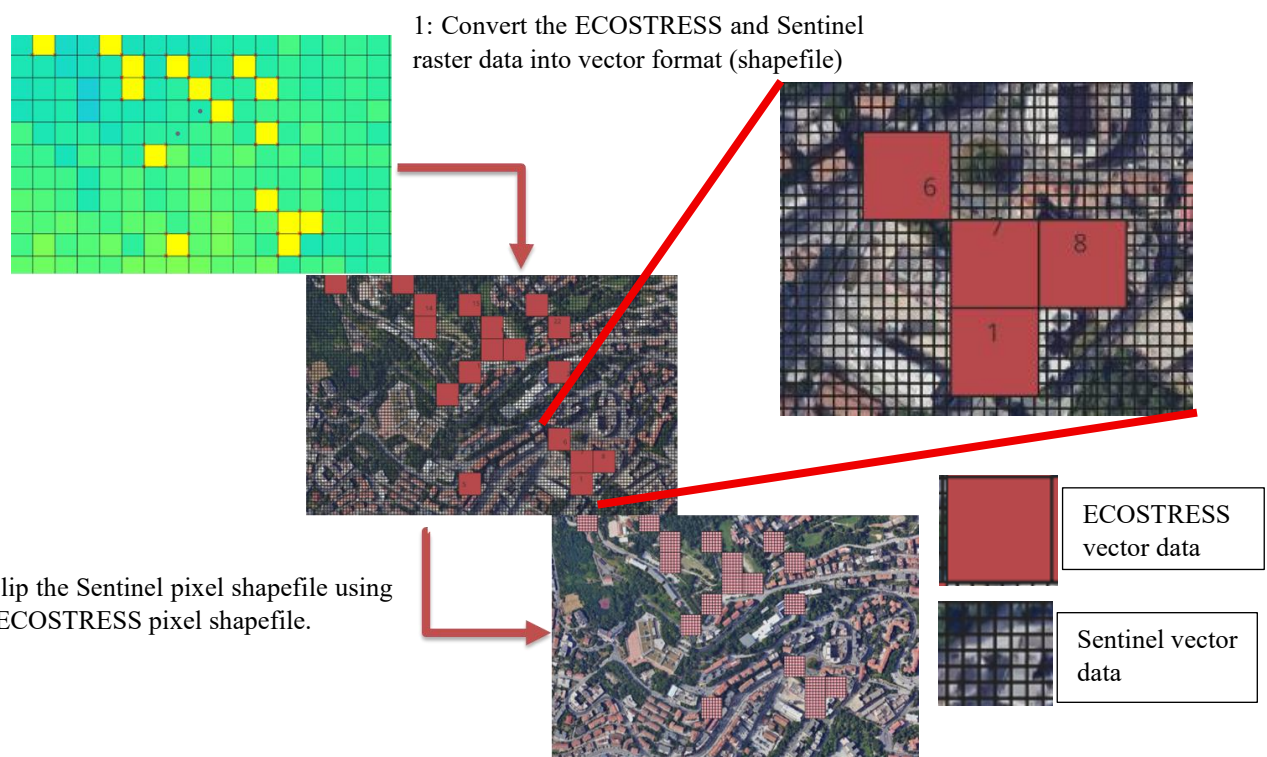


Figure 20. Loading ECOSTRESS/Landsat and Sentinel raster data, converting both to vector format, and clipping the Sentinel vector data using the ECOSTRESS and Landsat boundaries.

- Average Land Surface Temperature, or LST, for different vegetated areas

In pixels below each square represents a sample vegetation pixel which is extracted from satellite imagery, with its corresponding surface temperature value in degrees Celsius. The different types of vegetation record different LST, for this purpose we should calculate the mean value for different types of vegetation.

As we can see, the LST values range from about 29.9°C to 35.1°C across the selected areas. When averaged, the overall mean LST for vegetation is approximately 32.74°C.

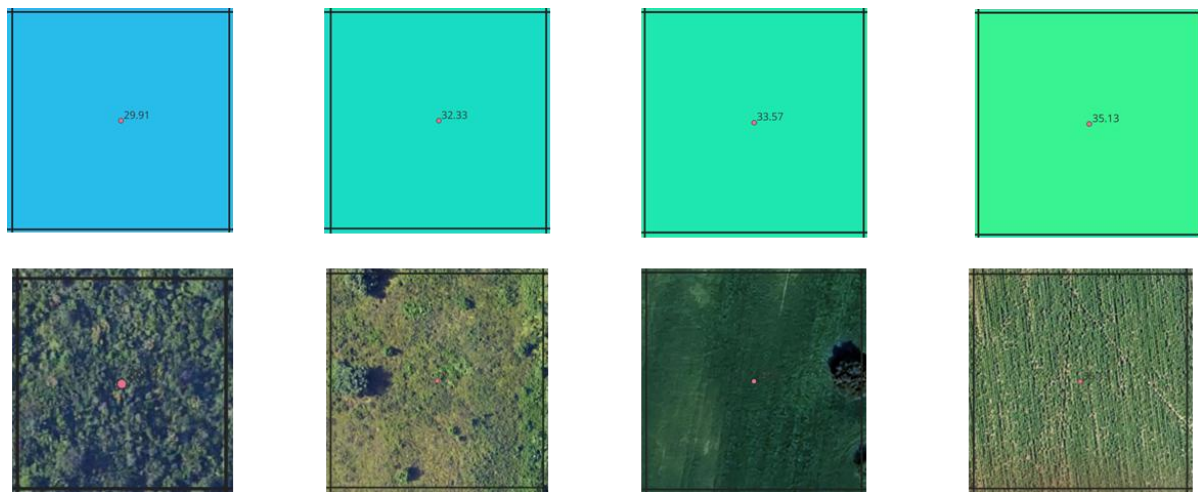


Figure 21. Average Land Surface Temperature, or LST, for different vegetated areas

- Average Land Surface Temperature (LST) for Soil Areas

The same for the soil pixels that different types of soil record different LST, then we have to find the mean value for this different class of soils. The figure bellow you can see the selected soil areas show varying surface temperatures ranging from 31.6°C to 36.3°C. By averaging these values $(34.49 + 36.27 + 33.17 + 31.61) \div 4$ the mean LST for soil areas is calculated as 33.89°C.

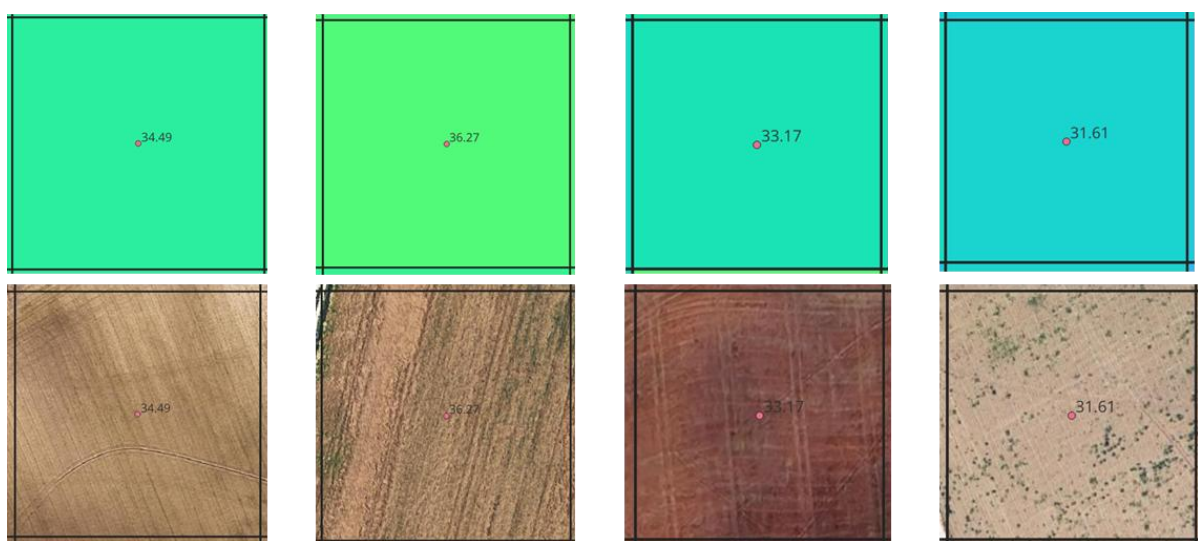


Figure 22. Average Land Surface Temperature (LST) for Soil Areas

- Average Land Surface Temperature (LST) for Asphalt/Concrete Areas

The same for the asphalted area which record different LST for different area, so we have to calculate the mean value for different classes. The selected asphalt and concrete surfaces exhibit higher surface temperatures, ranging from 35.6°C to 38.5°C. By averaging these values $(38.45 + 35.57 + 36.27 + 37.81) \div 4$ the mean LST is 37.03°C.



Figure 23. Average Land Surface Temperature (LST) for Asphalt/Concrete Areas

And at the end it is calculated the AWT using the mean value for vegetation, soil, and asphalt considering the percentage cover in one pixel.

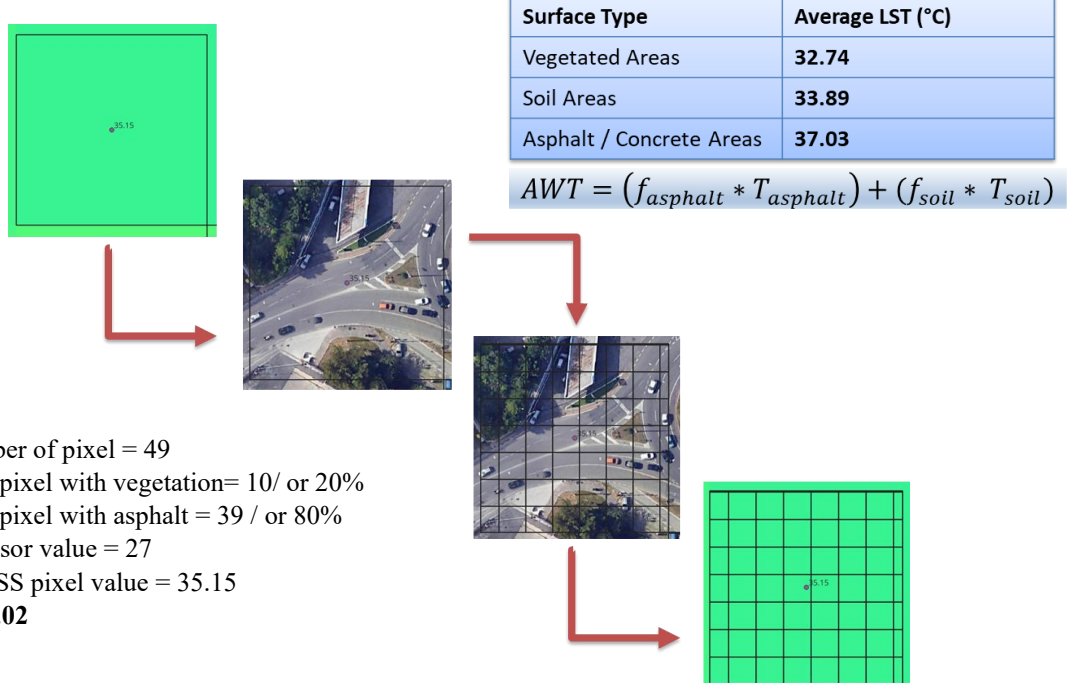


Figure 24. steps of LST calculation of one Landsat/ECOSTRESS pixel

3.14.5 Residual Result After Harmonizations

Sensor's Number	19 June Landsat	19 June ECOSTRESS	23 June ECOSTRESS	26 June Landsat	5 July Landsat
Column1	Residuals	Residuals	Residuals	Residuals	Residuals
1	2.467	2.37	0.05	0.108	2.421
2	2.38	2.79	1.27	3.179	1.771
3	0.538	1.83	-0.91	1.231	1.631
4	9.51	11.85	6.83	6.892	9.133
5	2.468	1.37	2.53	-1.343	4.497
6	2.46	0.47	-4.16	4.294	1.976
7	5.388	2.63	1.77	2.181	5.77
8	2.496	1.56	-0.59	-4.877	-3.781
9	2.987	4.15	3.23	-2.608	-1.838
10	1.522	2.07	0.51	6.523	3.122
11	1.915	2.97	-0.33	3.047	4.081
12	5.205	3.25	-0.91	2.793	4.135
13	1.454	3.65	2.91	4.187	4.871
14	1.747	5.37	1.55	2.853	6.078
15	7.217	1.81	0.91	1.006	1.292
16	3.923	5.43	3.71	3.664	8.73
17	4.14	6.79	2.21	6.896	6.993
18	5.95	7.03	2.77	5.825	-2.519
19	-0.502	0.63	3.39	0.777	-5.012
20	5.335	4.63	0.05	4.883	4.293
21	3.997	2.49	4.13	3.609	-2.933
22	0.708	0.11	-0.41	-0.284	2.848
23	3.888	4.25	4.07	2.411	-2.115
24	6.496	5.05	1.37	4.897	-2.188
25	lost sensor	lost sensor	lost sensor	lost sensor	lost sensor
26	0.15	0.99	0.15	2.379	-2.557
27	3.136	0.39	-0.59	1.242	-4.312
28	9.409	9.83	4.21	7.63	6.382
29	2.29	4.27	-0.05	-3.408	0.175
30	5.66	3.75	1.27	5.994	-5.659
31	-2.495	-2.39	4.69	-8.745	-10.198
32	-4.785	-1.73	1.47	-2.243	-5.201
33	1.529	-1.53	1.47	1.574	2.63
34	0.404	0.32	0.31	0.826	1.559
35	3.605	4.8	0.51	4.627	0.147
36	1.354	5.95	2.59	3.582	5.076
37	2.338	0.67	-0.85	-0.249	-2.435
38	-2.459	-3.45	-0.31	-0.845	-4.066
39	2.913	4.97	2.81	3.457	3.796
40	5.567	5.45	0.99	3.474	7.079
41	3.305	2.99	2.745	1.676	4.395
42	4.169	4.71	2.05	0.959	4.41
43	2.992	8.53	0.57	7.58	-2.251
44	2.078	2.39	2.17	4.705	5.44
45	2.248	6.97	3.83	2.252	6.569
46	1.806	-0.35	0.87	lost sensor	lost sensor
47	0.501	0.81	1.75	0.803	1.941
48	2.996	1.81	1.23	0.656	2.319
49	-1.149	-0.29	0.25	-4.947	-2.477
50	4.201	3.11	6.17	5.604	-7.241

Table 7. Residuals after calculating the AWT

Description of the table	
Yello colour	sensors on soil
Cement colour	sensor on asphalt or concrete
Green colour	sensor on vegetation
Red colour	lost sensor

3.15 Data Preparation and Validation Metric Computation in Python

In this step, the dataset collected from both ground sensors and satellite observations was loaded and prepared for validation in Python. Each record in the dataset includes a sensor ID, ground-measured temperature (VALUE), estimated temperature from satellite-based models (AWT), and the computed difference between them (Residuals). Missing or faulty sensor readings such as lost or malfunctioning sensors were identified and removed to ensure data quality and consistency.

After cleaning the data, it was structured into a Pandas DataFrame, which allows for efficient data manipulation and statistical analysis. Arrays were then extracted to represent the ground temperatures, satellite estimates, and their residuals. Using NumPy, several key statistical validation metrics were calculated to assess the accuracy of satellite-derived Land Surface Temperature (LST) data against ground-based measurements:

- a- Bias measures whether the satellite data tends to overestimate or underestimate temperatures.
- b- Mean Absolute Error (MAE) provides the average size of temperature errors, showing how close satellite estimates are to ground values.
- c- Root Mean Square Error (RMSE) emphasizes larger discrepancies, giving insight into overall accuracy.
- d- Pearson's R (correlation coefficient) evaluates the strength of the relationship between satellite and ground data, showing how well the two datasets follow similar patterns.

```
# Create DataFrame
df4 = pd.DataFrame(data4, columns=["Sensor_N", "VALUE", "AWT", "Residuals"])
df4 = df4.dropna(subset=["Residuals"])

# Extract arrays
ground4 = df4["VALUE"].values
satellite4 = df4["AWT"].values
residuals4 = df4["Residuals"].values

# =====
# Compute metrics
# =====
bias4 = np.mean(residuals4)
mae4 = np.mean(np.abs(residuals4))
rmse4 = np.sqrt(np.mean(residuals4**2))
r4, _ = pearsonr(satellite4, ground4)

# Print results
print("== Validation Metrics (Fourth Dataset) ==")
print(f"Bias : {bias4:.3f}")
print(f"MAE : {mae4:.3f}")
print(f"RMSE : {rmse4:.3f}")
print(f"Pearson R : {r4:.3f}")

data4 = [
    [1, 41.92133774, 39.5, 2.421],
    [2, 42.57076154, 40.8, 1.771],
    [3, 41.63080604, 40, 1.631],
    [4, 42.53316332, 33.4, 9.133],
    [5, 44.29686164, 39.8, 4.497],
    [6, 45.15136664, 43.175, 1.976],
    [7, 44.57030324, 38.8, 5.77],
    [8, 45.71875796, 49.5, -3.781],
    [9, 43.162079, 45, -1.838],
    [10, 42.62203184, 39.5, 3.122],
    [11, 41.08050482, 37, 4.0811],
    [12, 36.13462988, 32, 4.135],
    [13, 39.4706174, 34.6, 4.871],
    [14, 38.67763676, 32.6, 6.078],
    [15, 37.79236958, 36.5, 1.292],
    [16, 39.73038692, 31, 8.73],
    [17, 40.49260538, 33.5, 6.993],
    [18, 44.48143472, 47, -2.519],
    [19, 40.98821828, 46, -5.012],
    [20, 39.0433649, 34.75, 4.293],
    [21, 46.067396, 49, -2.933],
    [22, 41.64789614, 38.8, 2.848],
    [23, 40.98480026, 43.1, -2.115],
    [24, 43.71238022, 45.9, -2.188],
    [25, 41.77436288, None, None], # lost sensor
    [26, 41.44281494, 44, -2.557]
]
```

Figure 25. Data Preparation and Validation Metric Computation in Python

3.15.1 Residual Analysis as a Validation Metric

Residual analysis is one of the most straightforward ways to validate satellite-derived Land Surface Temperature (LST) data against ground-based observations. A residual represents the difference between satellite and in-situ temperature measurements at a specific point, calculated as:

$$\text{Residual} = T_{\text{satellite}} - T_{\text{ground}}$$

A positive residual indicates that the satellite recorded a higher temperature than the ground sensor, while a negative residual suggests the opposite. For example, if the satellite reports 35 °C and the ground measurement is 34 °C, the residual is +1 °C, meaning the satellite slightly overestimates the temperature.

3.15.2 Root Mean Square Error (RMSE) as a Validation Metric

The Root Mean Square Error (RMSE) is one of the most widely used indicators for assessing the accuracy of satellite-derived Land Surface Temperature (LST) compared to ground-based measurements. It quantifies the average magnitude of errors, showing how close the satellite temperature values are to the actual ground truth.

Mathematically, RMSE calculates as:

$$(RMSE) = \sqrt{\frac{1}{n} \sum_{i=1}^n (T_{\text{sat},i} - T_{\text{ground},i})^2}$$

- $(T_{\text{sat},i} - T_{\text{ground},i})^2$: this makes all values positive and penalizes large errors more strongly.
- n = the total number of observations.
- i = the index of each observation.
- Small RMSE: satellite is close to ground truth.
- Large RMSE: satellite is far from ground truth.
- Good for checking overall accuracy.
- RMSE = average error size + highlights the big mistakes.

A small RMSE indicates that satellite observations closely match ground temperatures, reflecting good model performance and data reliability. Conversely, a large RMSE implies greater deviation and reduced accuracy. This metric is particularly valuable because it not only measures overall error but also highlights significant mismatches that could arise due to surface heterogeneity, atmospheric effects, or calibration inconsistencies.

3.15.3 Mean Absolute Error (MAE) as a Validation Metric

The Mean Absolute Error (MAE) is a straightforward and intuitive metric used to assess the average difference between satellite-derived Land Surface Temperature (LST) and ground-based measurements. Unlike RMSE, which gives more weight to large errors, MAE treats all errors equally, making it a simple measure of the average error size in degrees Celsius (°C).

The formula is expressed as:

$$MAE = \frac{1}{n} \sum_{i=1}^n |T_{sat,i} - T_{ground,i}|$$

Here, n represents the total number of paired observations, and the absolute difference ensures that both positive and negative deviations are counted as errors. A lower MAE indicates a closer match between satellite and in-situ data, suggesting high reliability of the remote sensing product.

3.15.4 Bias (ΔT) as a Validation Metric

The Bias (ΔT) metric measures the average direction of error between satellite-derived Land Surface Temperature (LST) and ground-based observations. It helps identify whether the satellite tends to overestimate or underestimate surface temperatures. The bias is calculated as the mean of all residuals (differences between satellite and ground values):

$$Bias = \frac{1}{n} \sum_{i=1}^n (T_{sat,i} - T_{ground,i})$$

When the bias is positive, it means the satellite readings are usually warmer than what's recorded on the ground. A negative bias, on the other hand, indicates the satellite is underestimating surface temperatures. Small bias values close to zero suggest a good match between satellite and ground data, showing that the satellite measurements are well-calibrated and reliable.

3.15.5 Correlation Analysis (Pearson's R) - Evaluating the Relationship Between Satellite and Ground Temperatures

Pearson's correlation coefficient (R) is used to measure how closely the satellite-derived Land Surface Temperature (LST) values follow the same pattern as ground-based temperature observations. In simpler terms, it checks whether both datasets rise and fall together meaning if ground temperatures increase, do satellite temperatures show the same trend

$$R = \frac{\sum_{i=1}^n (X_i - \bar{X})(Y_i - \bar{Y})}{\sqrt{\sum_{i=1}^n (X_i - \bar{X})^2} \sqrt{\sum_{i=1}^n (Y_i - \bar{Y})^2}}$$

X = satellite LST values

Y = ground sensor values

$Y_i = Y^-$: how far each ground value is from the ground average

$X_i = X^-$: how far each satellite value is from the satellite average

Pearson's R (Correlation)

Checks if satellite and ground **rise and fall together**.

R=+1: perfect match in pattern (if ground heats up, satellite heats up the same way).

R=0: no relationship.

R=-1: opposite pattern.

Even if satellite has a bias (always too hot), it can still have **high correlation** if the *pattern* matches.

4 Result and Discussion

4.1 Land Cover Change Analysis in Ancona, Agugliano, and Camerata Picena

- Land Cover Classification Ancona, Agugliano, Camerata P, July 1996

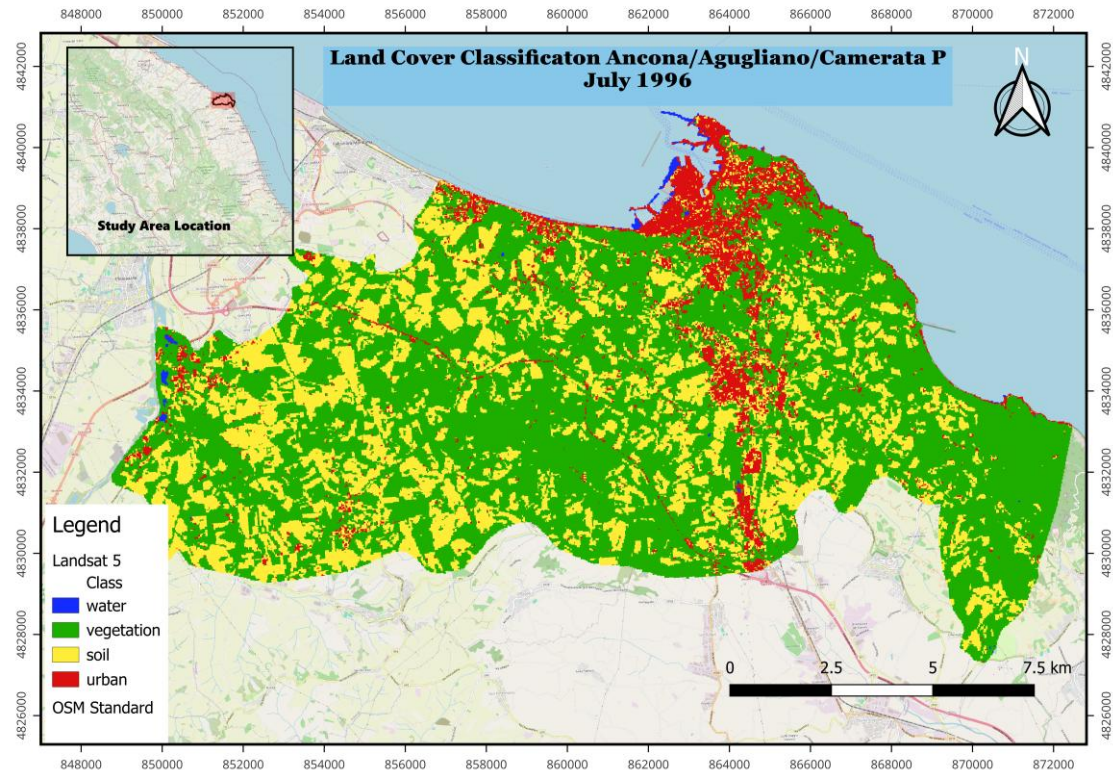


Figure 26. land cover classification

Raster Value	Class	Pixel Sum	Percentage %	Area [m ²]	Area [km ²]
1	water	1,049	0.34	565,907.09	0.57
2	vegetation	190,990	61.77	103,033,932.40	103.03
3	soil	92,364	29.86	49,827,876.47	49.83
4	Urban/road	24,899	8.05	13,432,336.15	13.43
Total	—	309,302	100%	166,860,051.11	166.86

Test Confusion Matrix

Test Confusion Landsat 5	
Class	Values
1	[0, 0, 0, 0, 0]
2	[0, 5, 0, 0, 0]
3	[0, 0, 37, 0, 0]
4	[0, 0, 5, 39, 0]
5	[0, 0, 1, 2, 19]
Training Accuracy: 0.99	
Training Kappa: 0.99	
Test Accuracy: 0.95	
Test Kappa: 0.92	

- Land Cover Classification Ancona/ Agugliano / Camerata P, July 2001

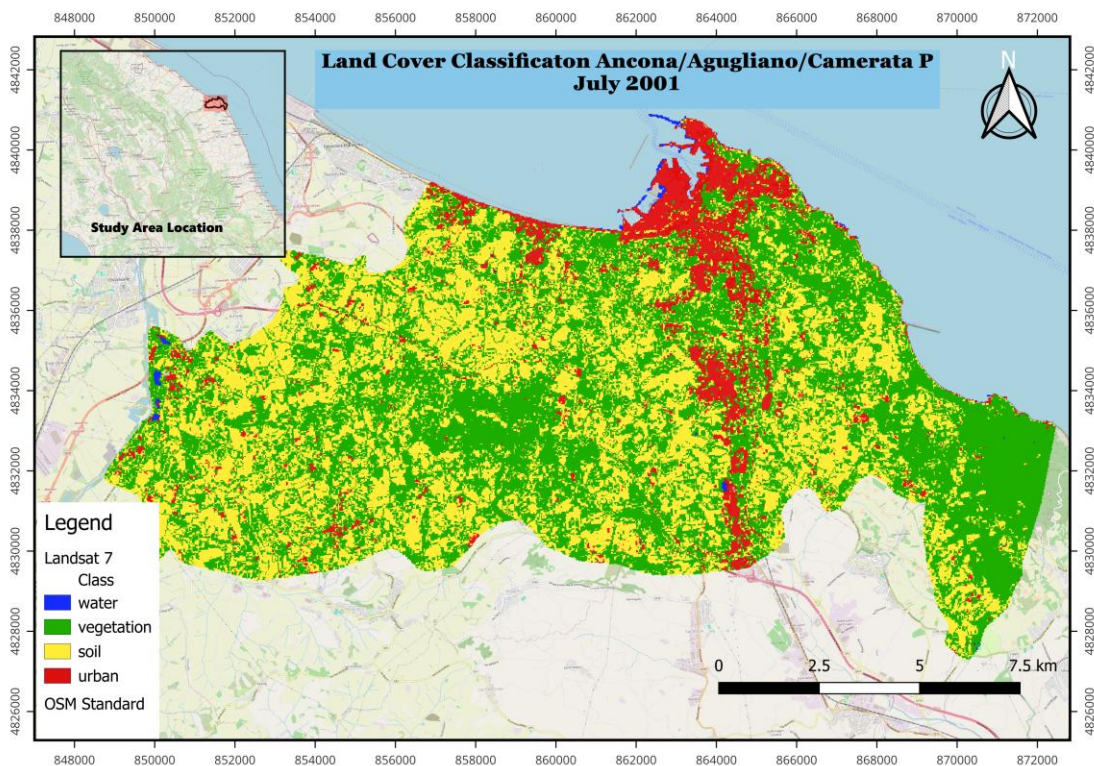


Figure 27. land cover classification

Raster Value	Class	Pixel Sum	Percentage %	Area [m ²]	Area [km ²]
1	water	818	0.26	441,288.85	0.44
2	vegetation	152,701	49.42	82,378,053.84	82.38
3	soil	128,599	41.62	69,375,677.61	69.38
4	urban	26,900	8.70	14,511,821.45	14.51
Total	—	309,018	100%	166,706,841.75	166.71

Test Confusion Matrix (2010)

Class	Values
1	[2, 0, 0, 0, 0]
2	[0, 19, 0, 0, 0]
3	[0, 1, 27, 2, 0]
4	[0, 0, 1, 18, 0]
5	[0, 0, 0, 0, 2]
Training Accuracy:	0.99
Training Kappa:	0.99
Test Accuracy:	0.83
Test Kappa:	0.80

- Land Cover Classification Ancona/ Agugliano / Camerata P, July 2010

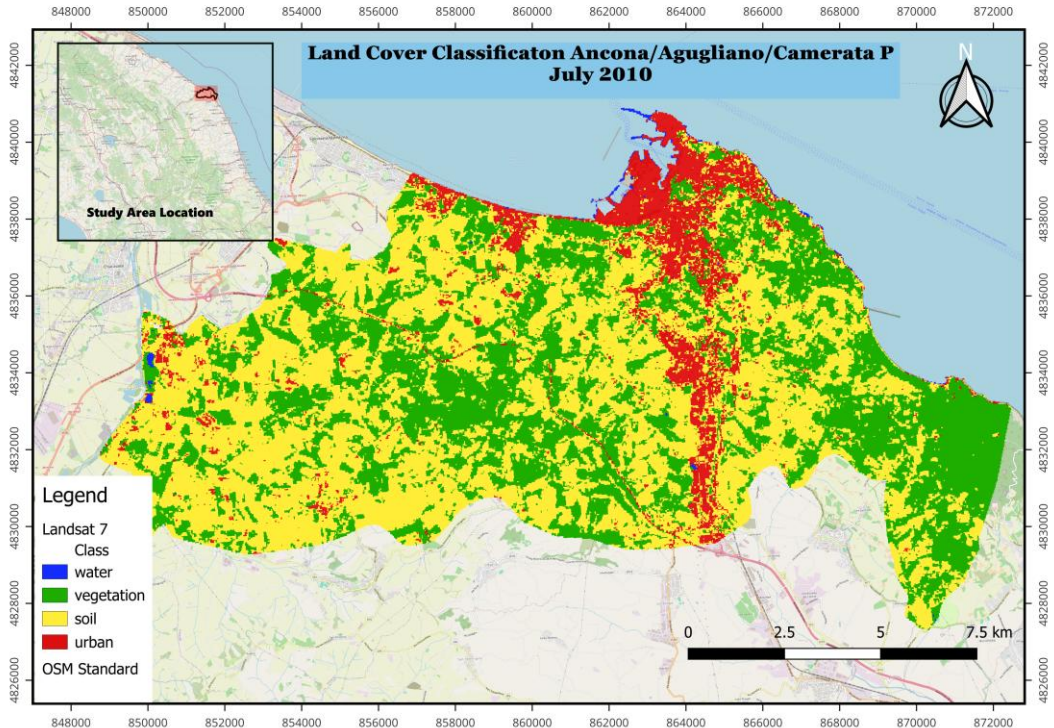


Figure 28. land cover classification

Land Cover Classification Ancona (Landsat 7)

Raster Value	Class	Pixel Sum	Percentage %	Area [m ²]	Area [km ²]
1	water	883	0.29	476,354.59	0.48
2	vegetation	118,324	38.27	63,832,593.39	63.83
3	soil	161,741	52.35	87,254,889.01	87.25
4	urban	28,110	9.10	15,164,583.68	15.16
Total	—	309,058	100%	166,728,420.67	166.73

Test Confusion Matrix (Landsat 7)

Class	Values
1	[1, 0, 0, 0, 0]
2	[0, 20, 0, 0, 0]
3	[0, 1, 28, 1, 0]
4	[0, 0, 0, 19, 0]
5	[0, 0, 0, 0, 2]
Training Accuracy:	0.99
Training Kappa:	0.99
Test Accuracy:	0.97
Test Kappa:	0.95

- Land Cover Classification Ancona/ Agugliano / Camerata P, July 2020

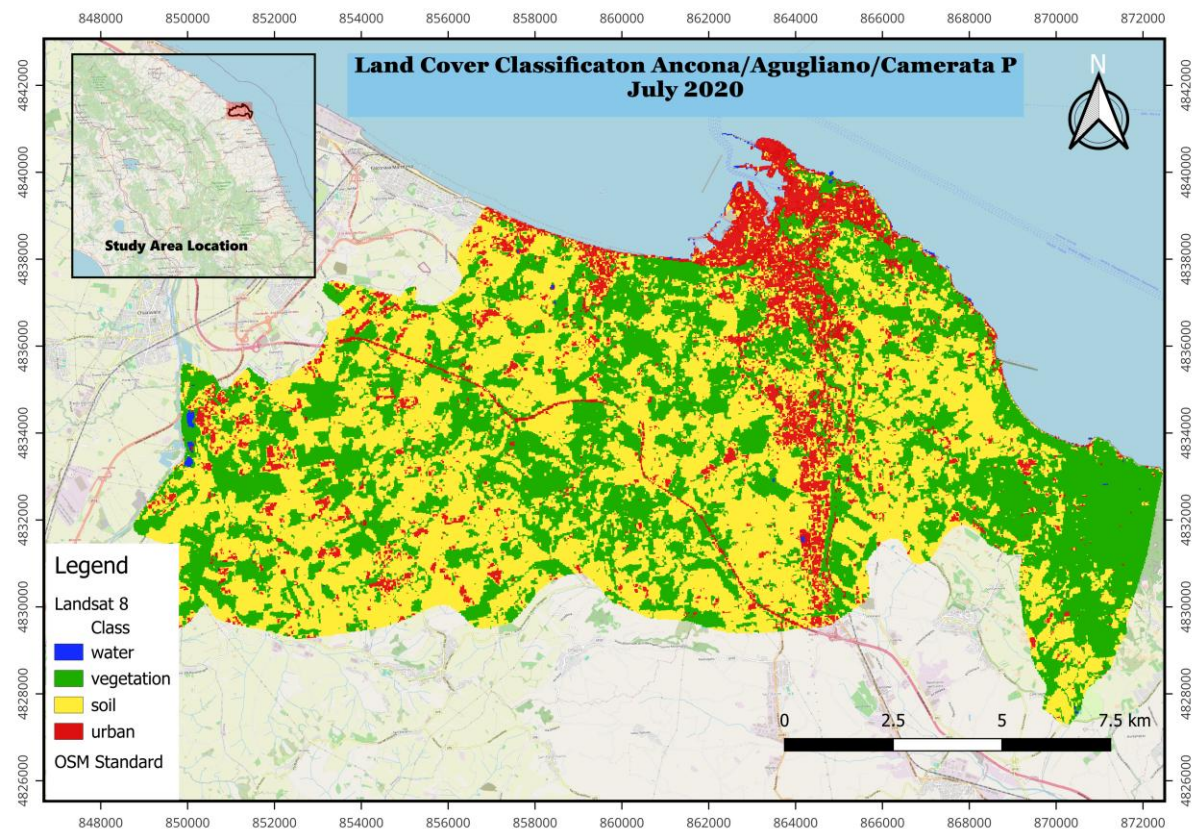


Figure 29. land cover classification

Land Cover Classification Ancona (Landsat 8)

Raster Value	Class	Pixel Sum	Percentage %	Area [m ²]	Area [km ²]
1	water	534	0.17	288,078.54	0.29
2	vegetation	123,045	39.83	66,379,445.03	66.38
3	soil	152,726	49.45	82,391,540.67	82.39
4	urban	32,535	10.54	17,551,751.34	15.59
Total	—	308,840	100%	166,610,815.58	166.61

Test Confusion Matrix (Landsat 8)

Class	Values
1	[2, 0, 0, 0, 0]
2	[0, 30, 0, 0, 0]
3	[0, 0, 33, 0, 0]
4	[0, 0, 5, 18, 0]
5	[0, 0, 1, 0, 2]
Training Accuracy:	1
Training Kappa:	1
Test Accuracy:	0.93
Test Kappa:	0.90

- Land Cover Classification Ancona/ Agugliano / Camerata P, July 2025

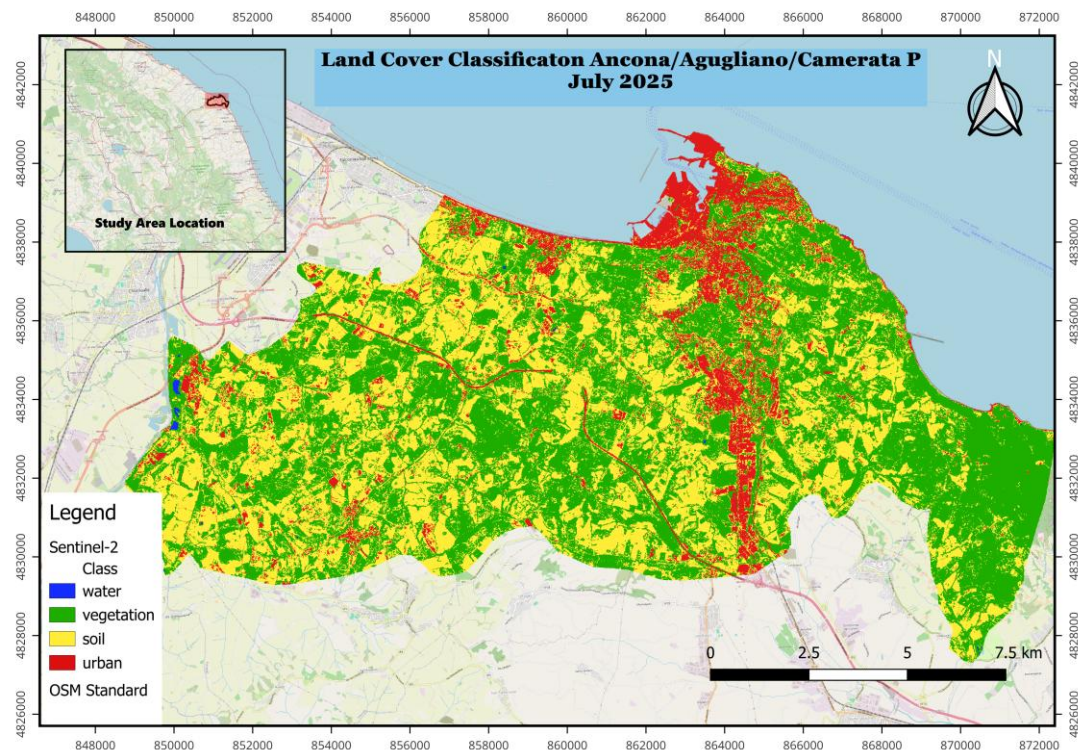


Figure 30. land cover classification

Raster Value	Class	Pixel Sum	Percentage %	Area [m ²]	Area [km ²]
1	water	2,238	0.04	134,129.38	0.13
2	vegetation	1,369,820	23.81	82,097,012.47	82.1
3	soil	1,127,982	19.6	67,603,007.93	67.6
4	urban	268.5	4.64	16,098,582.75	16.1
Total	—	2,768,651	48.12*	165,932,732.54	165.93

Test Confusion Sentinel-2

Class	Values
1	[3, 0, 0, 0, 0]
2	[0, 49, 0, 0, 0]
3	[0, 1, 58, 1, 0]
4	[0, 0, 1, 29, 0]
5	[0, 1, 0, 1, 17]
Training Accuracy:	0.99
Training Kappa:	0.99
Test Accuracy:	0.96
Test Kappa:	0.95

4.2 Urban Expansion Intensity (UEII)-Ancona

calculated the Urban Expansion Intensity Index (UEII) to measure how fast the urban area has grown from 1996 to 2025.

The urban area in Ancona increased by about 2.67 km^2 between 1996 and 2025. The UEII of 5.52% per year means that on average, only 5.52% of the total study area has been converted to urban land every year during this 28-year period.

$$UEII = \frac{(ULA_{t2} - ULA_{t1}) * 100}{TLA_i * \Delta T}$$

ULA_{t1} (Urban area in 1996): 13.43 km^2

ULA_{t2} (Urban area in 2025): 16.1 km^2

ULA_i (Total land area): 166.86 km^2

ΔT (Time period): $2025 - 1996 = 29 \text{ years}$

Step 1: Calculate change in urban area

$$ULA_{t2} - ULA_{t1} = 16.1 - 13.43 = 2.67 \text{ km}^2$$

Step 2: Apply the UEII formula:

$$UEII = \frac{(2.67) * 100}{166.86 * 29}$$

$$UEII = \frac{(2.67)}{4838.94} = 0.0552$$

$$\text{UEII} = 0.055 \text{ (or } 5.52\% \text{ per year)}$$

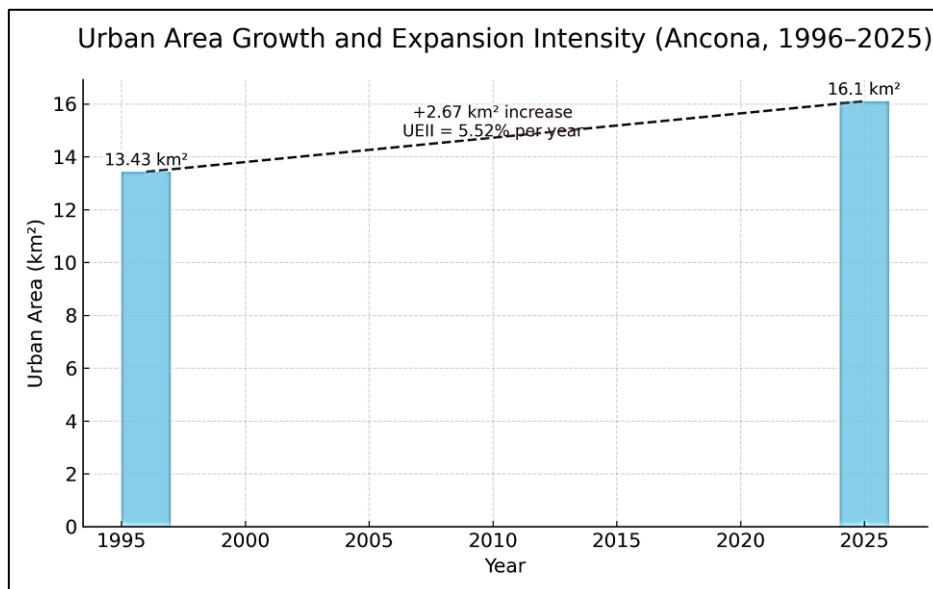


Figure 31. Urban area growth and expansion intensity (Ancona, 1996 to 2025)

- Land Cover Types and Land Surface Temperature in Ancona

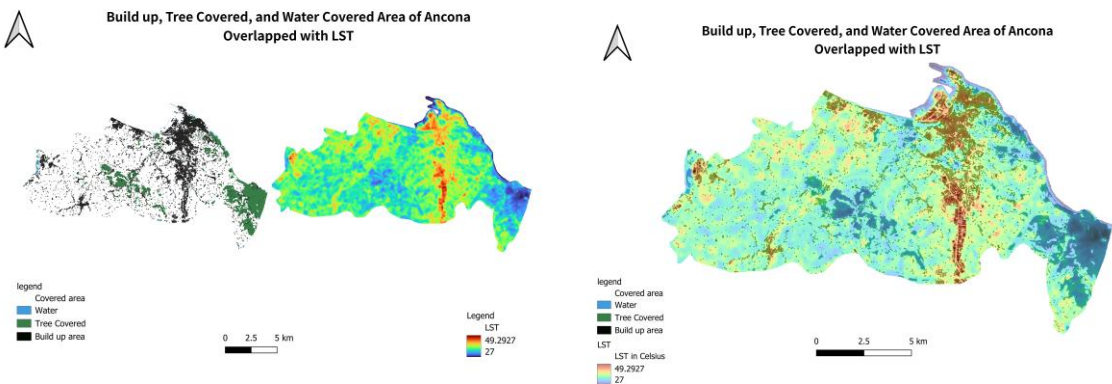


Figure 32. Relationship Between Land Cover Types and Land Surface Temperature

The maps above illustrate the spatial relationship between land cover types, including built-up areas, vegetation, and water bodies and land surface temperature (LST) across the municipality of Ancona. The land cover classification map highlights three primary surface categories: built-up and road surfaces (shown in red), tree-covered and vegetated areas (in green), and water bodies (in blue). These classes represent the major land cover features influencing the local thermal environment. Color range for LST is from 27.3 Cilsius to 49.6 Cilsius and shows a spatial distribution of surface temperatures across Ancona in mid June 2025.

Build up and urban area spots the area with a high temperature. Lack of vegetation and heat emitted form the buildings and vehicles. The second map shows the overlped of LST with build up area, covered area by tree and water body.

- Road Networks and Land Surface Temperature (LST) in Ancona

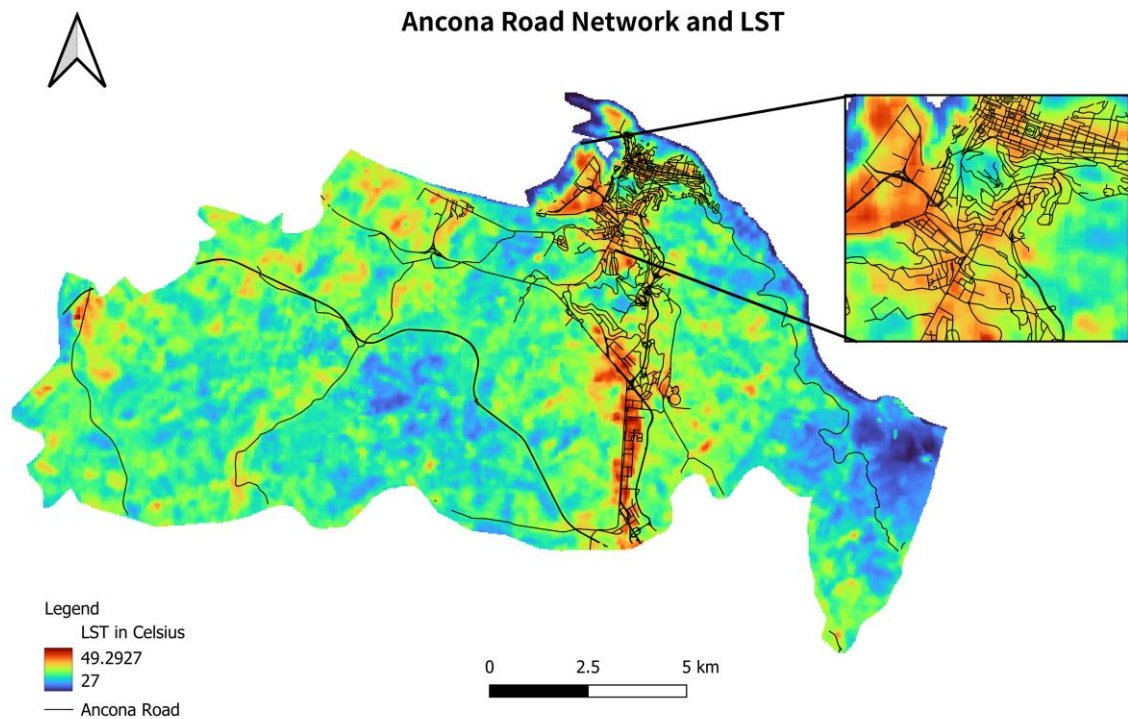


Figure 33. Ancona Road network and Land Surface Temperature

The map illustrates the relationship between Ancona's road network and Land Surface Temperature (LST) for the June 2025. The color gradient ranges from cooler zones (in blue and green, around 27°C) to hotter zones (in orange and red, approaching 49.2°C). The results clearly show that areas surrounding major roads and dense transport corridors exhibit higher LST values, highlighting how impervious materials such as asphalt and concrete absorb and retain more solar radiation compared to natural surfaces.

The highest surface temperatures are concentrated in central Ancona and along main transportation routes, where traffic density, building concentration, and reduced vegetation cover amplify heat retention. This spatial pattern supports the broader understanding that transport infrastructure significantly contributes to the urban heat island (UHI) effect, particularly in regions with limited greenery and dense built-up surfaces.

- Built-up Areas and Land Surface Temperature (LST) in Ancona

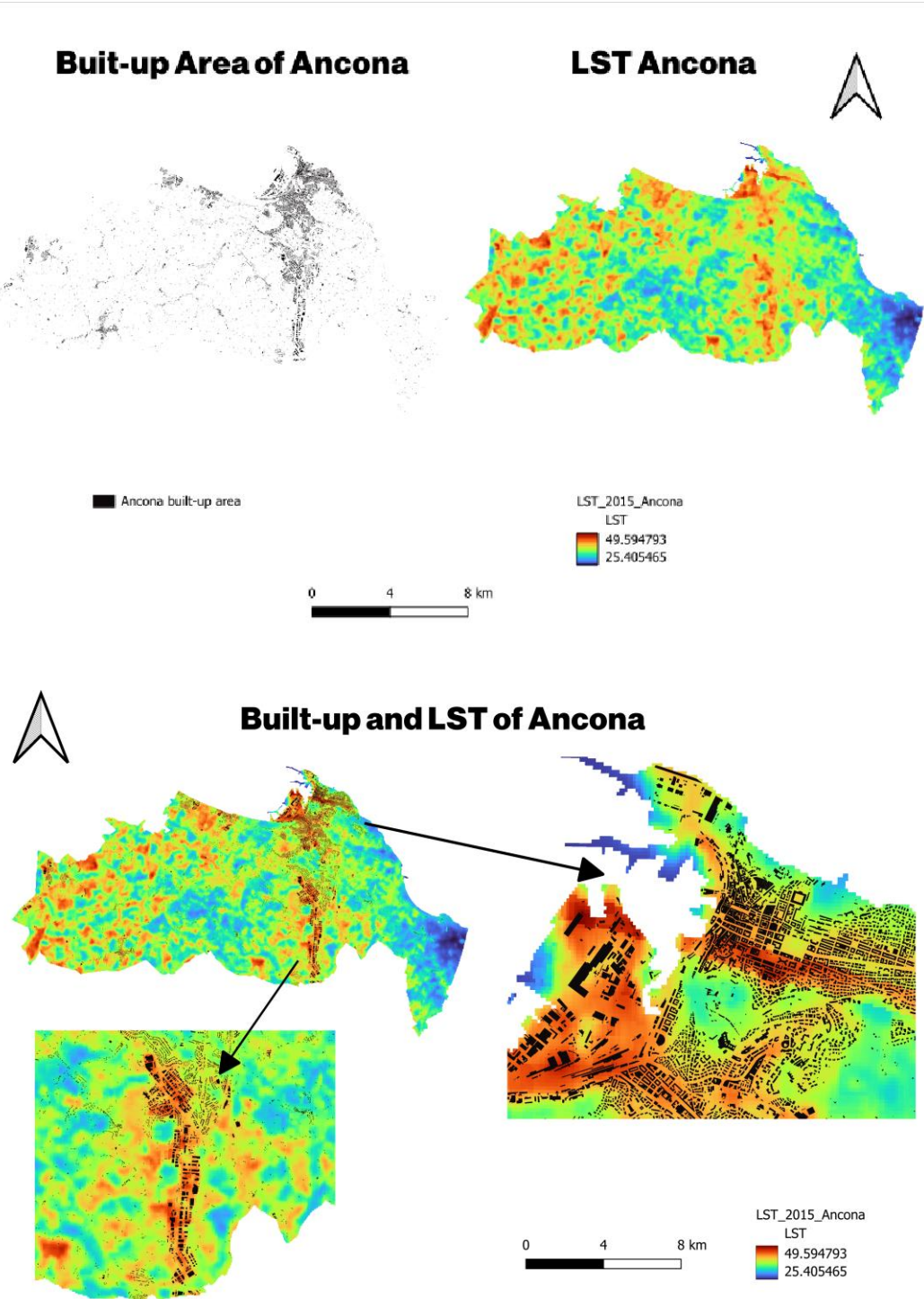


Figure 34. Relationship Between build-up area and LST

The maps illustrate the spatial relationship between **built-up** areas and **Land Surface Temperature (LST)** across Ancona for different years. The black polygons represent the city's built-up zones, while the colored LST maps highlight temperature variations, ranging from cooler areas in blue (around 25.4°C) to hotter areas in red (up to 49.5°C).

The analysis clearly shows that built-up and densely urbanized areas correspond to higher LST values, particularly within Ancona's city center and industrial zones. These hotspots are associated with impervious surfaces such as asphalt, concrete, and rooftops that absorb and retain solar heat. In contrast, vegetated and coastal areas display cooler temperatures due to evapotranspiration and proximity to the sea, which moderates local heat accumulation.

Zoomed-in sections emphasize how urban density and material composition directly affect surface temperature, reinforcing the well-known Urban Heat Island (UHI) phenomenon. Areas with more green cover or open spaces demonstrate lower LST, confirming the critical role of urban greenery and sustainable land management in mitigating heat impacts.

Overall, the spatial correlation between built-up expansion and rising LST suggests that urban growth has significantly influenced Ancona's microclimate, highlighting the need for climate-sensitive urban planning strategies that integrate vegetation, reflective materials, and sustainable design.

- Elevation and Land Surface Temperature (LST) in Ancona

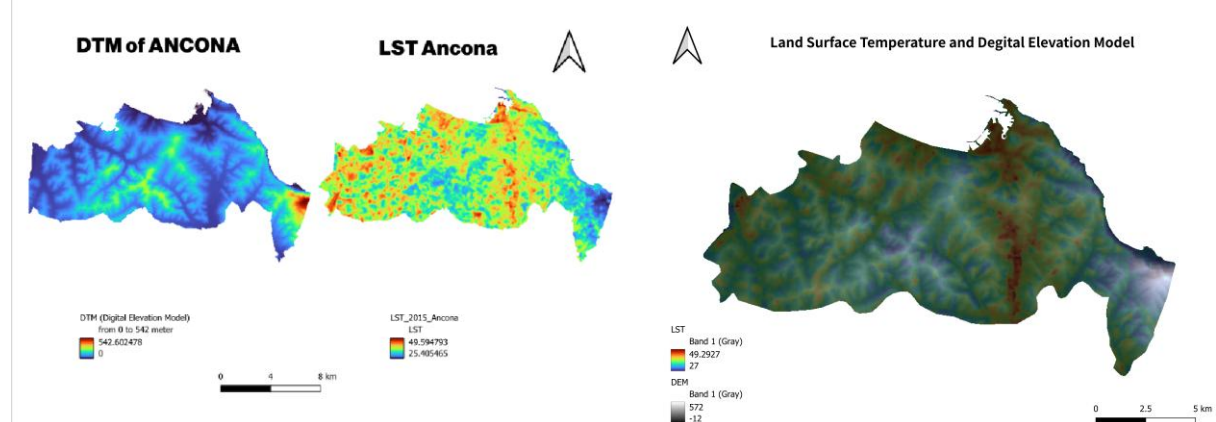


Figure 35. Relationship Between LST and DEM

The relationship between DEM and LST is very important, a Digital Elevation Model represents the terrain elevation, how high or low each pixel on land surface is above the sea level. Generally lowlands are with higher LST, there are some reason behind this. Lowlands are with denser air holds more heat, urban areas, less vegetation or the air usually stops, not moving a lot. But highlands are with lower LST, it is because cooler temperatures, more vegetation or snow and windy area which effect a lot.

4.3 Land Surface Temperature (LST) Change in Ancona (1996–2025)

Land Surface Temperature (LST) is basically how hot the ground feels when the sun warms it up whether that's soil, grass, pavement, or rooftops. Scientists measure it using satellites that detect heat energy coming from the Earth's surface. Tracking LST helps us understand important things like how much water is evaporating into the air, why cities get hotter than rural areas (the “urban heat island” effect), and how climate change is shifting temperatures across different regions.

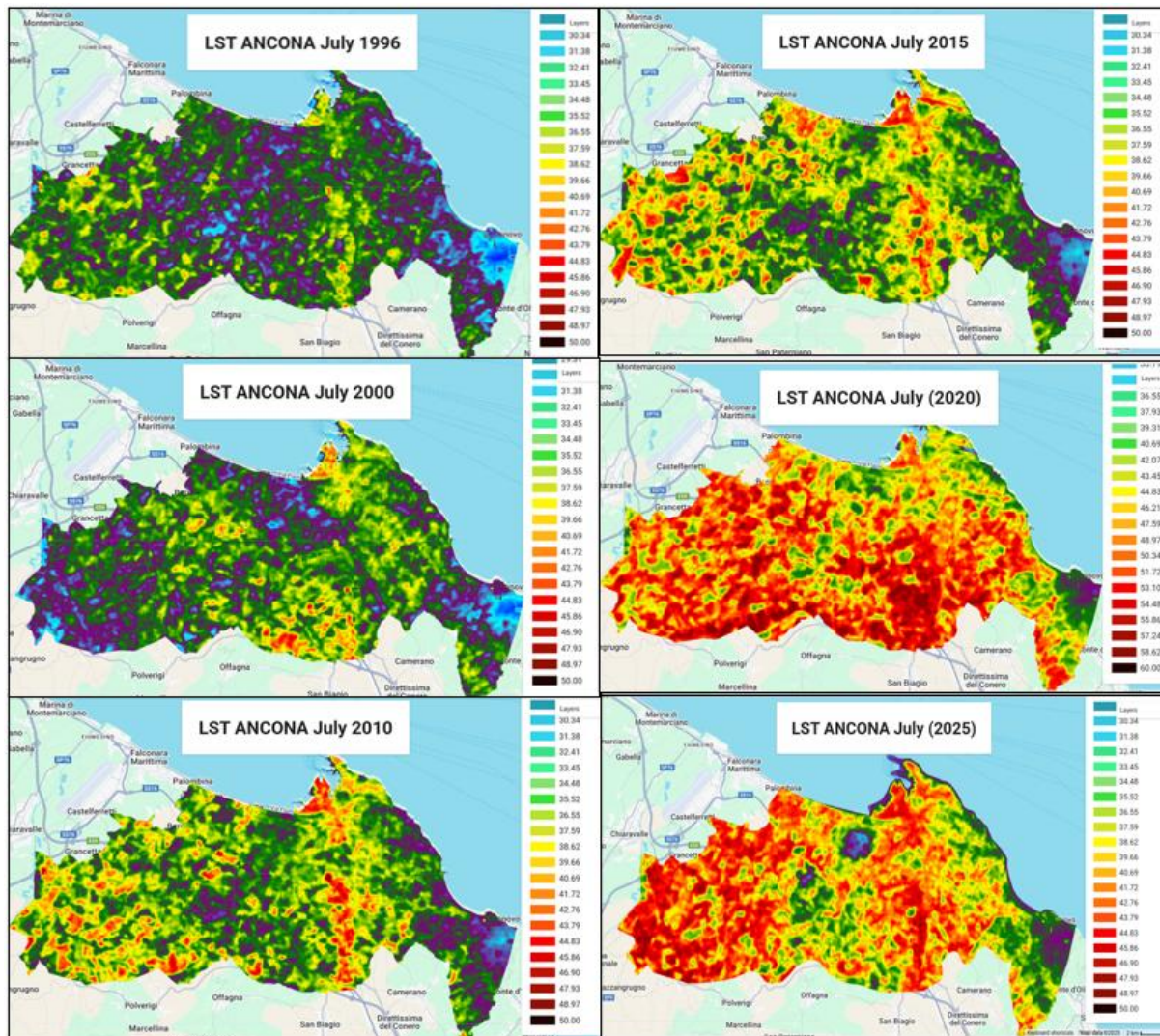


Figure 36. Land Surface Temperature (LST) Change in Ancona (1996–2025)

The maps above tell a powerful story about how the landscape of Ancona has changed in terms of LST over nearly three decades. They don't just show numbers or colors, they reveal how the land and climate are responding to human activities and natural processes over time. Each map represents the Land Surface Temperature (LST) in July of different years, a month when the region typically experiences high heat and when the urban heat island effect is most visible.

In 1996, as showed above the landscape looks relatively cool. Shades of **green**, **blue**, and **purple** dominate the map, representing temperatures mostly in the range of 32–36°C. Urban areas were smaller, vegetation was more abundant, and the land surface still retained its natural

ability to regulate heat. This was a period when the region's ecosystems were playing their role in balancing local microclimates. By 2000, the situation begins to shift. Patches of yellow and orange emerge, signaling higher temperatures creeping into parts of the territory. This gradual warming is often linked to increasing urban expansion, deforestation, and soil exposure. Where vegetation is replaced by built-up areas or bare soil, the land loses its cooling capacity and starts to store more heat.

Moving to 2010 which is showed above, the pattern becomes clearer. More yellow and orange tones cover the map, particularly around urban centers and roads. The heat is spreading. The urban fabric is denser, and the demand for space—buildings, infrastructure, and farmland has transformed large parts of the green landscape into hotter surfaces. Temperatures in many areas climb into the 38–42 °C range. What was once a patchy signal of heat becomes more continuous and noticeable.

By 2015, which showed on the map above the red zones intensify, signaling widespread land heating. This is a pivotal moment in the trend. The balance between vegetation and built-up land tips even further toward human-modified surfaces. More regions register above 42 °C, and the contrast between cooler vegetated patches and hot urban/bare zones grows sharper.

The situation takes a dramatic turn in 2020. Large swathes of the map are covered in fiery reds, representing land surface temperatures nearing or exceeding 46–50 °C. This surge cannot be ignored. It's not just a product of climate change, but also a reflection of how land use decisions amplify heat stress. The urban heat island effect dominates, and rural-urban contrasts are stark. Vegetation still cools certain areas, but these green patches are shrinking relative to the expanding heat. Finally, the 2025 projection shows a continuation of this worrying pattern. Much of the land is now engulfed in red and orange tones. Only isolated green patches remain, mostly forests and some agricultural areas. The heat signature suggests that if current trends continue, summers in Ancona could become increasingly intolerable, both for ecosystems and for people living in the region.

These maps are not just scientific outputs; they are warnings. They show how urban growth, deforestation, and soil degradation, when combined with global climate change, can transform a region's thermal landscape. But they also hint at solutions: the areas that remain green and cooler remind us of the protective role of vegetation. Expanding green spaces, restoring ecosystems, and integrating climate-conscious urban planning are not optional—they are essential if Ancona is to remain livable in the face of rising heat.

- Temporal Trends in Land Surface Temperature (1996–2025) Over Ancona

Year	Max Temp (°C)	Min Temp (°C)	Mean Temp (°C)	Std Dev (\pm °C)
1996	46.7	20.1	33	1.4
2001	48.3	20.6	33.99	2.6
2010	52.4	25.5	36.4	2.1
2015	49.5	25.4	36.9	4.7
2019	54.4	26.2	41.1	0.8
2025	53.8	25.1	39.8	2.7

Table 8. temporal trends in LST 1996–2025 over Ancona

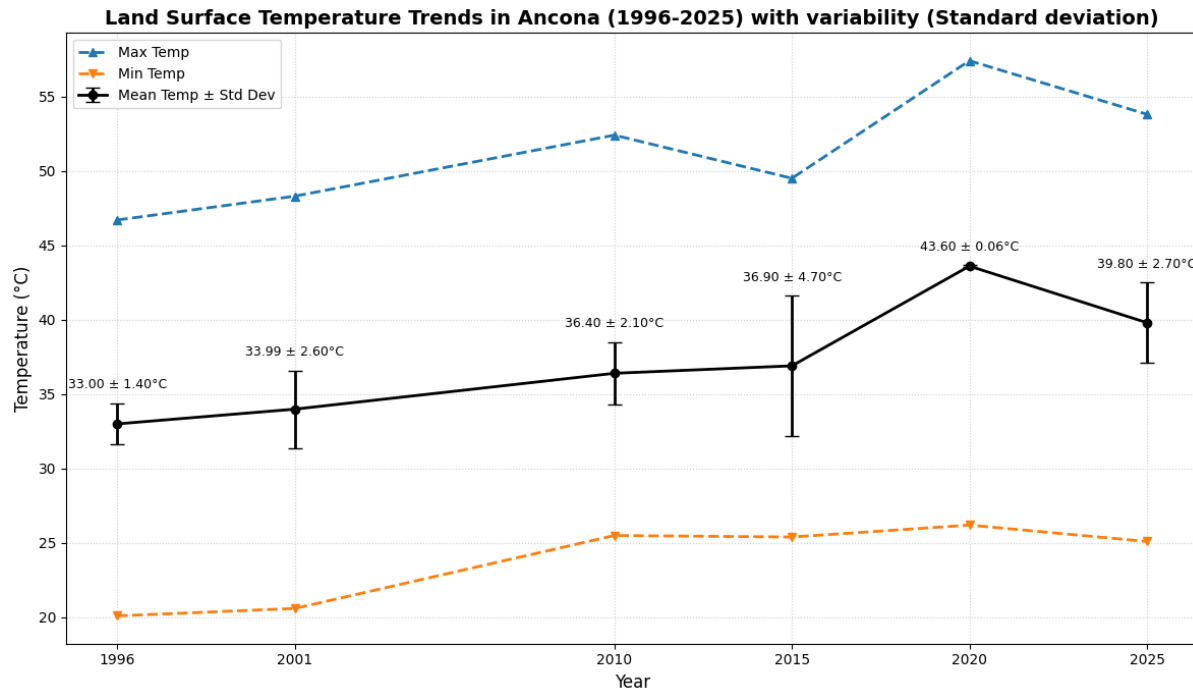


Figure 37. LST trends in Ancona

The analysis of Land Surface Temperature (LST) in Ancona from 1996 to 2025 shows a clear warming trend across the city. The mean temperature rose from about 33.0 °C in 1996 to nearly 39.8 °C in 2025, while maximum temperatures increased from 46.7 °C to 53.8 °C. This steady rise reflects both regional climate warming and urban growth, as more natural land has been replaced with built-up and impervious surfaces.

The standard deviation (SD) values indicate how varied surface temperatures were across the city. Between 1996 and 2015, higher SD values (up to 4.7 °C) suggest strong contrasts between hot built-up areas and cooler vegetated zones. However, an unusual pattern appeared in 2020, where despite a wide temperature range, the SD dropped to only 0.06 °C meaning the entire area was consistently hot. This likely occurred because there was less vegetation or water to create cooler zones, leaving the city's surfaces uniformly warm due to materials like asphalt and concrete.

Overall, the data highlight a progressive intensification of heat across Ancona, emphasizing the need for more urban greenery and sustainable planning to reduce surface temperatures and improve comfort for residents.

4.4 Urban Growth and Land Surface Temperature in Ancona

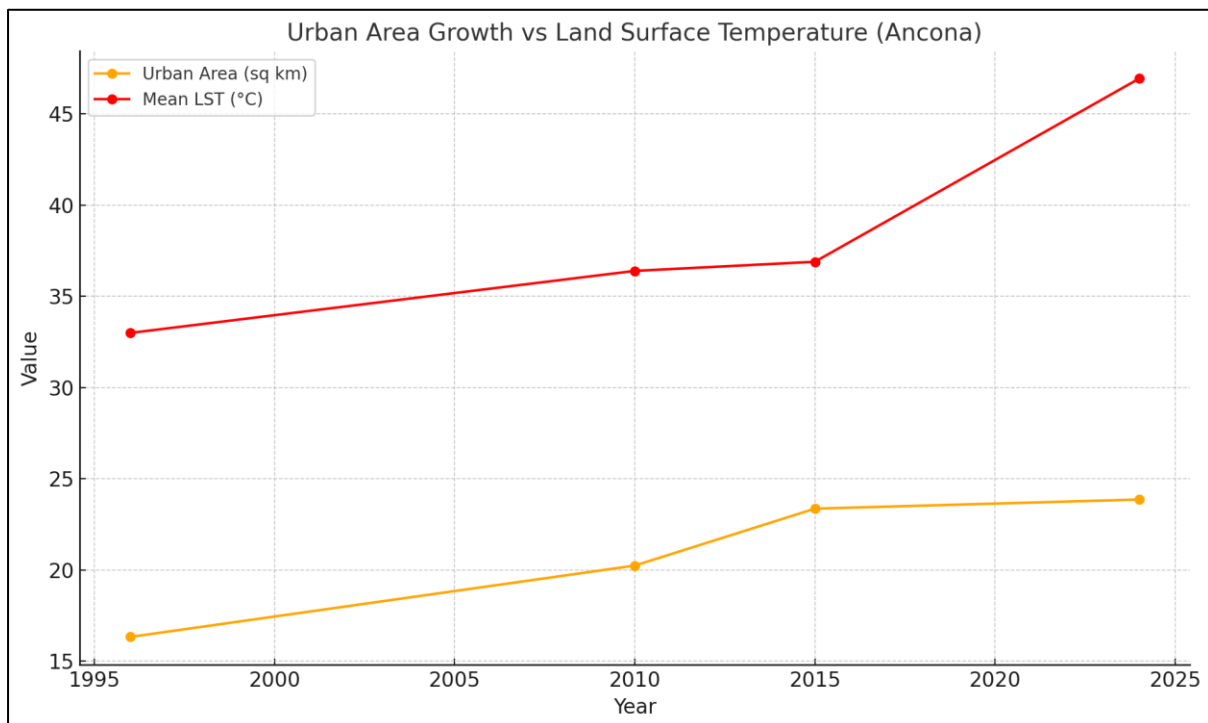


Figure 38. Urban Growth and Land Surface temperature

The graph above illustrates the relationship between urban expansion and Land Surface Temperature (LST) in Ancona from 1995 to 2025. Over this 30-year period, both indicators show a consistent upward trend a clear sign of how urbanization contributes to surface warming. The urban area expanded from approximately 16 km² in 1995 to nearly 23 km² in 2025, reflecting continuous growth driven by residential, commercial, and infrastructural development.

At the same time, the mean LST rose from about 33 °C in 1995 to around 46 °C in 2025, marking a significant increase in surface heat. This parallel rise between built-up area and surface temperature suggests that urban growth has directly influenced local thermal conditions, largely due to the replacement of natural surfaces (such as vegetation and soil) with impervious materials like asphalt, concrete, and rooftops.

4.5 Urban Heat Island Dynamics and Land Surface Temperature Variations in Ancona (1996–2025)

The analysis of Urban Heat Island (UHI) dynamics in Ancona from 1996 to 2025 reveals a consistent warming trend associated with urban expansion and surface modification.

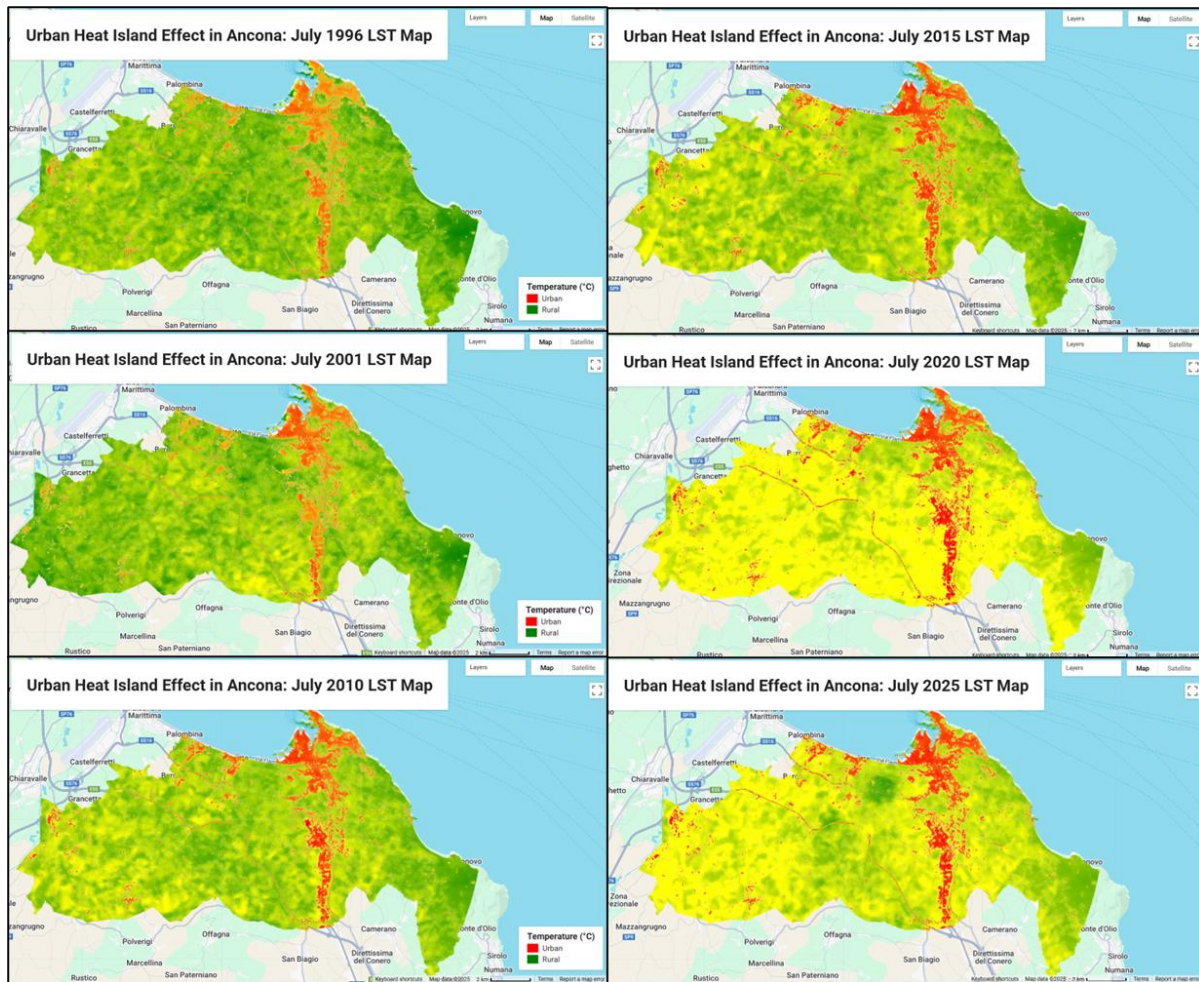


Figure 39. UHI dynamics and LST

- Urban vs Rural LST Statistics (Ancona, 1996–2025)

Year	Rural Mean LST (A°C)	Urban Mean LST (A°C)	UHI Intensity (A°C)
1996	32.82347944	35.17434511	2.350865675
2001	33.71680341	36.1113588	2.394555391
2010	36.06602542	39.96368104	3.897655619
2015	36.55997511	40.40313035	3.843155245
2020	43.65769991	43.70658097	0.04888098
2025	40.75740818	43.19179736	2.434389184

Table 9. urban and rural LST statistics, Ancona 199-2025

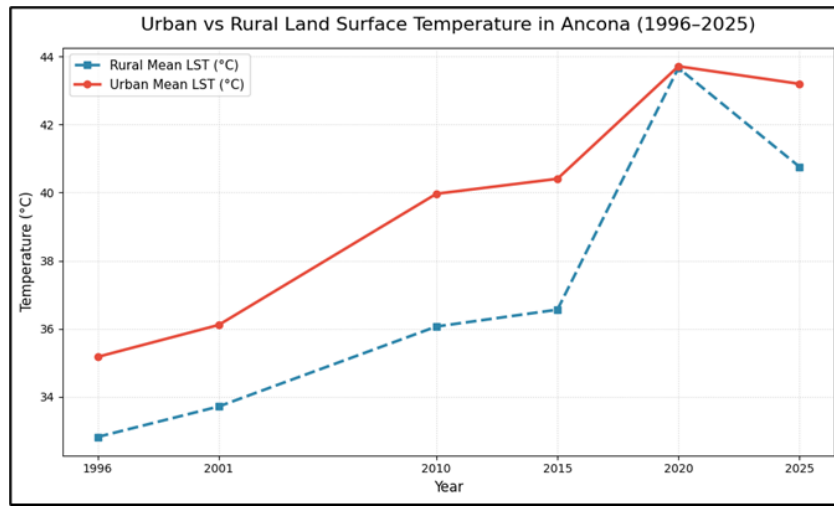


Figure 40. urban and rural LST trends

The series of Land Surface Temperature (LST) maps and statistical plots highlight how the city's built-up zones particularly the central, industrial, and transport corridors have gradually evolved into thermal hotspots over the past three decades.

The red zones on the maps represent areas with significantly higher LST values, corresponding to dense urban and impervious surfaces such as asphalt, concrete rooftops, and industrial facilities. In contrast, green and yellow areas mainly the vegetated and rural surroundings maintain lower temperatures, acting as cooling zones. This contrast between hot urban cores and cooler rural peripheries clearly illustrates the spatial manifestation of the UHI effect.

The accompanying graphs and statistical table provide quantitative insight into this pattern. Between 1996 and 2025, urban mean LST increased from 35.17 °C to 43.19 °C, while rural mean LST rose from 32.82 °C to 40.76 °C. Despite both showing warming, the UHI intensity (the temperature difference between urban and rural areas) fluctuated over time. It peaked at around 3.9 °C in 2010-2015, indicating a strong urban heat island effect during this period. Interestingly, 2020 recorded an unusually low UHI intensity (≈ 0.05 °C), suggesting a temporary levelling of urban–rural temperatures possibly due to consistent heat conditions across the region, reduced vegetation, or atmospheric factors such as heatwaves under cloud-free conditions.

By 2025, UHI intensity rose again to 2.4 °C, showing the persistence of heat concentration within built-up environments. These findings reflect the close link between urbanization, land cover change, and thermal patterns, emphasizing how expanding impervious surfaces trap more heat and diminish natural cooling. Maintaining or restoring vegetated zones within and around Ancona can help mitigate these effects by enhancing evapotranspiration and reducing surface heat accumulation.

4.6 Urban Heat Island Intensity (UHII)/ Its Implications in Ancona (1996–2025)

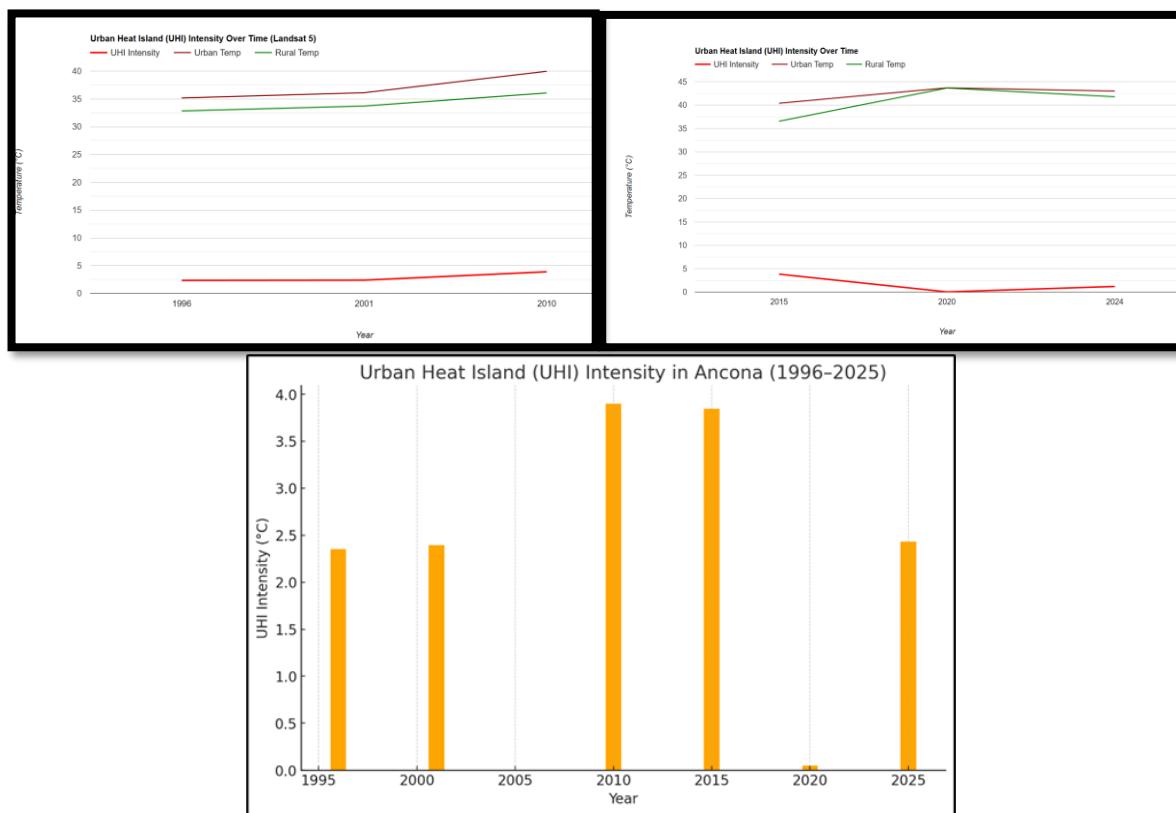


Figure 41. UHII and its Implications in Ancona

The **Urban Heat Island Intensity** (UHII) represents the temperature difference between urban and rural areas, highlighting how much **warmer** the city is compared to its natural surroundings. A higher UHII value indicates a larger temperature gap, meaning the urban environment retains significantly more heat. This typically occurs in cities with dense infrastructure, extensive asphalt and concrete surfaces, limited vegetation, and high population or energy use. In such cases, heat becomes trapped within the built environment, leading to increased thermal stress, particularly affecting vulnerable groups such as the elderly and children. Elevated UHII also contributes to higher energy demand for cooling and can worsen air quality and health outcomes due to stagnant heat and pollution buildup.

Conversely, a lower UHII suggests that the temperature difference between urban and rural areas is smaller, meaning the city is cooler and more climate resilient. This is often a result of increased vegetation, such as parks, street trees, and green roofs, as well as the use of reflective and permeable materials that help reduce surface heat absorption. Cities with low UHII values tend to experience lower energy consumption, better thermal comfort, and improved public health, especially during periods of extreme heat.

In the case of **Ancona (1996–2025)**, UHII trends show periods of strong heat concentration particularly around **2010 and 2015** reflecting years of intensified urban development and limited vegetation. The more moderate UHII values seen in later years

indicate progress toward a more balanced urban environment, possibly due to improved land management and green infrastructure efforts.

The formula to find the standard deviation:

$$s = \sqrt{\frac{\sum_{i=1}^N (X_i - \bar{X})^2}{N - 1}}$$

X_i : each LST value in each pixel

\bar{X} : mean LST value.

N: number of data points, means the number of pixels.

4.7 Land Use Land Cover (LULC) and Urban Heat Island (UHI)-Ancona

Since 1996 urban areas in Ancona have expanded significantly, leading to an increase in the Urban Heat Island (UHI) effect. In 1996 (Landsat 5), urban areas covered 16.34 km² (7.4%), but by 2025 (Landsat 9), buildings and roads combined covered 23.87 km² (10.81%). Meanwhile, vegetation decreased from 139.80 km² (63.29%) in 1996 to 87.21 km² (39.48%) in 2024. The rise in built-up areas, which absorb and retain heat, along with the loss of vegetation that provides cooling, has intensified the UHI effect. As a result, land surface temperatures have increased over time, reflecting the growing heat concentration in urban regions.

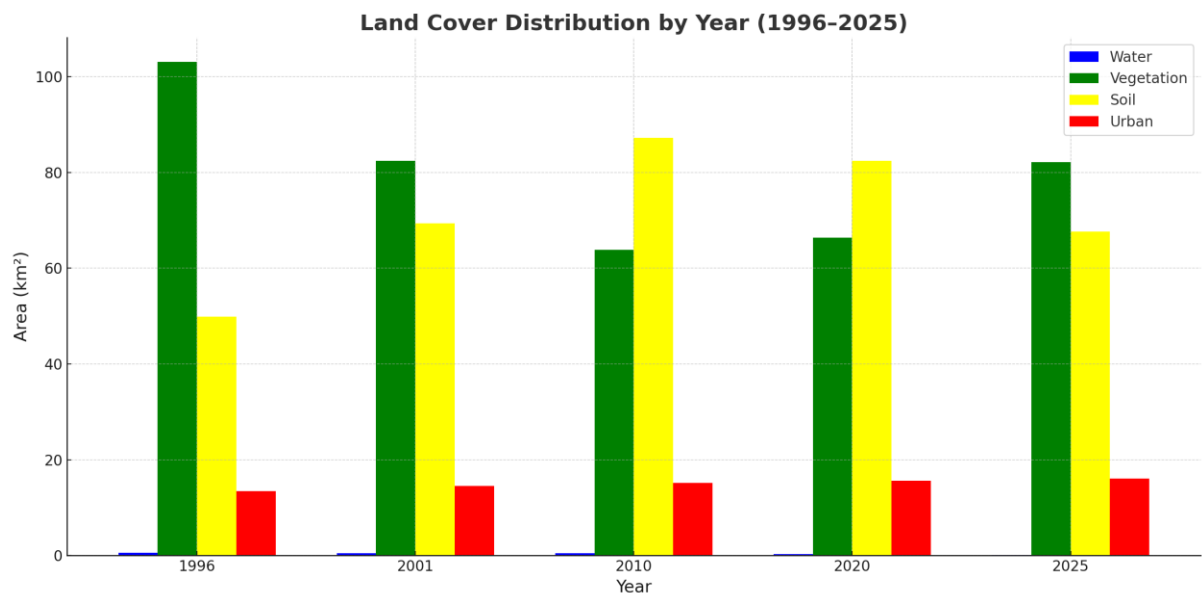


Figure 42. Land cover distribution by year 1996 to 2025

4.8 Land Surface Temperature (LST) Derived from Landsat and ECOSTRESS Data (Ancona, 19 June 2025)

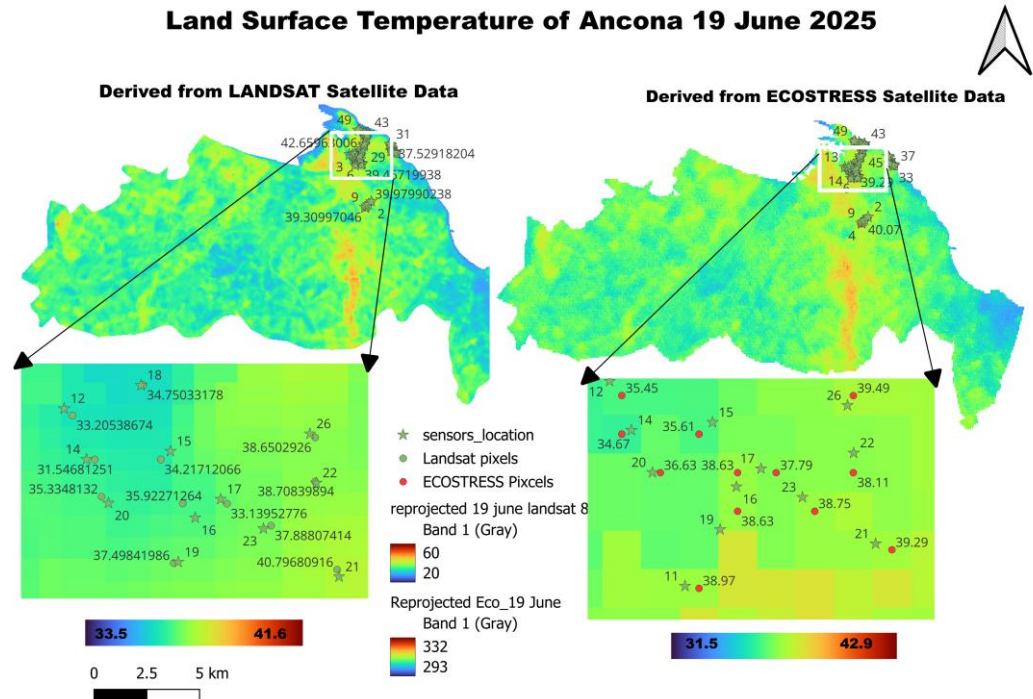


Figure 43 Land Surface Temperature Ancona 19 June 2025

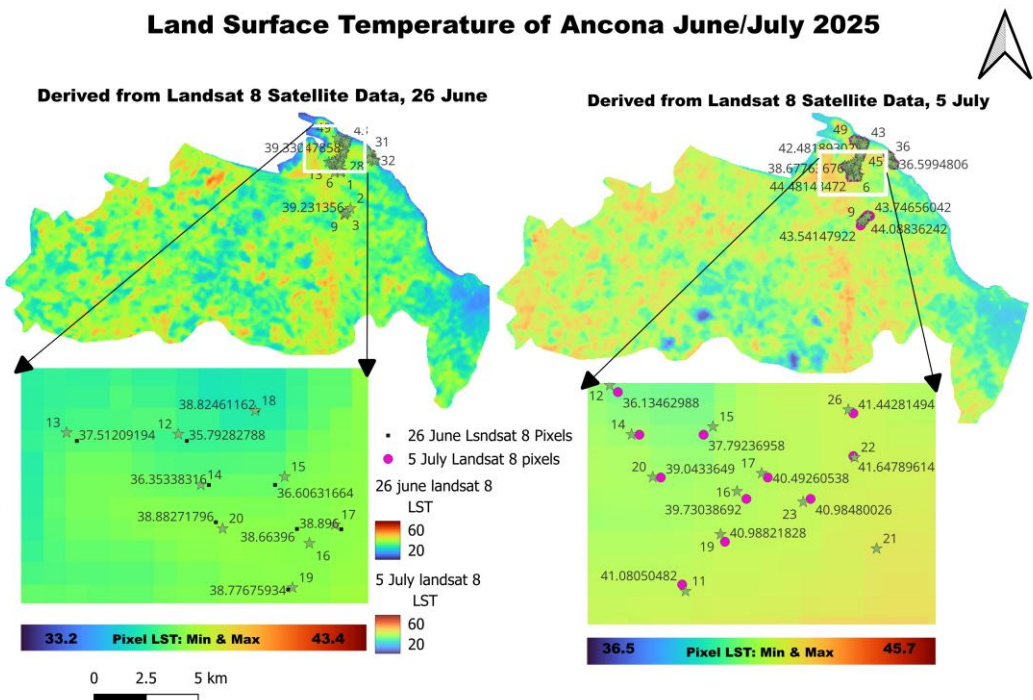


Figure 44 Land Surface Temperature Ancona 26 June and 5 July 2025

These figures 31 and 32 present a comparative analysis of Land Surface Temperature (LST) in Ancona on 19 and 26 of June, and 5 July 2025, derived from two satellite sources

Landsat 8 (left) and ECOSTRESS (right). Both datasets were harmonized spatially and temporally to ensure consistency, with ground sensor locations overlaid for validation.

4.8.1 Metrics Results

Satellite	Date	Bias (°C)	MAE (°C)	RMSE (°C)	Pearson R
ECOSTRESS	19/06/2025	3.011	3.408	4.262	0.488
LANDSAT 8	19/06/2025	2.764	3.229	3.862	0.678
LANDSAT 8	26/06/2025	2.098	3.330	3.993	0.423
LANDSAT 8	05/07/2025	1.225	4.007	4.592	0.604
ECOSTRESS	23/06/2025	1.597	1.969	3.535	0.553

Table 10. metrics results consistent

This table compare the validation metrics of satellite-derived Land Surface Temperature (LST) from ECOSTRESS and Landsat 8 with ground-based temperature observations, after incorporating the Average Weighted Temperature (AWT) adjustment. The number of Bias, MAE, RMSE and Pearson R formula related the dates as recorded the LST and for each data this formula used.

ECOSTRESS Performance:

ECOSTRESS shows Bias values between 1.60°C and 3.01°C, with RMSE values ranging from 3.54°C to 4.26°C. These numbers indicate a moderate but stable accuracy across both dates. The correlations ($R = 0.488$ and 0.553) are also consistent, reflecting a reliable relationship between ECOSTRESS temperatures and ground measurements.

Landsat 8 Performance:

Landsat 8 generally shows slightly lower Bias and MAE compared to ECOSTRESS on matching dates. For example:

- 19 June 2025: Landsat Bias = 2.764°C, lower than ECOSTRESS (3.011°C)
- 26 June 2025: Landsat Bias = 2.098°C, again lower
- 5 July 2025: Landsat Bias = 1.225°C, the lowest of all dates

Landsat also achieves the highest correlation in the table ($R = 0.678$ on 19 June), indicating that its temperature variations follow ground observations more closely than ECOSTRESS on most days.

Which Satellite Performs Better?

Overall, Landsat 8 performs slightly better than ECOSTRESS in this study, especially in terms of:

- Lower Bias (more accurate on average)
- Higher Pearson R (better agreement with the temporal pattern of ground temperatures)

ECOSTRESS, however, remains competitive and shows strong stability across days, with consistent MAE and RMSE values. ECOSTRESS also benefits from finer thermal detail due to its higher spatial resolution (70 m), which may explain some of the additional variability observed.

5 July, Landsat 8 Land Cover Types	Person R	Bias	MAE	RMSE
Asphalt/concrete	0.618	0.264	3.716	4.320
Soil/ Mixed	0.601	1.081	4.093	4.717
vegetation	0.590	2.471	4.125	4.602

Table 11. metric result for LANDSAT data on July 5th, 2025

19 June, Landsat 8 Land Cover Types	Person R	Bias	MAE	RMSE
Asphalt/concrete	0.689	1.999	2.274	2.775
Soil/ Mixed	0.650	2.651	3.462	4.062
vegetation	0.602	3.843	3.843	4.468

Table 12. metric result for LANDSAT data on June 19th, 2025

19 June, ECOSTRESS Land Cover Types	Person R	Bias	MAE	RMSE
Asphalt/concrete	0.475	2.548	2.804	3.631
Soil/Mixed	0.430	2.829	3.487	4.101
vegetation	0.422	4.348	4.348	5.568

Table 13. metric result for ECOSTRESS data on June 19th, 2025

23 June, ECOSTRESS Land Cover Types	Person R	Bias	MAE	RMSE
Asphalt/concrete	0.602	1.722	1.891	2.458
Soil/Mixed	0.534	1.371	1.879	2.410
vegetation	0.520	1.716	2.123	2.877

Table 14. metric result for ECOSTRESS data on June 23th, 2025

26 June, Landsat Land Cover Types	Person R	Bias	MAE	RMSE
Asphalt/concrete	0.480	1.323	2.189	2.932
soil	0.431	2.519	3.813	4.438
vegetation	0.400	2.032	3.504	3.973

Table 15. metric result for LADSAT data on June 26th, 2025

4- Asphalt and Concrete

Hard surfaces such as asphalt and concrete consistently showed higher Bias and RMSE across all times or dates. Asphalt pixels showed the largest overestimations, which explains the higher error values. Despite this, the correlation (Pearson R) for asphalt surfaces remained moderate to strong in most cases. This indicates that although the absolute deviations can be larger, satellite observations still follow the overall trend of ground temperature variations for these surfaces.

5- Soil

Soil surfaces/some cases mixed surfaces produced intermediate error values. The Bias and RMSE for soils were generally lower than for asphalt but slightly higher than for vegetation. The soil category consistently displayed stable correlation values, demonstrating that its thermal response, although variable.

6- Vegetation

Vegetated areas consistently presented the lowest MAE and RMSE values, indicating that the satellite retrieval performed best over these surfaces. In some cases vegetation exhibited slightly higher Bias than soil but still maintained the lowest spread of errors (MAE, RMSE). This means that although the satellite may systematically over- or underestimate vegetated surfaces by a small amount, the predictions remain consistent and reliable.

Overall Interpretation, looking across all the analysed dates, the surface-specific metrics show:

- a- Vegetation shows the best agreement between satellite and ground temperatures.
- b- Soil performs moderately, with stable correlations but slightly higher error magnitudes.
- c- Asphalt/concrete remains the most challenging, with the highest errors due to thermal complexity and extreme heating behaviour.

These findings highlight the importance of considering surface composition when validating satellite LST. Urban areas in particular, dominated by asphalt and concrete, require careful interpretation because their thermal properties differ significantly from natural surfaces.

4.9 Conclusion

The aim of this study is to compare and connect satellite thermal data and ground temperature measurements to better monitor long-term climate changes in Ancona and nearby towns. By combining data from Landsat 8 TIRS and ECOSTRESS with ground sensors the studies showed that matching data in space and time and correcting for emissivity can make satellite and ground readings more similar and reliable. The results from Landsat data processing showed a clear increase in land surface temperature (LST) between 1996 and 2025. This rise is strongly linked to urban expansion and the loss of vegetation in years. The Urban Heat Island (UHI) effect became stronger over time, proving that more buildings and less green space cause higher surface temperatures.

Among the two satellite sources, Landsat 8 gave more stable temperature patterns, while ECOSTRESS was better at capturing the real temperature values. When both are used together after harmonization, they provide a clearer and more accurate picture of how heat is spread across the land. These findings also remind us that how cities' grow has a big impact on their local climate. The warming trend seen almost over the past thirty years shows the need for more green spaces, as long as the urban expand by years.

In summary, harmonizing satellite and ground data is not only a technical process, it is also an important way to understand and manage climate change better. The approach used in this study can be applied in other regions to monitor temperature changes and support smart planning for a hotter future.

4.10 References

1. Ewa Głowienka; Eva Savina Malinvernì; Marsia Sanità; Krystyna Michalowska; and Marcin Kucza: *Harmonizing satellite thermal data with ground-based observations for climate long-term monitoring*. [[2025](#)].
2. Sofia L. Ermida; Patrícia Soares; Vasco Mantas; Frank-M. Götsche; and Isabel F. Trigo: *Google Earth Engine Open-Source Code for Land Surface Temperature Estimation from the Landsat Series*. [[2020](#)].
3. Mehmet Cetin; Mehtap Ozenen Kavlak; Alper Cabuk: *Determination of land surface temperature and urban heat island effects with remote sensing capabilities: the case of Kayseri, Türkiye*. [[2024](#)].
4. Zhao-Liang Li a b; Bo-Hui Tang a; Hua Wu a; Huazhong Ren c; Guangjian Yan c; Zhengming Wan d; Isabel F. Trigo e f; José A. Sobrino g: *Satellite-derived land surface temperature: Current status and perspectives* [[2013](#)].
5. Nasa website, Landsat 8 and Landsat 7 completed information: [[lunch date](#)].
6. Nasa website, Landsat 5 completed information: [[launched on March 1984](#)].
7. Nasa website, ECOSTRESS full information and data acquisition website [[website](#)].
8. Lili Liang; Yu Feng ; Jie Wu; Xinyue He; Shijing Liang; Xin Jiang; Gabriel de Oliveira; Jianxiu Qiu; Zhenzhong Zeng: *Evaluation of ECOSTRESS evapotranspiration estimates over heterogeneous landscapes in the continental US*. [[2022](#)]
9. Huanyu Zhang; Amber N. Mahmood; Tian Hu; Kanishka Mallick; Yoanne Didry; Patri; Hitzelberger; Zoltan Szantoi: *Global evaluation of high-resolution ECOSTRESS land surface temperature and emissivity products: Collection 1 versus Collection 2* [[2025](#)].
10. Prof. S. V. Sabale1, Piyush S. Hokarne2, Nikita D. Kale3, Ketan S. Gambhire4: *Review Paper on Applications of Q-GIS Software* . [[2021](#)].
11. Qihao Weng; Dengsheng Lu; Jacquelyn Schubring: *Estimation of land surface temperature-vegetation abundance relationship for urban heat island studies* [[2004](#)].
12. Jose Sobrino; Juan-Carlos Jimenez Leo Paolini: *Land surface temperature retrieval from LANDSAT TM 5* [[2004](#)].
13. Graduate School of Global Environmental Studies (GSGES), Kyoto University, Kyoto 606-8502, Japan; Graduate School of Agriculture (GSA), Kyoto University, Kyoto 606-8502, Japan; 3SIWIL Division, P4W/CRESTPENT, IPB University, Bogor 16153, Indonesia: *Retrieving Spatial Variation of Land Surface Temperature Based on Landsat OLI/TIRS: A Case of Southern part of Jember, Java, Indonesia* : [[2019](#)].
14. Thanh Noi Phan, Verena Kuch, and Lukas W. Lehnert: *Land Cover Classification using Google Earth Engine and Random Forest Classifier—The Role of Image Composition* [[2020](#)]
15. Google earth engine platform and website [[official website](#)]